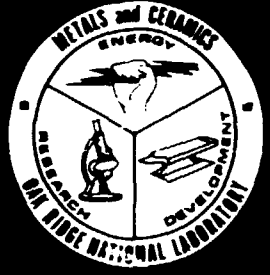

ORNL-5428

DR 2319

Operation and Postirradiation Examination of ORR Capsule OF-2: Accelerated Testing of HTGR Fuel

T. N. Tiegs
K. R. Thoms

ORNL-5428
Distribution
Category UC-77

Contract No. W-7405-eng-26

Metals and Ceramics Division

Engineering Technology Division

HTGR Fuel Recycle Development Program (189a 0H045)
General Support-Task 800

OPERATION AND POSTIRRADIATION EXAMINATION OF ORR CAPSULE OF-2: ACCELERATED TESTING OF HTGR FUEL

T. N. Tiegs and K. R. Thoms

Date Published: March 1979

OAK RIDGE NATIONAL LABORATORY
Oak Ridge, Tennessee 37830
operated by
UNION CARBIDE CORPORATION
for the
DEPARTMENT OF ENERGY

TABLE OF CONTENTS

OPERATION AND POSTIRRADIATION EXAMINATION OF ORR CAPSULE OF-2: ACCELERATED TESTING OF HTGR FUEL

T. N. Tiegs and K. R. Thoms*

ABSTRACT

Irradiation capsule OF-2 was a test of High-Temperature Gas-Cooled Reactor fuel types under accelerated irradiation conditions in the Oak Ridge Research Reactor. The results showed good irradiation performance of Triso-coated weak-acid-resin fissile particles and Biso-coated fertile particles. These particles had been coated by a fritted gas distributor in the 0.13-m-diam furnace. Fast-neutron damage ($E > 0.18$ MeV) and matrix-particle interaction caused the outer pyrocarbon coating on the Triso-coated particles to fail. Such failure depended on the optical anisotropy, density, and open porosity of the outer pyrocarbon coating, as well as on the coke yield of the matrix. Irradiation of specimens with values outside prescribed limits for these properties increased the failure rate of their outer pyrocarbon coating. Good irradiation performance was observed for weak-acid-resin particles with conversions in the range from 15 to 75% UC_2.

1. INTRODUCTION

Irradiation capsule OF-2 was a test of High-Temperature Gas-Cooled Reactor (HTGR) fuel types under accelerated irradiation conditions in the Oak Ridge Research Reactor (ORR). The irradiation of capsule OF-2 started June 21, 1975 and ended Aug. 1, 1976 after 8440 hr of reactor full-power irradiation (30 MW).

The OF-2 irradiation experiment was the second in a series of HTGR fuel irradiations in the ORR.[1,2] Fuel was irradiated to approximately 80% of HTGR burnup and fast-neutron exposure ($E > 0.18$ MeV).† Details of the capsule design, instrumentation (both thermometry and dosimetry), and fuel types have been reported previously.[1,3,4] For completeness, this report presents a summary of the test objectives and capsule design. The objectives of this experiment are:

---

*Engineering Technology Division.

†The capsule was removed from the reactor about three months ahead of schedule because the ORR was shut down for an extended period.

1. to test the performance of reference Triso-coated weak-acid-resin fissile particles and reference Biso-coated fertile particles, both fuels coated in the 0.13-m-diam furnace;
2. to study the matrix-particle interaction phenomenon and the effects of particle strength, matrix type, and particle surface conditions on irradiation performance;
3. to investigate the irradiation behavior of coating microstructures created by a variation in one of the coating process conditions — gas concentration, deposition rate, deposition temperature, or batch size;
4. to investigate the influence of stoichiometry and kernel density on the irradiation performance of weak-acid-resin-derived fuels;
5. to verify the adequacy of the performance of fissile fuel to be irradiated later in early proof-test elements in the Fort St. Vrain Reactor;
6. to compare the performance of coatings deposited in the 0.13-m coater by fritted and cone gas distribution systems. (The fritted system is the reference for the HTGR Recycle Demonstration Facility); and
7. to test the feasibility of removing fuel rods from the graphite holder after full-life irradiation, particularly rods carbonized in-block.

In addition to the ORNL specimens, Los Alamos Scientific Laboratory (LASL) tested loose ZrC particles and two fuel rods (to be described later). Detailed descriptions of their fabrication and analysis are reported elsewhere.[5]

1.1 Description of the OF-2 Capsule and Fuel Specimen Holders

The OF-2 irradiation capsule was similar in design to the OF-1 capsule,[2] being a double-walled water-cooled stainless steel vessel. The total active test space was a cylinder 0.610 m long with a 62.0-mm diameter (24.0 by 2.44 in.). This test space was divided into two compartments by a copper bulkhead brazed in the primary containment tube 85.73 mm (3.375 in.) below the horizontal midplane of the reactor. The

upper compartment — designated cell 2 — contained three-fifths of the test space and was used for objectives 2, 3, and 4. The lower compartment — designated cell 1 — contained the remaining two-fifths of the test space and was used for objectives 1, 5, 6, and 7. Each compartment had its own sweep-gas system and was independently swept with a helium and neon gas mixture to control temperature and monitor fission gas release. The entire in-core section of the capsule is shown in Fig. 1.1.

The upper experimental compartment (cell 2) contained two H-451 graphite* specimen holders with a 9.53-mm-diam (0.375-in.) central spline hole and four 15.95-mm-diam (0.628-in.) peripheral fuel holes. The upper holder, specimen holder A, was 168.3 mm (6.625 in.) long and 61.34 mm (2.415 in.) in diameter, and was designed to operate at a maximum temperature of 1150°C. The lower holder, specimen holder B, was 168.3 mm (6.625 in.) long and 61.16 mm (2.408 in.) in diameter, and was designed to operate at a maximum temperature of 1350°C. Each specimen holder contained 36 fuel rods; Figs. 1.2 and 1.3 represent specimen holders A and B, respectively. Holes 1 and 2 each contained six 25.4-mm-long by 15.75-mm-diam (1.00- by 0.620-in.) fuel specimens; holes 3 and 4 each contained twelve 12.7-mm-long by 15.75-mm-diam (0.50- by 0.620-in.) fuel specimens. In addition specimen holder B contained about two cubic centimeters of LASL loose-coated inert particles.

Specimen holder A contained 12 thermocouples — 11 Chromel-P vs Alumel (C-A) and one platinum-molybdenum (Pt-Mo). Specimen holder B contained seven thermocouples — 6 C-A and 1 Pt-Mo. These were used to monitor axial, peripheral, and centerline graphite temperatures. Flux monitors were also built into each specimen holder and central graphite spline.

The lower experiment compartment (cell 1) contained one H-451 graphite specimen holder with a 9.53-mm-diam (0.375-in.) central spline hole and four 15.95-mm-diam (0.628-in.) peripheral fuel holes. This holder, specimen holder C, was designed to operate at a maximum temperature of 1350°C and was 222.25 mm (8.750 in.) long with a 61.054-mm (2.4037-in.)

---

*H-451 graphite manufactured by Great Lakes Carbon Company (GLCC), New York.

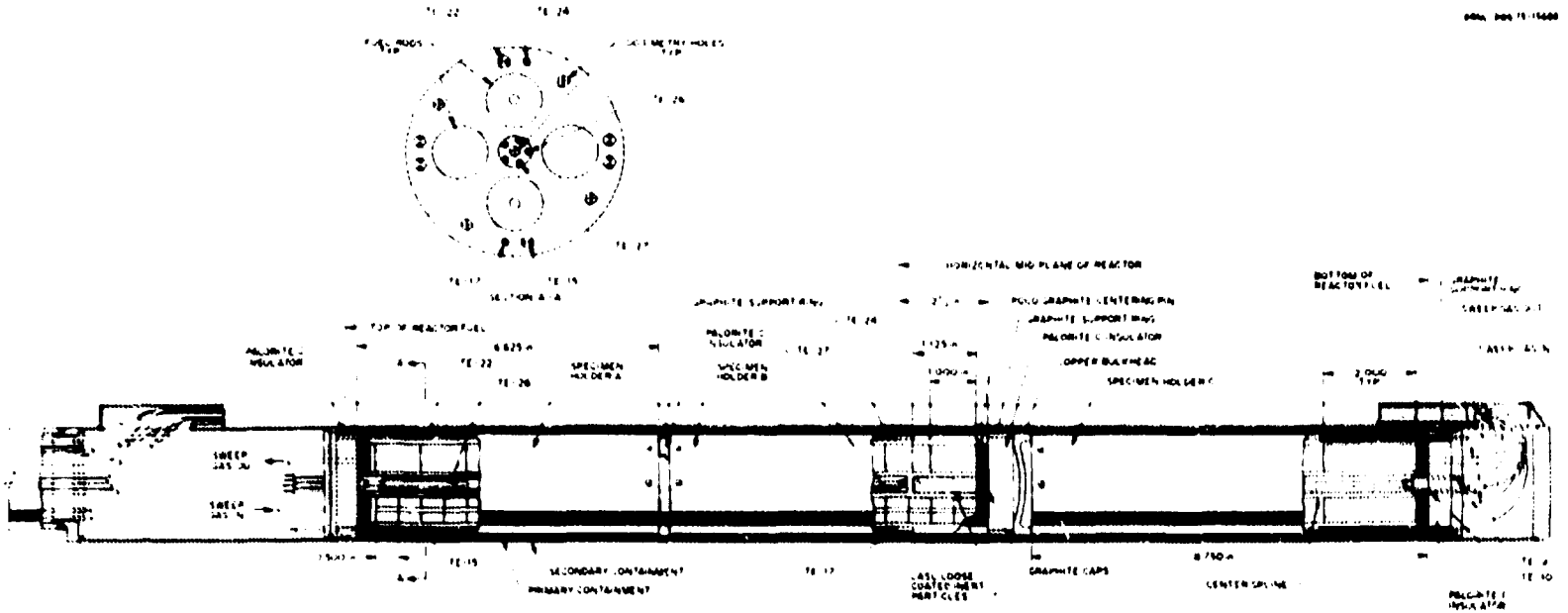

Fig. 1.1. In-core Section of OF-2 Capsule. To convert dimensions to millimeters, multiply by 25.4.

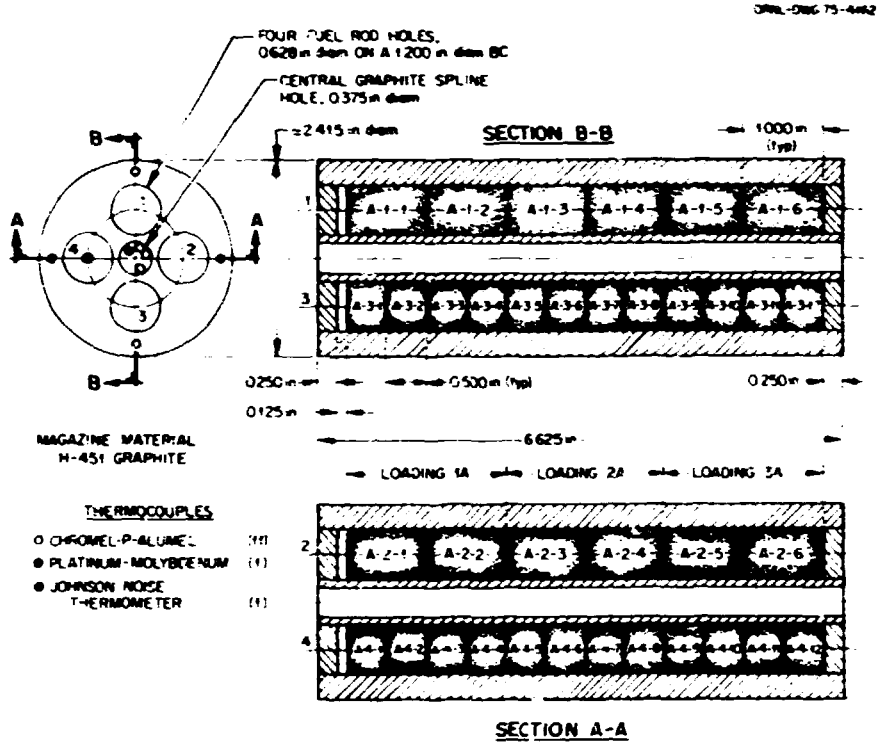

Fig. 1.2. Specimen Holder A of Irradiation Capsule OF-2. To convert dimensions to millimeters, multiply by 25.4.

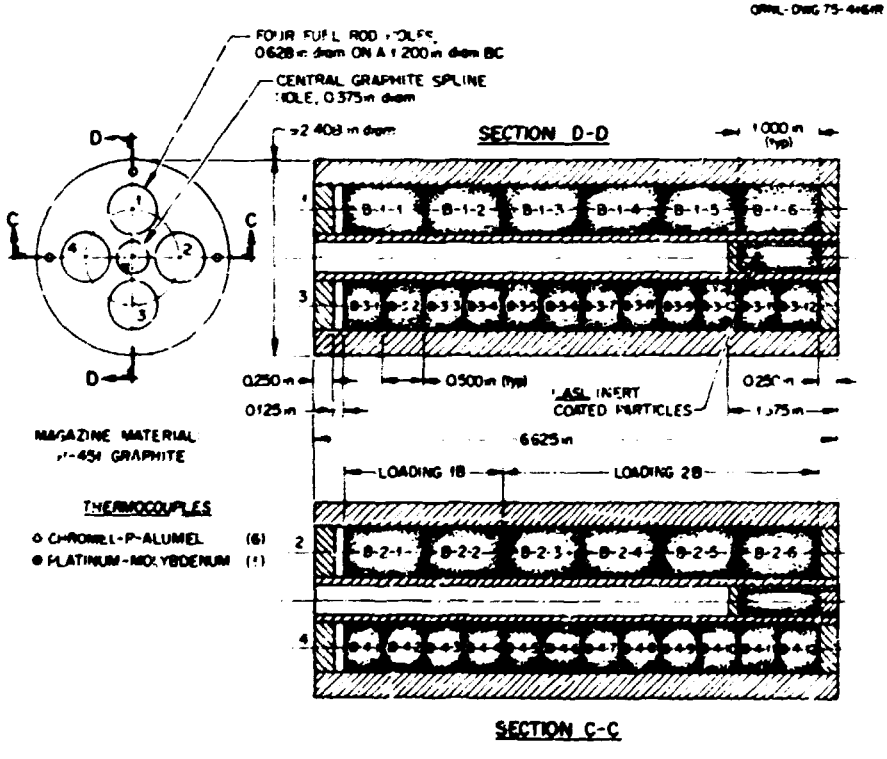

Fig. 1.3. Specimen Holder B of Irradiation Capsule OF-2. To convert dimensions to millimeters, multiply by 25.4.

diameter. Figure 1.4 describes specimen holder C. Each fuel hole contained four 50.8-mm-long by 15.75-mm-diam (2.00- by 0.620-in.) fuel rods. Nine C-A thermocouples were incorporated to monitor axial, peripheral, and centerline graphite temperatures. Flux monitors were placed in the central graphite spline only.

1.2 Description of OF-2 Fuel Specimens: Coated Particles

Capsule OF-2 required 88 fuel specimens. Of these, 86 were fabricated at ORNL and two specimens at LASL. The Triso-coated fissile particle test set consisted of 12 batches of weak-acid-resin derived (WAR) particles with a wide range of stoichiometries, from uranium oxide to uranium carbide; one batch of WAR U(C,N) particles; one batch of sol-gel $(4Th,U)O_2$ particles; and one batch of General Atomic Company's

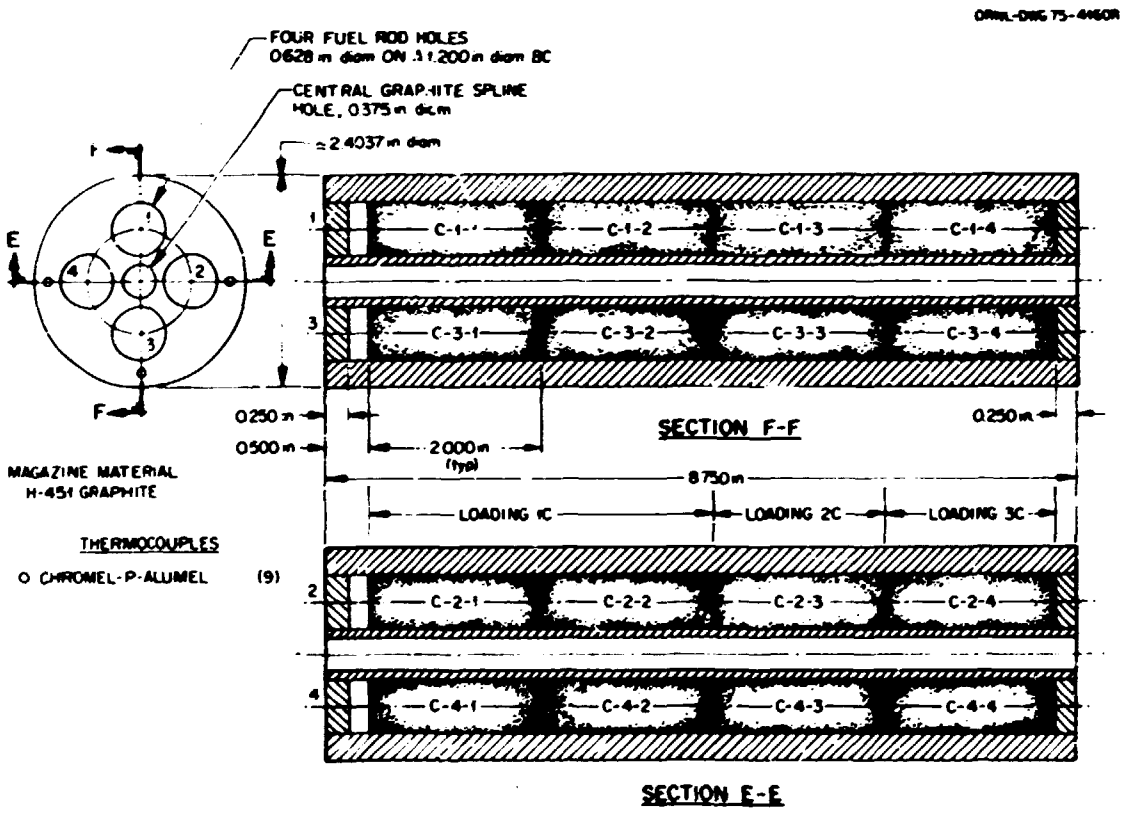

Fig. 1.4. Specimen Holder C of Irradiation Capsule OF-2. To convert dimensions to millimeters, multiply by 25.4.

VSM UC_2 particles. Each fissile particle batch is described in Table 1.1. All particle batch types except type 15 were included in the fuel specimens in the upper experimental compartment, cell 2. Fabricated for the lower experimental compartment, cell 1, particle types 13, 14, and 15 were coated in the large-diameter coating furnace. Types 13 and 14 were coated by the reference fritted gas distribution system, and type 15 by the cone distribution system. Particle types 1 through 11 were annealed at 1800°C for 10 min in a fluidized bed after the outer low-temperature isotropic (oLTI) coating had been deposited. Particle types 13 through 15 were similarly annealed after the inner low-temperature isotropic (iLTI) coating had been deposited.

Sixteen batches of Biso-coated fertile particles were selected for OF-2. Nine of the fertile batch types were coated in the large-diameter coating furnace. Batch types G through J, and M through P were coated by the fritted gas distributor, and batch type K by the cone distribution system. Specific coating parameters — deposition rates, geometries, and densities — are described in Table 1.2. Fertile particle types A through L were annealed at 1800°C for 10 min in a fluidized bed, but the remaining types were not annealed.

1.3 Fuel Pods

For each fuel rod specimen fabricated, one batch each of fissile and fertile particles was selected from its proper test set and combined with a particular matrix type. The matrix test set for OF-2 is described in Table 1.3.

For the upper experimental compartment 72 fuel rod specimens were fabricated. Each specimen contained a mixture of Triso-coated fissile particles, Biso-coated fertile particles, and Biso-coated carbon particles. All specimens were fabricated by the slug-injection technique.[2] Forty-six fuel rods were fabricated to nominal dimensions of 15.75 mm OD by 3.30 mm ID by 12.70 mm long (0.620 by 0.130 by 0.500 in.). The fuel rods used matrix type d with 28.5 wt % Asbury 6353 graphite in Ashland Oil Company A-240 petroleum pitch. Specimens were injected at 180°C (453 K) and 4.1 MPa (600 psi) and carbonized in a bed of high-fired 3000°C (3273 K)

Table I.1. Fissile Particle Test Set for OF-2

Type	Batch	Kernel Composition	Nominal Conversion (%)	Carbonization Rate (°C/min)	Coater		Annealed	Mean Dimensions,[a] μm					Mean Densities, mg/m³					Coating Rates μm/min	
					Diameter (mm)	Type		Kernel	Buff	iLTI	SiC	oLTI	Kernel[b]	Buffer	iLTI	SiC	oLTI	SiC	oLTI
1	OR-2332-H	WAR $UC_{5.43}O_{1.95}$	0	2	64	Cone	Yes	373.1	39.2	32.3	32.9	32.2	3.23	1.24[j]	1.949	3.199	2.025	0.30	4.95
2	OR-2329-H[c]	WAR $UC_{5.53}O_{1.97}$	0	2	64	Cone	Yes	371.9	23.0	40.6	31.8	30.8	3.22	0.87[c,j]	1.949	3.198	2.023	0.29	4.97
3	OR-2218-H[d]	WAR $UC_{4.58}O_{2.04}$	0	40	64	Cone	Yes	371.3	69.3	42.0	30.7	44.6	3.66	1.12[j]	1.945	3.193	1.994	0.17	5.25
4	OR-2322-H[e]	WAR $UC_{5.54}O_{1.69}$	15	2	64	Cone	Yes	379.7	49.8	35.7	32.3	39.4	3.12	1.14[j]	1.941	3.207	1.971	0.23	6.06
5	OR-2320-H	WAR $UC_{5.12}O_{1.54}$	25	2	64	Cone	Yes	374.0	43.8	36.8	34.3	38.6	3.17	1.30[j]	1.953	3.205	1.995	0.22	7.02
6	OR-2211-H[d]	WAR $UC_{4.61}O_{0.97}$	50	2	64	Cone	Yes	363.0	59.3	37.5	30.2	42.0	3.11	ND	1.948	3.202	1.997	0.16	4.94
7	OR-2207-H[d,f]	WAR $UC_{4.14}O_{0.53}$	75	2	64	Cone	Yes	366.4	62.7	38.9	31.1	42.7	3.03	1.13[j]	1.941	3.199	2.009	0.17	5.02
8	OR-2208-H[d]	WAR $UC_{3.68}O_{0.01}$	100	2	64	Cone	Yes	366.5	59.2	38.4	27.9	40.0	3.01	1.11[j]	1.947	3.199	1.997	0.15	4.71
9	OR-2121-H[d,f,g]	WAR $UC_{2.61}O_{0.16}$	100	6	64	Cone	Yes	314.3	74.6	36.1	28.4	49.2	5.28	1.10[j]	2.0	3.188	1.982	0.32	4.28
10	OR-2219-H[d]	WAR $UC_{3.68}N_{0.53}$	NA[m]	2	64	Cone	Yes	365.3	66.3	44.0	31.9	43.5	3.02	1.09[j]	1.947	3.192	1.977	0.17	5.12
11	OR-2321-H[e]	Sol-gel $Th_{0.8}U_{0.2}O_2$	NA	NA	64	Cone	Yes	361.1	83.3	37.2	34.4	41.1	9.9	1.08[j]	1.938	3.206	1.993	0.22	6.32
12	6151-00-035[i]	VSM UC_2	NA	NA	NA[l]	NA[l]		196.0	99	33	32	38	10.99	1.07	1.92	3.20	1.85	ND[l,n]	ND[l]
13	A-601	WAR $UC_{4.38}O_{0.61}$	75	2	127	Frit	No	354.2	58.8	35.4[h]	30.0	35.8	3.03	1.217[j]	1.713[k]	3.206	1.724[k]	ND	4.84
14	A-611	WAR $UC_{5.45}O_{1.75}$	15	2	127	Frit	No	366.4	47.6	36.8	30.5	35.5	3.10	1.159[j]	1.753[k]	3.204	1.696[k]	0.15	5.14
15	A-615	WAR $UC_{4.12}O_{0.47}$	75	2	127	Cone	No	354.1	51.0	30.7[h]	29.5	32.4	3.08	1.330[j]	1.857[k]	3.200	1.910[k]	ND	4.00

[a] Kernel diameter, buffer, inter LTI, SiC, and outer LTI thicknesses.
[b] Mercury gradient column measurement, uncorrected.
[c] Thin buffer.
[d] Irradiated in HRB-9 and -10.
[e] Similar batch irradiated in HRB-7, -8, -9, -10, and MET VII.
[f] Irradiated in Dragon MET VII.
[g] Irradiated in HRB-7 and -8.
[h] Buffer thickness corrected for uranium entering it during subsequent coating.
[i] Coated at General Atomic Company.
[j] Density after depositing LTI.
[k] Corrected gradient density.
[l] Top density.
[m] NA: Not applicable.
[n] ND: Not determined.

Table 1.2. Fertile Particle Test Set for OF-2

Type	Batch	Coater		Coating parameters			LTI deposition		Dimensions,[a] μm			Density,[b] g/cm³		Anneal
		Type	Diameter (mm)	Gas	Concentration (%)	Diluent (%)	Temperature (°C)	Rate (μm/min)	Kernel	Buffer	LTI	Uncorrected	Corrected	
A	OR-2266-HT[c]	Cone	64	MAPP[d]	100		1275	14.1	506	94.8	91.3	2.02		Yes
B	OR-2265-HT[c]	Cone	64	MAPP	100		1325	15.7	508	96.1	94.2	1.95		Yes
C	OR-2262-HT[c]	Cone	64	MAPP	50	50 Ar	1275	6.5	507	98.0	85.1	2.01		Yes
D	OR-2261-HT[c]	Cone	64	MAPP	50	50 Ar	1325	7.4	506	95.8	88.9	1.89		Yes
E	OR-2264-HT[c]	Cone	64	MAPP	25	75 Ar	1275	3.2	507	96.5	91.6	1.99		Yes
F	OR-2263-HT	Cone	64	MAPP	25	75 Ar	1325	3.6	506	92.8	90.5	1.84		Yes
G	J-488[e,f]	Frit	127	C_3H_6	50	50 He	1375	7.4	497.9	82.7	80.7	1.98	1.87	Yes
H	J-489[e]	Frit	127	C_3H_6	50	50 He	1375	5.8	499.0	81.4	77.7	1.90	1.79	Yes
I	J-490[e]	Frit	127	C_3H_6	100		1375	6.2	495.9	80.2	74.7	1.99	1.86	Yes
J	J-491[e]	Frit	127	C_3H_6	100		1375	9.3	497.1	79.5	77.5	2.00	1.86	Yes
K	J-262[g]	Cone	127	C_3H_6	100		1350	8.4	497	84.0	86.1	2.01		Yes
L	OR-1849-HT	Cone	25	C_3H_6	75	25 He	1400[h]	21.5	508	79.4	74.7	1.94		Yes
M	J-481[i]	Frit	127	C_3H_6	50	50 He	1375	7.4	497.9	82.7	80.7	1.94	1.84	No
N	J-483	Frit	127	C_3H_6	100		1375	6.2	495.9	80.2	74.7	1.96	1.83	No
O	J-482	Frit	127	C_3H_6	50	50 He	1375	5.8	499.0	81.4	77.7	1.88	1.78	No
P	J-487	Frit	127	C_3H_6	100		1375	9.3	497.1	79.5	77.5	1.95	1.81	No

[a] Mean dimensions of kernel diameter, buffer, and LTI thickness.

[b] Mercury gradient column measurement.

[c] Irradiated in HT-30.

[d] MAPP gas is marketed by AIRCO, Inc., and consists primarily of methylacetylene and propadiene with alkanes as stabilizers.

[e] Batch J-488 rupture load was 26.11 N (5.92 lb), strong particle in matrix interaction experiment.

[f] Irradiated in HRB-7 and -8, OF-1.

[g] Temperature measured at different point in furance; actual bed temperature approximately 1325°C.

[h] Batch J-481 rupture load was 22.42 N (5.04 lb), weak particle in matrix interaction experiment.

Table 1.3. Matrix Test Set for OF-2

Type	Pitch		Additive	Filler		Average coke yield (%)	Carbonization technique
	Wt %	Type		Wt %	Type		
a	71	A-240	None	29	Asbury 6353	18.3	Al_2O_3
b	71	A-240	None	29	Asbury 6353	37.3	In-tube
c		GA	Proprietary			25.7-30.0[a]	In-block or in-tube[b]
d	71.5	A-240	None	28.5	Asbury 6353	15.6	Graphite flour

[a]The first number is the mean of rods carbonized in Magazine C and the second number is the average for the rods in Magazines A and B.

[b]Fuel rods in Magazines A and B were carbonized in-tube, while fuel rods in Magazine C were carbonized in-block.

graphite flour at a heating rate of 1 K/min. The remaining 26 fuel specimens were fabricated to nominal dimensions of 15.7 mm diam by 25.4 mm long (0.620 by 1.00 in.) with matrix types a, b, and c. Matrix types a and b were the same types as in the 12.70-mm-long (0.500-in.) specimens; matrix type c is GA's proprietary matrix. Specimens were injected at 180°C (453 K) and 5.5 MPa (800 psi), except for those containing unannealed fertile batches M and N, which were injected at 4.1 MPa (600 psi). Eight fuel rods with matrix type a were carbonized in a bed of Al_2O_3 at a heating rate of 6 K/min, producing a coke yield of 18.3%. Eight rods with matrix type b were carbonized in a graphite tube (to simulate in-block carbonization) at a heating rate of 2 K/min, producing a coke yield of 37.1%. And eight fuel rods with matrix type c were carbonized in a graphite tube at a heating rate of 11.5 K/min, producing a coke yield of 29.8%. All specimens were subjected to a final heat treatment at 1800°C (2073 K) in argon for 30 min. For each of the fuel rods in specimen holders A and B (Figs. 1.2 and 1.3), Tables 1.4 and 1.5 describe the fissile and fertile particle types and matrix types used, along with the total weights of ^{235}U and ^{232}Th contained in each rod.

For the lower experimental compartment 16 fuel rod specimens were fabricated. Each specimen contained a mixture of Triso-coated fissile particles, Biso-coated fertile particles, Triso- and Biso-coated carbon particles, and H-451 shim particles. The rods in position 4, however, contained no inert particles. To keep dimensional changes of the fuel rods uniform in this compartment, the ratio of Biso- to Triso-coated

Table 1.4. Fuel Rods for OF-2 Irradiation Capsule, Holder A

Specimen location[a]	Particle types		Matrix type	Pitch-coke yield (%)	Loading, g	
	Fissile	Fertile			^{235}U	^{232}Th
		25.4-mm-long (1.00-in.) Specimens				
1-1	14	M	b	39.97	0.2380	3.980
-2	13	M	a	16.99	0.2380	3.980
-3	14	G	a	16.16	0.1350	2.610
-4	14	G	c	31.09	0.1350	2.610
-5	13	G	b	36.23	0.1060	2.190
-6	13	M	c	30.86	0.1060	2.190
2-1	14	M	a	18.2	0.2380	3.980
-2	14	G	b	37.65	0.2380	3.980
-3	13	M	b	37.62	0.1350	2.610
-4	13	G	c	30.88	0.1350	2.610
-5	14	M	c	29.20	0.1060	2.190
-6	13	G	a	17.38	0.1060	2.190
		12.7-mm-long (0.50-in.) Specimens				
3-1	12	M	d	18.4	0.1190	1.990
-2	2	I	d	18.1	0.1190	1.990
-3	11	H	d	17.0	0.1190	1.990
-4	2	G	d	19.6	0.1190	1.990
-5	4	K	d	24.7	0.0675	1.805
-6	6	J	d	19.2	0.0675	1.805
-7	8	G	d	15.2	0.0675	1.805
-8	10	H	d	14.6	0.0675	1.805
-9	4	I	d	16.5	0.0530	1.095
-10	2	C	d	14.1	0.0530	1.095
-11	8	A	d	15.7	0.0530	1.095
-12	12	B	d	14.7	0.0530	1.095
4-1	9	G	d	N.D.[b]	0.1190	1.990
-2	1	H	d	N.D.	0.1190	1.990
-3	9	I	d	N.D.	0.1190	1.990
-4	1	J	d	13.5	0.1190	1.990
-5	3	A	d	15.2	0.0675	1.805
-6	5	B	d	14.8	0.0675	1.805
-7	7	C	d	34.7	0.0675	1.805
-8	11	D	d	10.8	0.0675	1.805
-9	3	E	d	12.6	0.0530	1.095
-10	1	F	d	34.4	0.0530	1.095
-11	7	A	d	13.9	0.0530	1.095
-12	LASL	LASL	LASL		0.0530	1.095

[a] Hole number followed by position from top.

[b] N.D.: Not determined.

Table 1.5. Fuel Rods for OF-2 Irradiation Capsule, Holder B

Specimen location[a]	Particle types		Matrix type	Pitch-coke yield (%)	Loading, g	
	Fissile	Fertile			^{235}U	^{232}Th
		25.4-mm-long (1.00-in.) Specimens				
1-1	13	M	b	38.56	0.0814	1.530
-2	13	G	a	17.89	0.0814	1.530
-3	13	G	c	30.62	0.0690	1.260
-4	14	M	a	20.08	0.0690	1.260
-5	14	G	b	37.06	0.0690	1.260
-6	14	M	c	27.75	0.0690	1.260
2-1	13	G	b	36.36	0.0814	1.530
-2	14	M	b	36.82	0.0814	1.530
-3	14	G	a	18.89	0.0690	1.260
-4	13	M	a	20.78	0.0690	1.260
-5	13	M	c	29.63	0.0690	1.260
-6	14	G	c	29.79	0.0690	1.260
		12.7-mm-long (0.50-in.) Specimens				
3-1	12	A	d	15.7	0.0407	0.765
-2	2	B	d	17.4	0.0407	0.765
-3	4	C	d	15.8	0.0407	0.765
-4	6	D	d	15.4	0.0407	0.765
-5	8	E	d	N.D.	0.0345	0.630
-6	10	F	d	14.6	0.0345	0.630
-7	2	L	d	14.1	0.0345	0.630
-8	4	G	d	12.0	0.0345	0.630
-9	3	H	d	16.4	0.0345	0.630
-10	8	I	d	15.8	0.0345	0.630
-11	2	J	d	15.5	0.0345	0.630
-12	4	K	d	15.2	0.0345	0.630
4-1	11	G	d	N.D.	0.0407	0.765
-2	1	H	d	N.D.	0.0407	0.765
-3	3	I	d	11.5	0.0407	0.765
-4	5	J	d	16.4	0.0407	0.765
-5	7	A	d	15.5	0.0345	0.630
-6	9	B	d	15.5	0.0345	0.630
-7	1	C	d	16.0	0.0345	0.630
-8	3	D	d	15.1	0.0345	0.630
-9	5	E	d	15.1	0.0345	0.630
-10	7	F	d	15.6	0.0345	0.630
-11	1	A	d	15.7	0.0345	0.630
-12	LASL	LASL	LASL		0.0345	0.630

[a]Hole number followed by position from top.

particles was kept constant for each loading. Each specimen contained 20 vol % shim particles. Specimens were fabricated to nominal dimensions of 15.75 mm diam by 50.8 mm long (0.620 by 2.00 in.) by the slug-injection technique and used matrix type c. Specimens were injected at 180°C (453 K) and 5.5 MPa (800 psi), except that rods containing unannealed fertile particles types M and N were injected at 4.1 MPa (600 psi). Placement of fuel rod specimens in cell 1 (Fig. 1.4) was based on a statistical experimental design to minimize interaction effects. Rods were carbonized by the reference in-block technique with a heating rate of 11.5 K/min, producing an average coke yield of 25.7%. All fuel rods were subjected to a final heat treatment at 1800°C (2073 K) in argon for 30 min. Table 1.6 describes the fissile and fertile particle types and the total weights of ^{235}U and ^{232}Th used in each fuel rod of specimen holder C.

Table 1.6. Fuel Rods for OF-2 Irradiation Capsule, Holder C[a,b]

Specimen Location[c]	Particle types		Loading, g	
	Fissile	Fertile	^{235}U	^{232}Th
1-1	13	N	0.1338	2.780
-2	13	I	0.1338	2.780
-3	14	G	0.1590	3.460
-4	13	O	0.3640	7.900
2-1	15	O	0.1338	2.780
-2	13	G	0.1338	2.780
-3	15	H	0.1590	3.460
-4	15	P	0.3640	7.900
3-1	14	M	0.1338	2.780
-2	14	P	0.1338	2.780
-3	13	J	0.1590	3.460
-4	14	M	0.3640	7.900
4-1	15	H	0.1338	2.780
-2	14	J	0.1338	2.780
-3	13	I	0.1590	3.460
-4	13	N	0.3640	7.900

[a] All specimens were 50.8 mm (2.00 in.) long, fabricated with type c matrix.

[b] Since test specimens were not removed from the magazine, actual coke yields were not available. However, typical sample specimens were processed in another holder at the same time as the actual test specimens. Coke yield data from the sample specimens are: mean coke yield = 25.7%; high = 29.5%; low = 23.6%; number of samples = 16, standard deviation = 1.56; 95% confidence interval = 25.7 ± 4.53%.

[c] Hole number followed by position from top.

2. CAPSULE IRRADIATION

Capsule OF-2 began irradiation in the E-7 position of the ORR core on June 21, 1975, and terminated irradiation on Aug. 1, 1976 following 8440 hr at reactor full power (30 MW).

During initial operation the total reaction rates were higher in the ends of the capsule because of a change in the neutron spectrum. The result was an increase of approximately 20% in heat generation rate for fuel rods located at the top of Magazine A and at the bottom of Magazine C, that is, rods at the ends of the capsule. The major temperature changes were for fuel rods in the top 50 mm (2 in.) in Magazine A, which operated at approximately 100 K above the design temperature of 1150°C (1423 K) and for fuel rods at the bottom of Magazine C, where the maximum temperature was 1350°C (1623 K). Details of these results are presented in ref. 3.

A complete listing of fission gas release-to-birth rate ratios (R/B) for cells 1 and 2 is presented in Fig. 2.1. Cell 1 was occupied by Magazine C, while Magazines A and B were in cell 2.

The R/B measurements can be used for qualitative evaluation of fuel performance during irradiation. At the beginning of irradiation, contamination- and fabrication-induced fuel failures, but not irradiation-induced fuel failures presumably cause the fission gas release.

In cell 1 containing just Magazine C, the R/B remained relatively constant (e.g., ^{85m}Kr was in the range of $2\text{-}3 \times 10^{-5}$) until approximately 4000 hours. At that time the R/B began to increase and rose to where the ^{85m}Kr was in the range 1×10^{-4}. Cell 1 contained only three types of fissile particles and eight types of fertile particles. All of these particle types were contained in cell 2 under similar conditions (approximately half the test space was comprised of these particle types), with the exception of fissile particle batch A-615. However the R/B measurements in Cell 2 decreased throughout the irradiation. Thus, we decided that the fissile batch A-615 caused the increase in R/B. As the metallographic section will present later, batch A-615 had very anisotropic pyrocarbon coatings, which failed during irradiation.

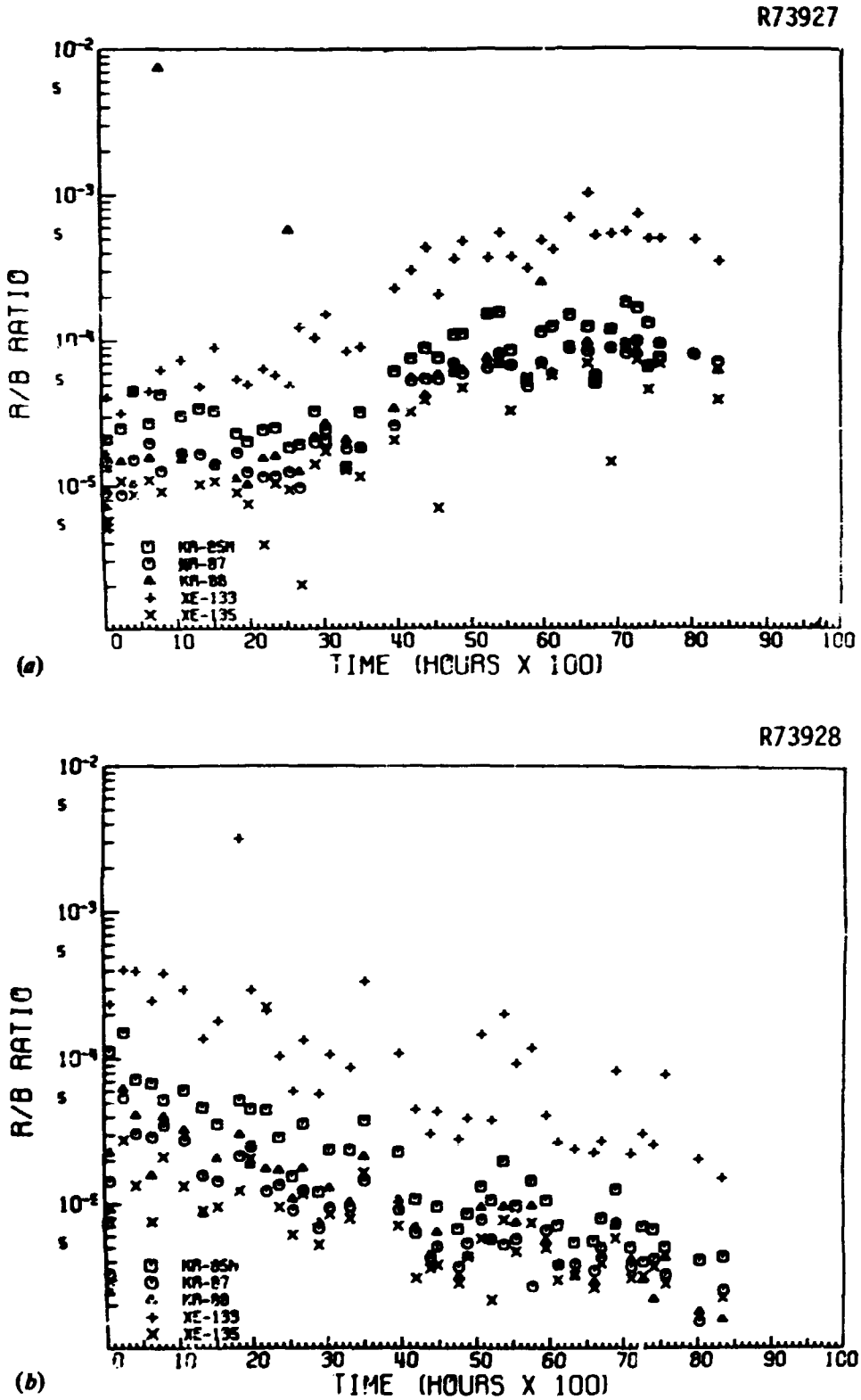

Fig. 2.1. Fission Gas Release-to-Birth Rate Ratios for OF-2 During Irradiation. (a) Cell 1. (b) Cell 2.

We note that at the beginning of irradiation the R/B measurements in Cell 2 were higher than in Cell 1: ^{85m}Kr was 1×10^{-4}. During the metallographic examination the fuel was in generally good condition. However, faulty fabrication caused some fertile particles to fail. These fabrication failures may have produced the high initial R/B in Cell 2.

Preliminary estimates of fast-neutron fluence and fuel burnup have been made and are presented in Figs. 2.2 through 2.4. We emphasize that these are preliminary values that will be revised when the dosimetry analysis is completed.[6]

R73931

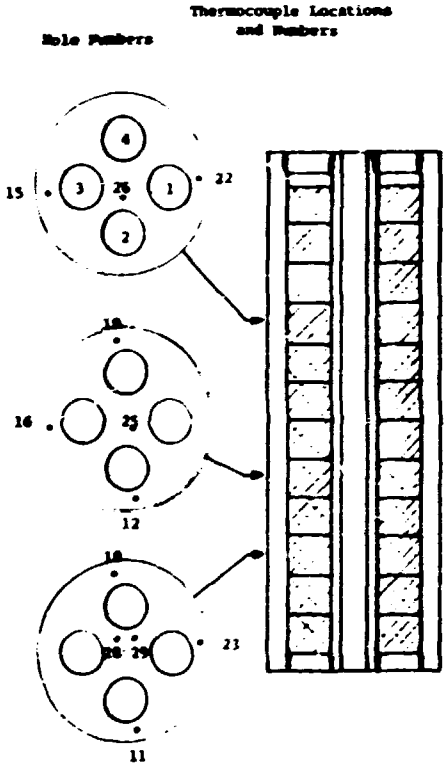

Distance Above MHP (in.)	Estimated Average Fast Fluence (E >0.18 MeV) (Neutrons/cm^2) × 10^{21}	Estimated Average Burnup (% FIMA) ^{235}U	^{238}U	^{232}Th
10.50	1.94	50.0	2.29	0.59
10.00	2.25	54.1	2.83	0.74
9.50	2.55	58.3	3.48	0.94
9.00	2.83	61.7	4.14	1.13
8.50	3.19	59.9	4.20	1.14
8.00	3.57	63.0	4.89	1.35
7.50	3.92	65.2	5.46	1.53
7.00	4.24	67.1	6.01	1.71
6.50	4.56	69.0	6.63	1.91
6.00	4.88	70.4	7.15	2.08
5.50	5.23	71.2	7.74	2.28
5.00	5.58	73.0	8.31	2.48

Fig. 2.2. Preliminary Estimates of Neutron Fluence and Fuel Burnup in Specimen Holder A of Capsule OF-2.

R73929

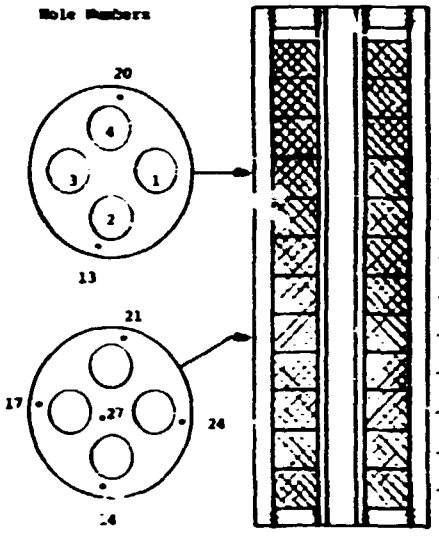

Distance Above MHP (in.)	Estimated Average Fast Fluence (E >0.18 MeV) (Neutrons/cm^2) × 10^{21}	Estimated Average Burnup (% FIMA) ^{235}U	^{238}U	^{232}Th
3.625	6.38	75.5	9.69	2.96
3.125	6.64	76.1	10.1	3.13
2.625	6.86	76.7	10.6	3.29
2.125	7.11	77.3	11.0	3.44
1.625	7.31	77.8	11.4	3.60
1.125	7.56	78.1	11.7	3.71
0.625	7.75	78.4	12.1	3.84
0.125	7.92	78.7	12.4	3.94
-0.375	8.01	79.0	12.7	4.07
-0.875	8.20	79.2	12.9	4.15
-1.375	8.26	79.4	13.1	4.22
-1.875	8.36	79.5	13.2	4.28

Fig. 2.3. Preliminary Estimates of Neutron Fluence and Fuel Burnup in Specimen Holder B of Capsule OF-2.

R73930

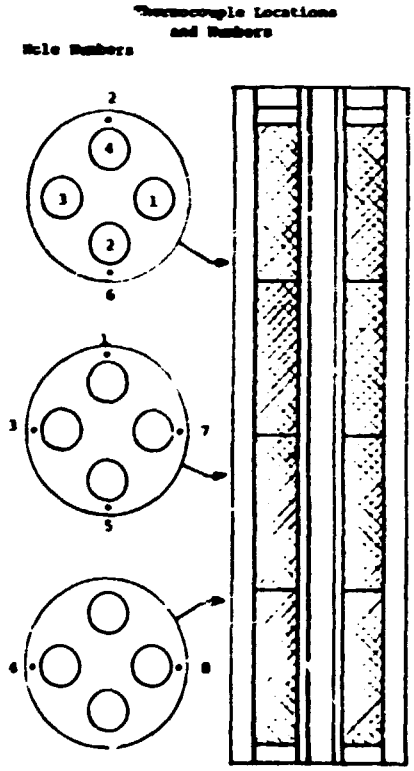

Distance Above MHP (in.)	Estimated Average Fast Fluence (E >0.18 MeV) (Neutrons/cm^2) × 10^{21}	Estimated Average Burnup (% FIMA) ^{235}U	^{238}U	^{232}Th
-4.875	8.91	79.6	13.4	4.34
-6.875	8.50	79.0	12.7	4.07
-8.8[illegible]	7.62	77.5	11.2	3.50
-10.875	5.86	75.9	9.15	2.77

Fig. 2.4. Preliminary Estimates of Neutron Fluence and Fuel Burnup in Specimen Holder C of Capsule OF-2.

3. POSTIRRADIATION EXAMINATION

3.1 Disassembly

The OF-2 capsule was sectioned and the end bulkheads and accompanying thermocouples were removed. All three graphite magazines were retrieved in excellent condition. In addition the fibrous carbon insulators used at the ends of the magazines were removed.

The primary and secondary containments were slit open to expose their inner surfaces. As shown in Fig. 3.1, the secondary containment had a dark sooty film deposited on the inner surface, in contrast to the primary containment, which remained shiny. The inner surface of both cells 1 and 2 were equally sooty in appearance.

R72838

Fig. 3.1. Inner (Bottom) and Outer (Top) Containments. Note the sooty appearance of the inner containment as compared with the outer containment.

All three magazines were opened easily and the spines and fuel rods removed easily. This included the fuel rods carbonized in-block and contained in Magazine C. In previous tests,[2,5] rods carbonized in-block had been very difficult to remove. We assumed that a bond had been established between the rods and the graphite to make removal difficult.

However, in those earlier tests the pitch-coke yield was always more than 40%, whereas Magazine C had a pitch-coke yield of 25.7%. This difference may have resulted in a weaker bond between the fuel rods and the graphite in Magazine C than in the previous tests and it may explain the ease of their removal.

3.2 Gamma Scanning

Gross gamma scans (0.55–0.75 MeV) were made along the lengths of each magazine and indicated some inhomogeneity in the fissile and fertile fuel particles in the fuel rod. The burnup profiles along the magazines were fairly constant except for the bottom portion of Magazine C. Fuel rods located at this position had been loaded with much more fuel to compensate for the lower neutron reaction rates expected at this axial position of the ORR core. This problem is discussed in detail in ref. 3. The gamma scans showed that the loadings were too high, as the burnup profiles were much higher than those of neighboring fuel rods.

Additional gross gamma scans (0.55–0.75 MeV) were made of the fuel rod stacks after their removal from the graphite magazines (Figs. 3.2–3.4). These scans resembled those made of the magazines before the fuel rods were removed. Inhomogeneity in the fissile and fertile fuel particles is shown by the change in gamma activity along the length of the fuel rods. Of particular interest were the scans made of the fuel rods from Magazine C. Ten activity peaks, and hence, ten valleys were associated with each fuel rod; they resulted from the use of a 20-way splitter-blender during fuel rod fabrication. This inhomogeneity causes the temperature profile to differ by ±2 K from the homogeneous situation.[7]

In conjunction with the gross gamma scans, gamma spectra to identify particular isotopes were acquired on each fuel rod. To obtain a representative spectrum, each rod was moved very slowly - less than 2.5 mm/min (0.1 in./min) — past a 0.51- by 25- by 425-mm (20-mil by 1.0-in. by 17-in.) collimator. The spectra were always taken from the middle portion of the fuel rod to minimize any edge effects. The profiles of the following isotopes were determined along each fuel stack: ^{95}Zr, ^{103}Ru, ^{125m}Te, ^{134}Cs, ^{137}Cs, ^{141}Ce, and ^{144}Ce (see Appendix).

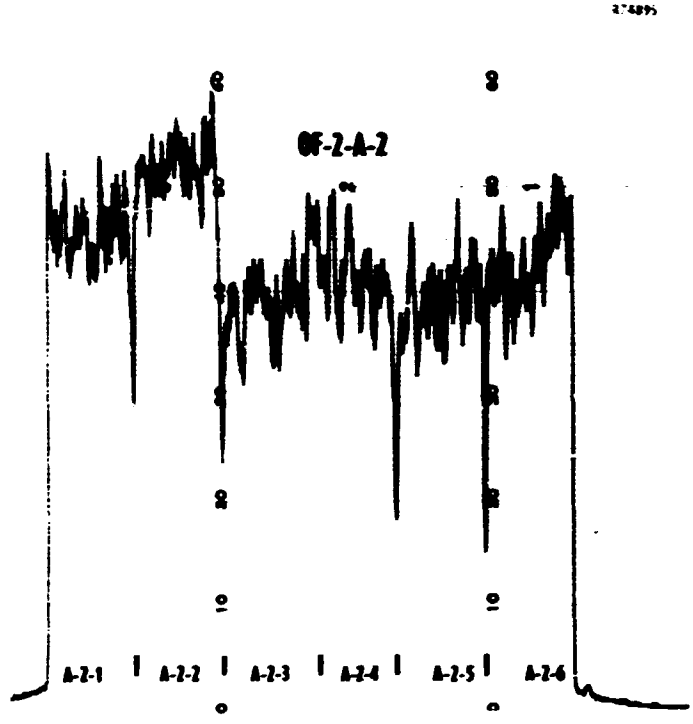

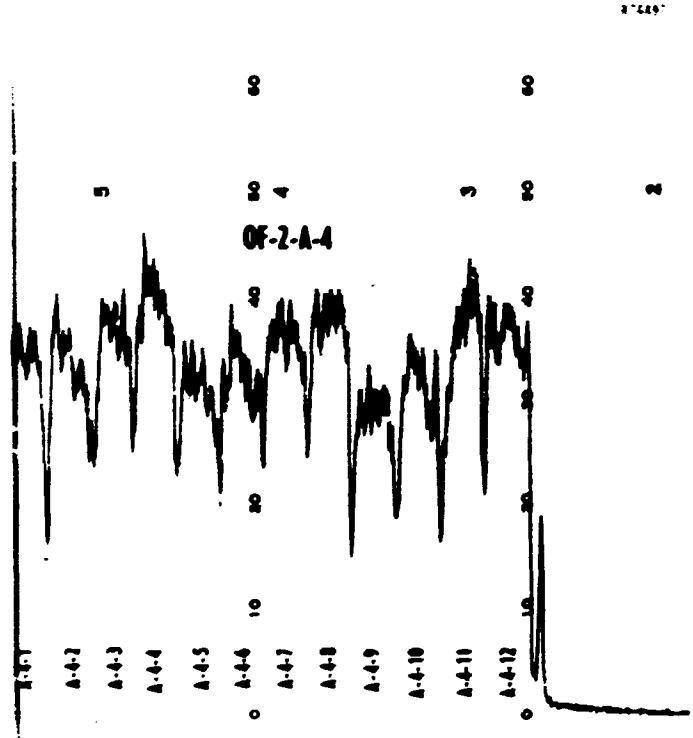

Rods After Their Removal from Graphite
. (d) Stack A-4. Fuel rod 1 is on the
ounts/min. A 0.51- by 1090-mm

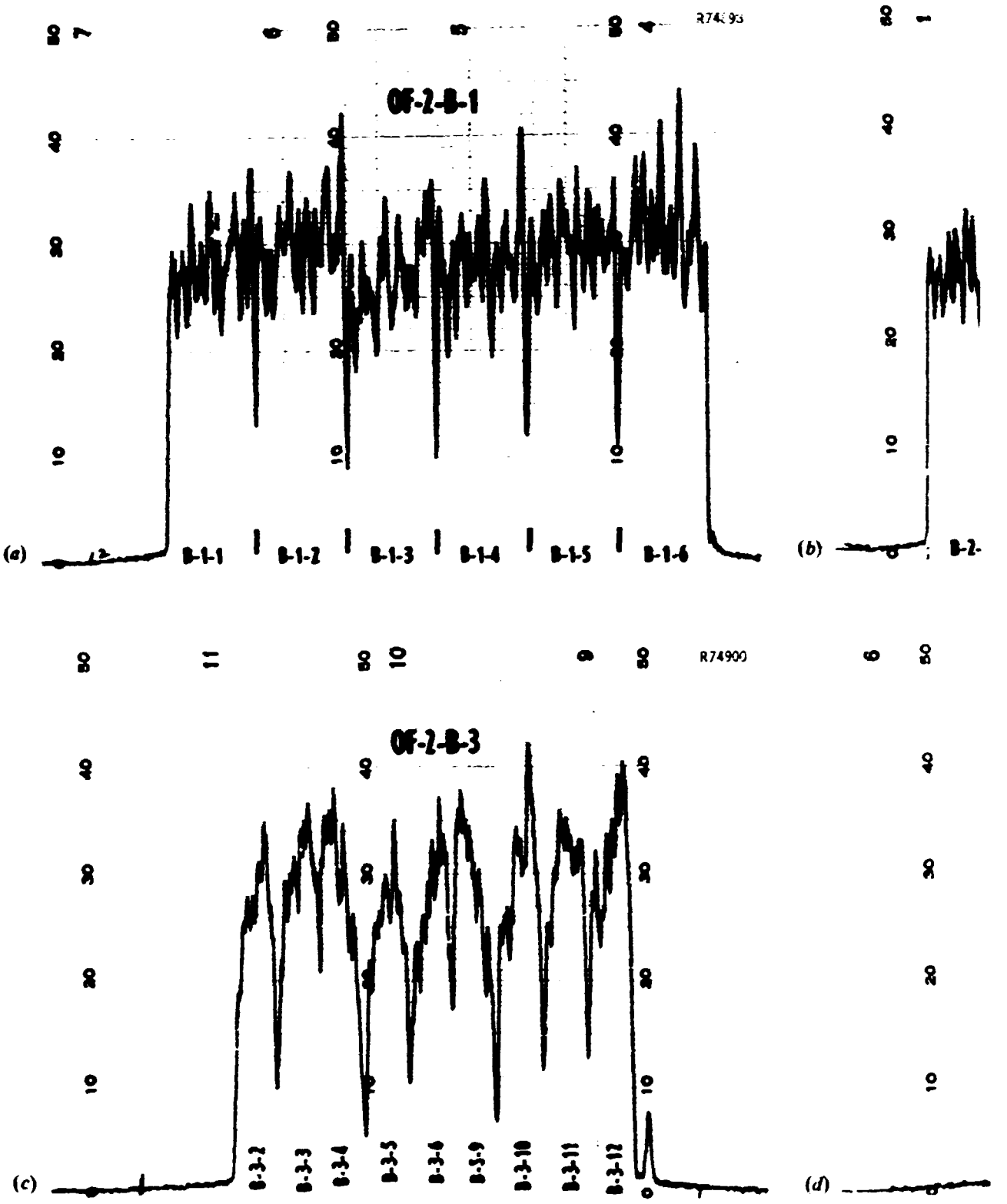

Fig. 3.3. Gross Gamma Scans (0.55–0.75 MeV) of Fuel Rods I Magazine B. (a) Stack B-1. (b) Stack B-2. (c) Stack B-3. (d) left. Each division corresponds to a count rate of 1000 counts/ (0.02- by 43-in.) collimator was used. In stack B-3 fuel rods F In stack B-4 fuel rods B-4-1, B-4-2, and B-4-11 are missing.

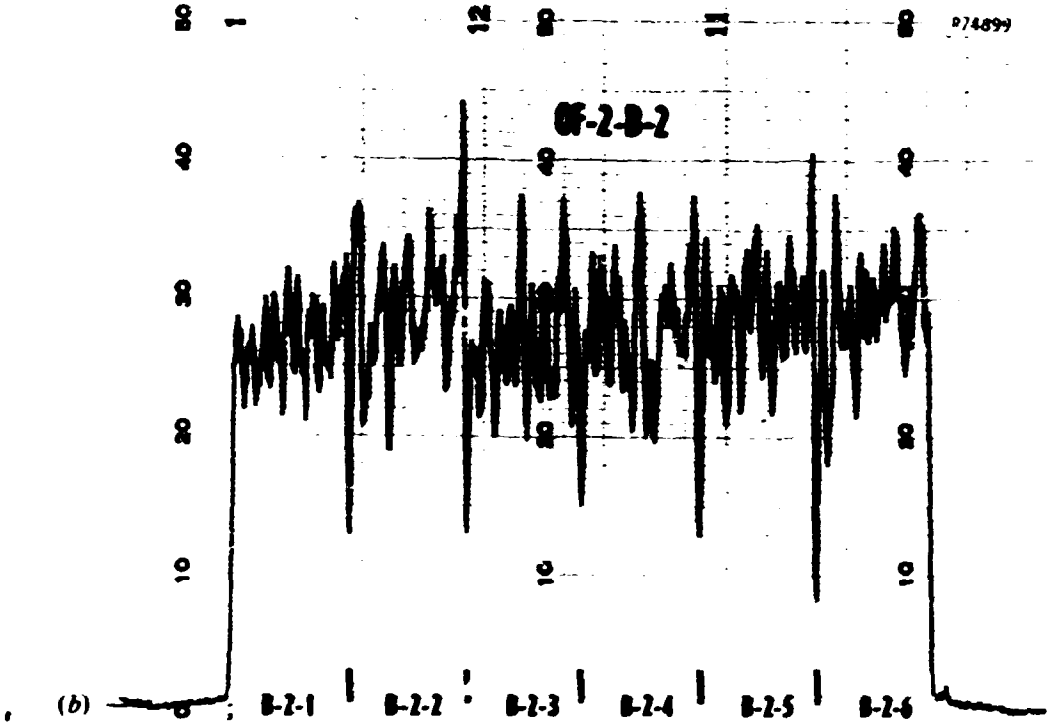

(b)

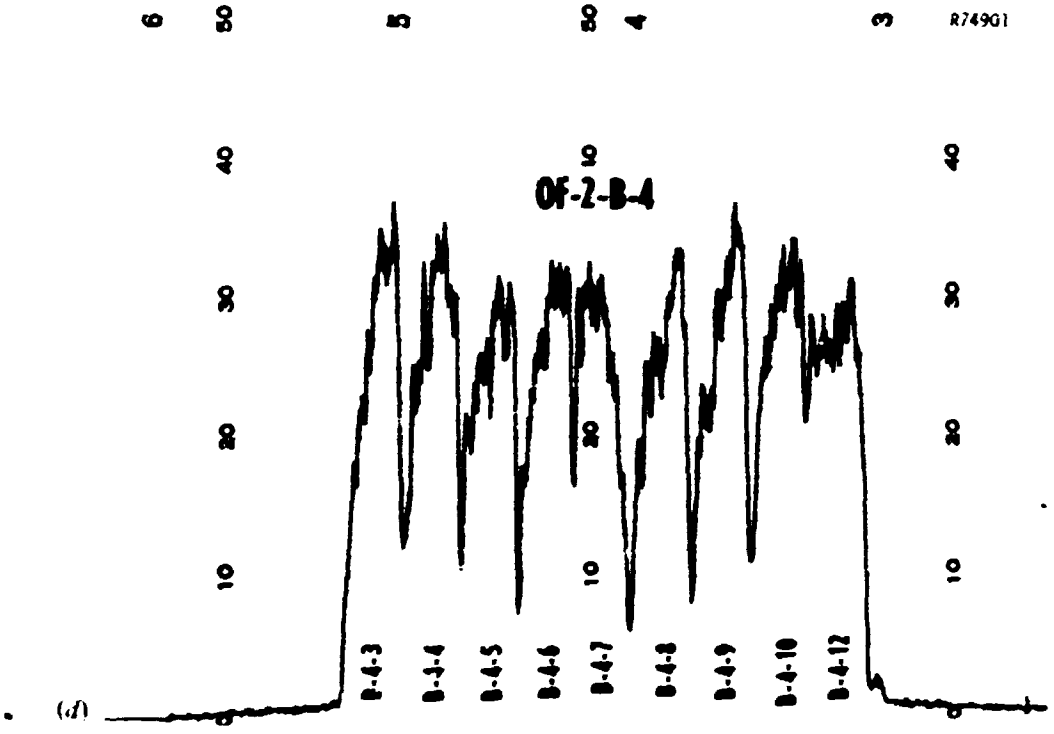

(d)

MeV) of Fuel Rods After Their Removal from Graphite
(c) Stack B-3. (d) Stack B-4. Fuel rod 1 is on the
rate of 1000 counts/min. A 0.51- by 1090-mm
tack B-3 fuel rods B-3-1, B-3-7, and B-3-8 are missing.
-11 are missing.

BLANK PAGE

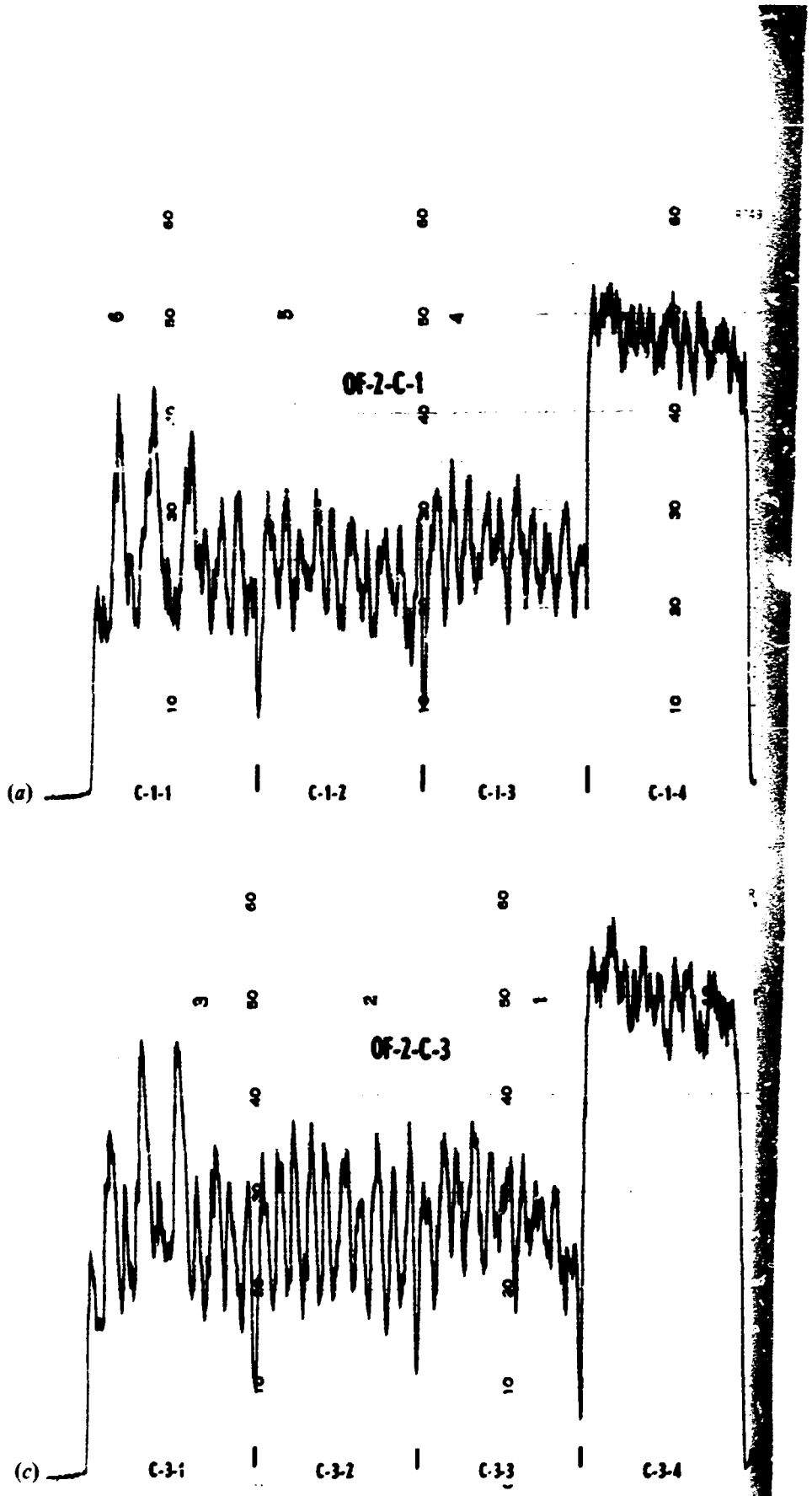

Fig. 3.4. Gross Gamma Scans (0.55–0.75 MeV
(a) Stack C-1. (b) Stack C-2. (c) Stack C-3.
corresponds to a count rate of 1000 counts/min.
used.

BLANK PAGE

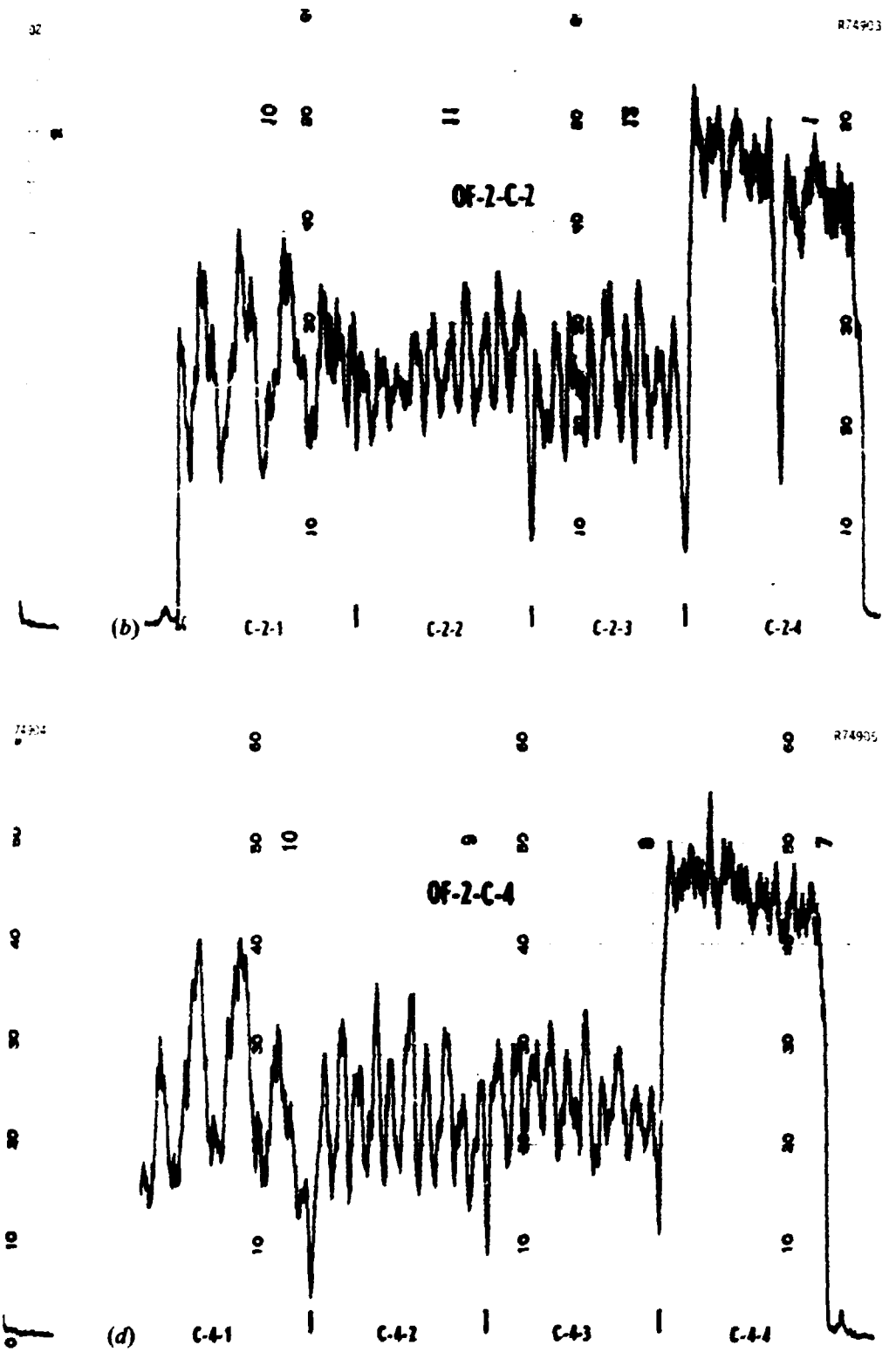

) of Fuel Rods After Removal from Graphite Magazine C.
(d) Stack C-4. Fuel rod 1 is on the left. Each division
A 0.51- by 1090-mm (0.02- by 43-in.) collimator was

After removal of the fuel rods, spectral gamma scans were made along the length of the empty graphite magazines, as well. The collimator used was 6.3 by 25 by 425 mm (0.25 by 1.0 by 17 in.) long. The following isotopes were identified in the graphite: ^{110m}Ag, ^{134}Cs, ^{137}Cs, ^{144}Ce. The profiles for each magazine are given in Figs. 3.5 through 3.7. As shown, the gamma activity in Magazine A is relatively constant with an increase near the bottom. On the other hand, the profile from Magazine B shows an increase in cesium activity from top to bottom, while silver activity remains fairly constant. Magazine C shows a similar increase in cesium activity from top to bottom, with very high activity at the bottom of hole 2. These high activities at the bottom of Magazine C indicate a high failure fraction of particles in that area. Remember, the heavy-metal loading at this position was too high, resulting in a relatively high power density. Interestingly, ^{144}Ce was observed at the bottom of each magazine and nowhere else. We have found no plausible explanation for this. The silver activity in the graphite magazines generally followed the burnup profile across the capsule. This indicates that the release of silver from the particles and fuel rods — not observed in the fuel rod scans — was constant and the same for all particle types.

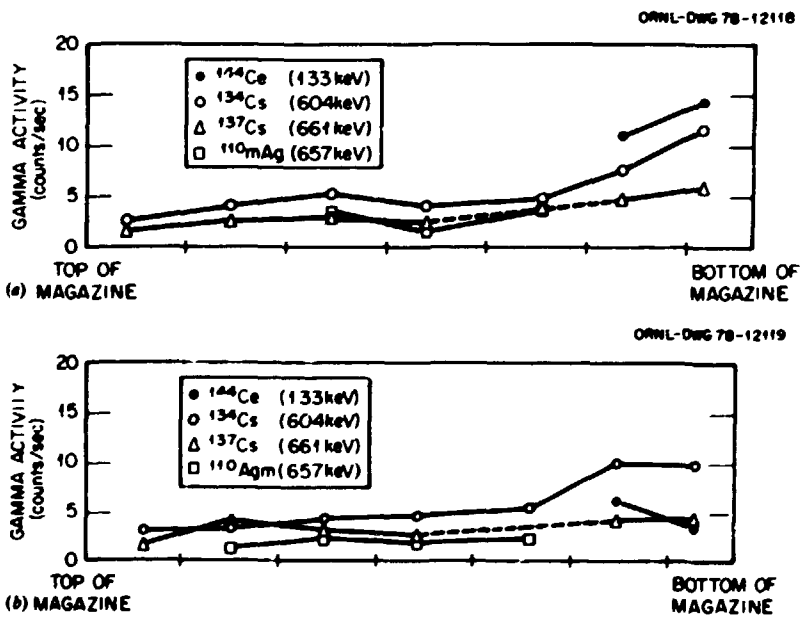

Fig. 3.5. Gamma Activity of Empty Graphite Magazine A from Capsule OF-2. (a) Along holes 1 and 3. (b) Along holes 2 and 4.

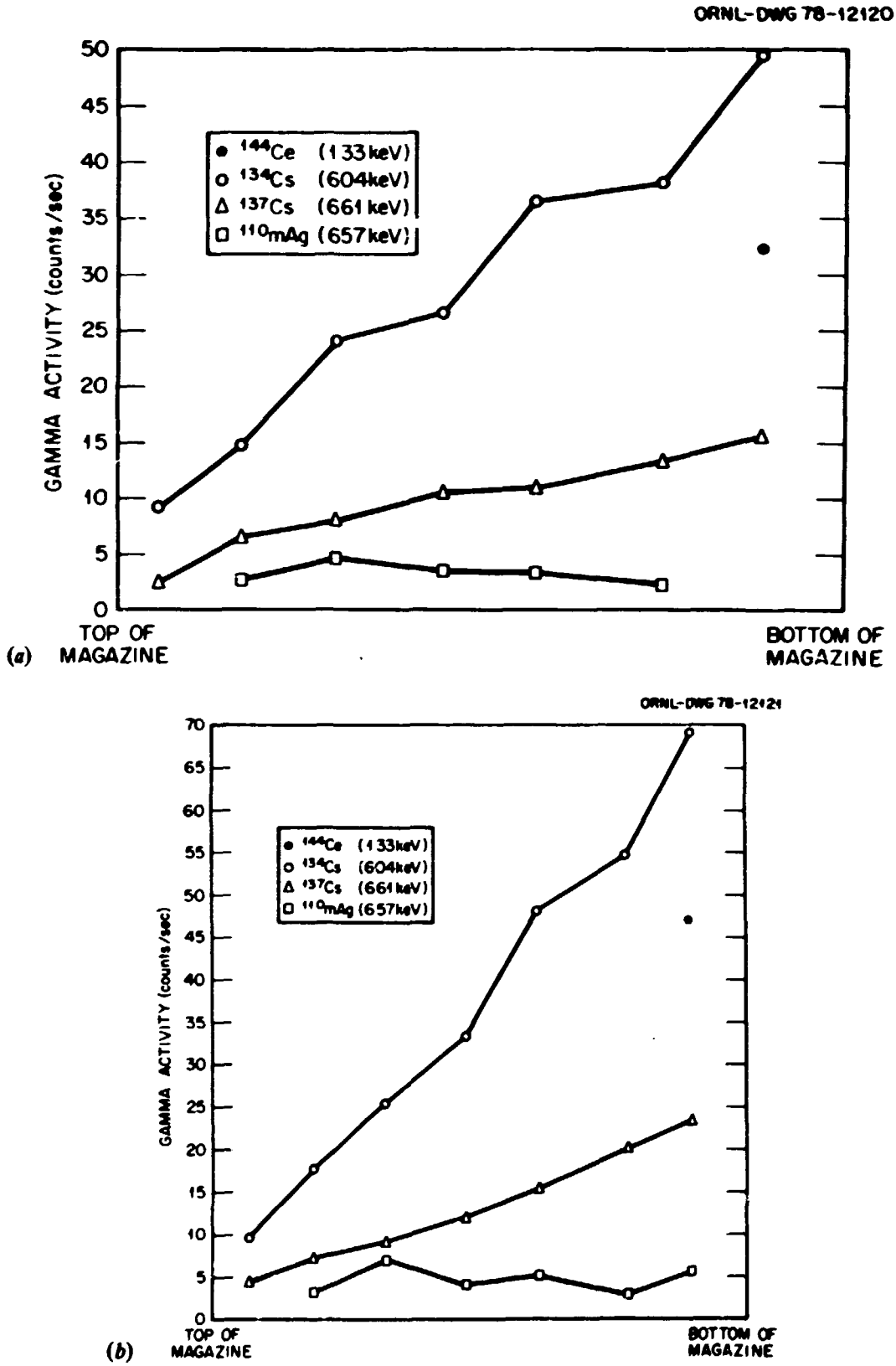

Fig. 3.6. Gamma Activity of Empty Graphite Magazine B from Capsule OF-2. (a) Along holes 1 and 3. (b) Along holes 2 and 4.

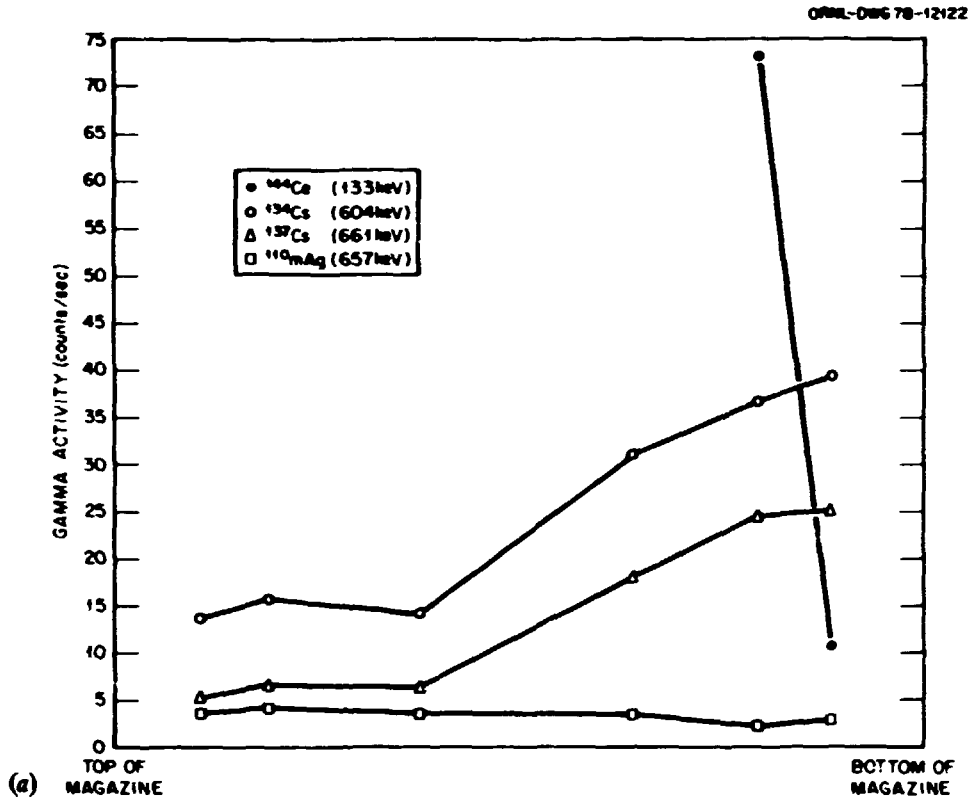

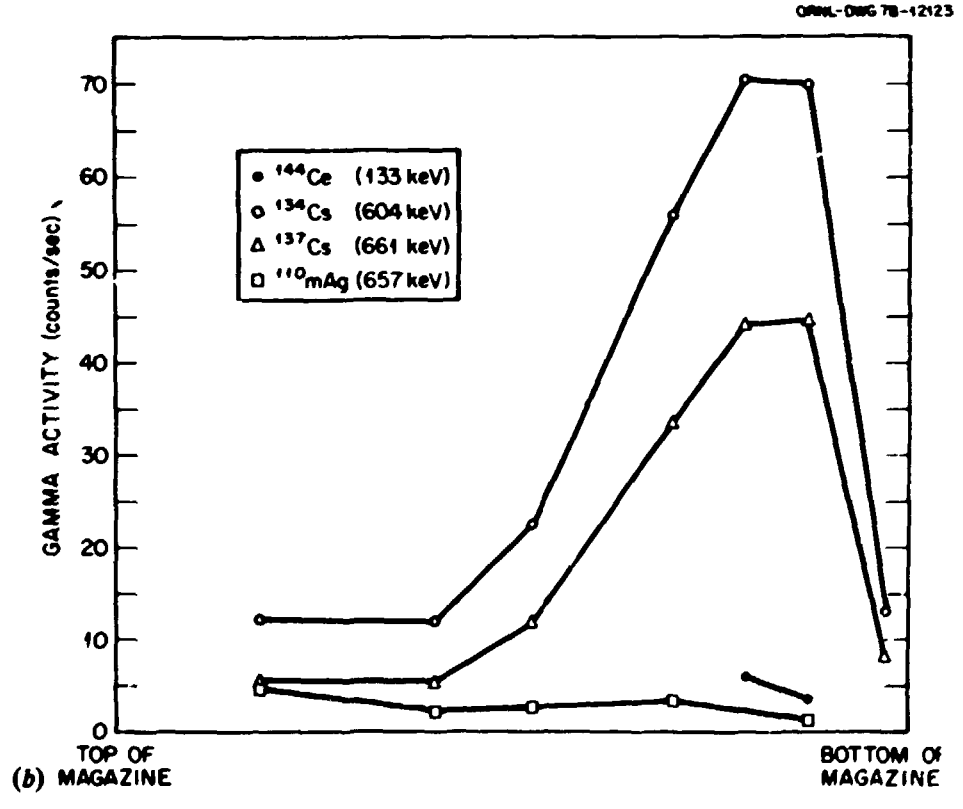

Fig. 3.7. Gamma Activity of Empty Graphite Magazine C from Capsule OF-2. (a) Along holes 1 and 3. (b) Along holes 2 and 4.

3.3 Visual Examination

After the fuel rods were removed from the magazines they were visually examined. The results are given below:

Magazine A. Fuel rods from this magazine were in good condition, with only slight debonding. Fuel holes 1 and 2 each contained six 25-mm-long (1-in.) rods, and fuel holes 3 and 4 each contained twelve 13-mm-long (0.5-in.) rods. Visual inspection of the surface of each of the fuel rods indicated that in ten rods, from 1 to 12 failed particles were visible. The remaining 26 rods indicated no visible failures on the fuel rod surface.

Magazine B. Fuel rods from holes 1 and 2 were in good condition, with only slight debonding at their edges. Fuel rods from holes 3 and 4 were in much worse condition. Eight fuel rods had completely debonded and had no apparent structure. These rods were located in positions B-3-1, -2, -6, -7, -8, B-4-1, -2, and -11. Because the matrix used to fabricate the rods from holes 3 and 4 was characterized by low coke yields (12-17.4%), the resulting fuel rods were weak. Thus, we can conclude that generally, during irradiation, the integrity of fuel rods with coke yields lower than 18% is poor. Therefore, the use of such rods should be discouraged. The eight completely debonded rods were not visually examined for particle failures. From one to twelve failed particles were seen on the surface of eight of the remaining 28 fuel rods, but none were seen on the other 20 fuel rods.

Magazine C. The fuel rods from this magazine were in good condition with only moderate debonding of a few rods. Visual examination at high magnification revealed many outer pyrocarbon coating failures on the surface of several fuel rods. Failures were most prevalent on the surface of rods containing fissile particle batch A-615 (Fig. 3.8). Those fuel rods with high loadings at the bottom of the magazine also had many OPyC failures on their surfaces.

Fig. 3.8. Surface of Fuel Rod C-2-1 Showing Numerous oLTI Failures. The arrow points to one of many outer pyrocarbon coating failures.

3.4 Dimensional Analysis

We inspected each fuel rod by measuring its diameter at the top, midlength, and bottom at 0 and 90° with a dial gage comparator and V-block assembly. A maximum length was also determined. The results are given in Table 3.1. The diametral shrinkage as a function of fast-neutron fluence ($E > 0.18$ MeV) is shown in Fig. 3.9. The fuel rods from Magazines A and B exhibited shrinkage up to a fast fluence of 7×10^{25} n/m^2 ($E > 0.18$ MeV), at which point a minimum was reached and the rods began to swell. The rods carbonized in Robinson graphite shrank more than did those rods carbonized in-tube or in packed Al_2O_3. As shown in Table 1.3, these rods had the lowest average coke yield.

Because the rods in Magazine C were carbonized in-block, their diametral changes were calculated from the preirradiation dimensions of

Table 3.1. OF-2 Fuel Rod Dimensional Change

Specimen	Diameter after irradiation (in.)	Change (%)	Length after irradiation (in.)	Change (%)	Estimated average fast fluence[a] (n/cm^2)	Specimen	Diameter after irradiation (in.)	Change (%)	Length after irradiation (in.)	Change (%)	Estimated average fast fluence[a] (n/cm^2)
OF-2A-1-1	0.6061	-2.32	0.9715	-2.85	2.09×10^{21}	OF-2B-1-1	0.6001	-3.46	0.9517	-3.60	6.51×10^{21}
-2	0.6051	-2.53	0.9655	-2.87	2.69	-2	0.5986	-3.61	0.9528	-3.66	6.99
-3	0.6018	-2.94	0.9650	-3.46	3.38	-3	0.5991	-3.84	0.9593	-4.20	7.44
-4	0.6026	-3.09	0.9708	-3.68	4.08	-4	0.5966	-3.84	0.9623	-4.10	7.85
-5	0.6031	-3.05	0.9692	-3.07	4.72	-5	0.6011	-3.47	0.9559	-4.07	8.11
-6	0.6025	-3.17	0.9530	-3.89	5.40	-6	0.6009	-3.56	0.9499	-3.69	8.31
OF-2A-2-1	0.6063	-2.38	0.9668	-2.48	2.09	OF-2B-2-1	0.5982	-3.58	0.9697	-2.65	6.51
-2	0.6040	-2.85	0.9630	-3.14	2.69	-2	0.5996	-3.51	0.9583	-3.58	6.99
-3	0.6017	-3.08	0.9520	-3.66	3.38	-3	0.5977	-3.71	0.9540	-3.98	7.44
-4	0.6035	-2.82	0.9682	-4.29	4.08	-4	0.5982	-3.78	0.9573	-4.19	7.85
-5	0.6005	-3.50	0.9680	-3.35	4.72	-5	0.5971	-3.71	0.9653	-3.95	8.11
-6	0.6000	-3.26	0.9681	-3.38	5.40	-6	0.6006	-3.35	0.9693	-3.95	8.31
OF-2A-3-1	0.6034	-2.63	0.4874	-2.44	1.94	OF-2B-3-1		Debonded			6.38
-2	0.6036	-2.71	0.4842	-2.08	2.25	-2	0.5837	-5.9[illegible]	0.4485	-5.92	6.64
-3	0.5984	-3.55	0.4797	-3.75	2.55	-3	0.5936	-4.32	0.4612	-7.87	6.86
-4	0.6011	-3.14	0.4869	-2.42	2.83	-4	0.5765	-7.03	0.4694	-5.34	7.11
-5	0.5994	-3.35	0.4861	-3.01	3.19	-5	0.5872	-5.78	0.4721	-4.86	7.31
-6	0.6000	-3.38	0.4747	-3.02	3.57	-6		Debonded			7.56
-7	0.5995	-3.35	0.4760	-3.72	3.92	-7		Debonded			7.75
-8	0.5986	-3.51	0.4866	-1.76	4.24	-8		Debonded			7.91
-9	0.5980	-3.64	0.4841	-3.51	4.56	-9	0.5939	-4.16	0.4787	-4.72	8.01
-10	0.5968	-3.83	0.4764	-3.85	4.88	-10	0.5937	-4.26	0.4702	-4.61	8.20
-11	0.5966	-3.76	0.4770	-3.54	5.23	-11	0.5934	-4.31	0.4799	-4.82	8.26
-12	0.5967	-3.80	0.4802	-3.13	5.58	-12	0.5946	-4.07	0.4750	-4.06	8.36
OF-2A-4-1	0.6074	-2.16	0.4843	-2.00	1.94	OF-2B-4-1		Debonded			6.38
-2	0.6062	-2.29	0.4862	-2.05	2.25	-2		Debonded			6.64
-3	0.6069	-2.14	0.4743	-2.73	2.55	-3	0.5943	-4.19	0.4654	-4.49	6.86
-4	0.6027	-2.82	0.4745	-3.56	2.83	-4	0.5930	-4.45	0.4849	-4.17	7.11
-5	0.6046	-2.58	0.4832	-2.56	3.19	-5	0.5946	-4.16	0.4682	-4.91	7.31
-6	0.5992	-3.40	0.4772	-3.46	3.57	-6	0.5910	-4.69	0.4714	-5.11	7.56
-7	0.6013	-3.11	0.4822	-2.35	3.92	-7	0.5913	-4.61	0.4699	-5.19	7.75
-8	0.6010	-3.14	0.4872	-2.85	4.24	-8	0.5910	-4.74	0.4716	-5.30	7.91
-9	0.6001	-3.33	0.4833	-2.82	4.56	-9	0.5923	-4.48	0.4765	-4.64	8.01
-10	0.5960	-3.86	0.4759	-4.09	4.88	-10	0.5936	-4.29	0.4730	-6.36	8.20
-11	0.6009	-4.01	0.4756	-3.16	5.23	-11	0.5924	-4.42	0.4881	-2.30	8.26
-12	0.5914	-4.40	0.4896	-3.20	5.58	-12		Debonded			8.36
OF-2C-1-1[b]	0.6103	-1.69	1.9641	-4.32	8.91						
-2	0.6094	-2.12	1.9741	-2.05	8.50						
-3	0.6086	-2.23	1.9411	-2.37	7.62						
-4	0.6053	-2.61	1.9128	-2.13	5.86						

Table 3.1 (continued)

Specimen	Diameter after irradiation (in.)	Change (%)	Length after irradiation (in.)	Change (%)	Estimated average fast fluence[a] (n/cm^2)	Specimen	Diameter after irradiation (in.)	Change (%)	Length after irradiation (in.)	Change (%)	Estimated average fast fluence[a] (n/cm^2)
OF-2C-2-1	0.6083	-2.28	ND		8.91×10^{21}						
-2	0.6088	-1.76	ND		8.50						
-3	0.6151	-0.73	1.9580	-1.40	7.62						
-4	0.6104	-1.50	1.9953	0.01	5.86						
OF-2C-3-1	0.6105	-2.26	2.0146	0.41	8.91						
-2	0.6108	-1.83	1.9611	-2.75	8.50						
-3	0.6075	-2.53	1.9663	-2.36	7.62						
-4	0.6027	-3.01	1.9201	-3.23	5.86						
OF-2C-4-1	0.6115	-1.99	1.9582	-3.24	8.91						
-2	0.6086	-2.30	2.0228	-0.40	8.50						
-3	0.6084	-2.39	1.9583	-3.31	7.62						
-4	0.6082	-1.97	1.9204	-1.84	5.86						

[a] $E > 0.18$ MeV.

[b] Since actual specimens for holder C were not removed from the holder, the preirradiation dimensions were from typical as-fired sample specimens processed at the same time as the actual test specimens.

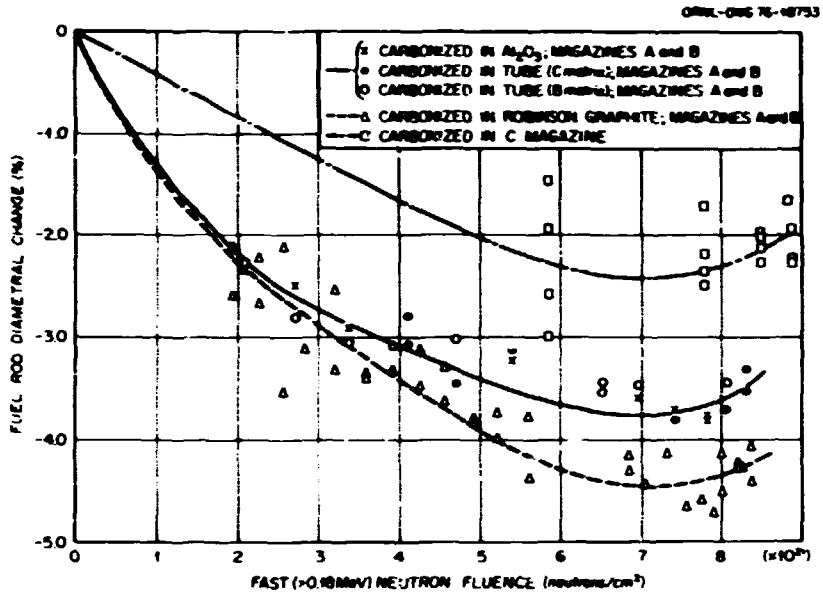

Fig. 3.9. OF-2 Fuel Rod Dimensional Changes Versus Estimated Fast Fluences.

rods fabricated and processed exactly as the irradiated ones were. These rods shrank less than did rods carbonized by any other procedure. We should note that the rods in Magazine C contained many more Triso-coated particles (in the form of inerts and fissiles) than did rods irradiated in the other two magazines. The increase in Triso-particle packing fractions apparently resulted in less irradiation-induced shrinkage. This agrees with other data that indicate that fuel rod dimensional changes are primarily controlled by the dimensional changes of the constituent fuel particles.[8,9]

The graphite magazines were also dimensionally measured by opposing dial indicators. The results are presented in Fig. 3.10. Magazines B and C behaved similarly and both shrank up to a fast fluence of 8-8.5 x 10^{25} n/m^2 (E > 0.18 MeV), at which point a minimum was reached and the graphite began to swell. These magazines experienced similar temperatures. On the other hand, Magazine A, which operated at a much lower temperature and neutron fluence, did not swell and shrank more at the same fast fluence.

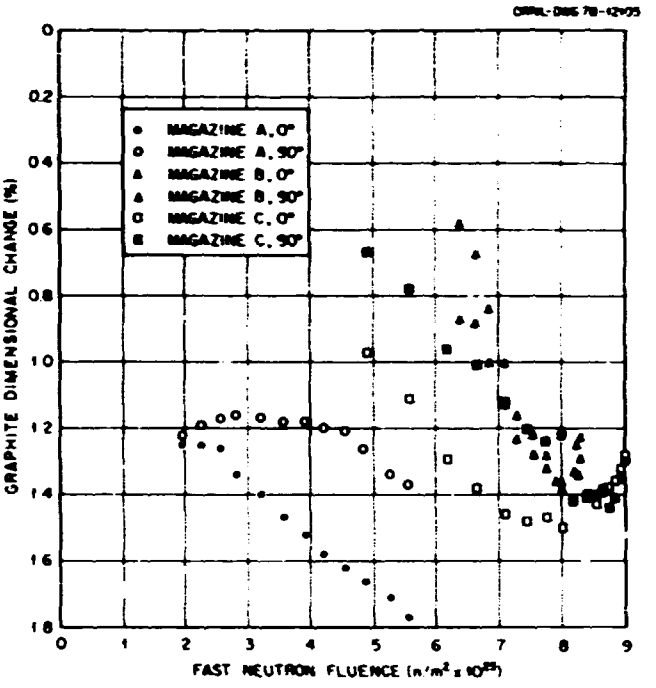

Fig. 3.10. OF-2 Graphite Magazines' Dimensional Change as a Function of Fast-Neutron Fluence.

3.5 Metallographic Examination

3.5.1 Fissile particles made in 0.13-m-diam coater

As mentioned previously, many coating failures were observed in the fuel rods from Magazine C. Selected fuel rods from Magazine C were examined metallographically to determine the cause of the coating failures. Metallography revealed coating failures of the oLTI coatings on the Triso particles but with none of the Biso coatings of fertile or inert particles. No failed SiC coatings were observed, either.

The oLTI coating failures were attributable to fast-neutron damage (Fig. 3.11) and matrix-particle interaction (Fig. 3.12). Because only one random plane is observed in the metallographic cross sections, it was not possible confidently to distinguish between fast-neutron damage and matrix-particle interaction. To supplement the observations from Magazine C fuel rods, further metallography was performed on rods from Magazines A and B; these rods contained the same particle batches. The rods differed only in carbonization method. Metallography was performed

Fig. 3.11. Failure of the oLTI Coating Caused by Fast-Neutron Damage (E > 0.18 MeV). Particle batch A-601 irradiated in fuel rod C-2-2.

Fig. 3.12. Failure of the oLTI Coating Caused by Matrix-Particle Interaction. Particle batch A-615 irradiated in fuel rod C-2-1.

to determine whether the oLTI coating failures resulted from characteristics of the matrix or of the particles: we found a combination of both was responsible. Table 3.2 presents the tabulated results of the oLTI coating failures on the Triso-coated particles. As shown, failures were observed in most fuel rods that included all particle batches (that is, A-601, -611, and -615). Table 3.3 lists the important properties of the oLTI coatings for the fissile particles examined, and Fig. 3.13 shows the relationship between oLTI coating failure and pitch-coke yields.

Table 3.2. Failure Fraction of oLTI Coatings on Triso-Coated Particles in OF-2

Fuel rod[a]	Matrix type[b]	Pitch-coke yield (%)	Fissile particle batch	oLTI failure fraction[c] (%)
A-1-1	b	38.0	A-611	8
A-1-2	a	17.0	A-601	3
A-1-3	a	16.2	A-611	0
A-1-4	c	31.0	A-611	7
A-1-5	b	36.2	A-601	22
A-1-6	c	30.9	A-601	6
A-2-3	b	37.6	A-601	19
B-1-2	a	17.9	A-601	0
B-1-3	c	30.6	A-601	7
B-1-4	a	20.1	A-611	0
B-1-6	c	27.8	A-611	0
C-2-1	f	25.7[d]	A-615[e]	100[e]
C-2-2	f	25.7[d]	A-601[e]	0-7[e,f]
C-3-4	f	25.7[d]	A-611	33

[a]Letter indicates magazine; first number indicates hole, second number indicates rod.

[b]Matrix types are as follows:

Type	Pitch	Additive	Filler	Carbonization technique
a	A-240	none	Asbury 6353	Packed Al_2O_3
b	A-240	none	Asbury 6353	In-tube
c		GA proprietary		In-tube
d		GA proprietary		In-block

[c]Determined metallographically.

[d]Estimated.

[e]Fuel rod also contained Triso-coated inert particles.

[f]All oLTI failures attributable to Triso-coated inert particles.

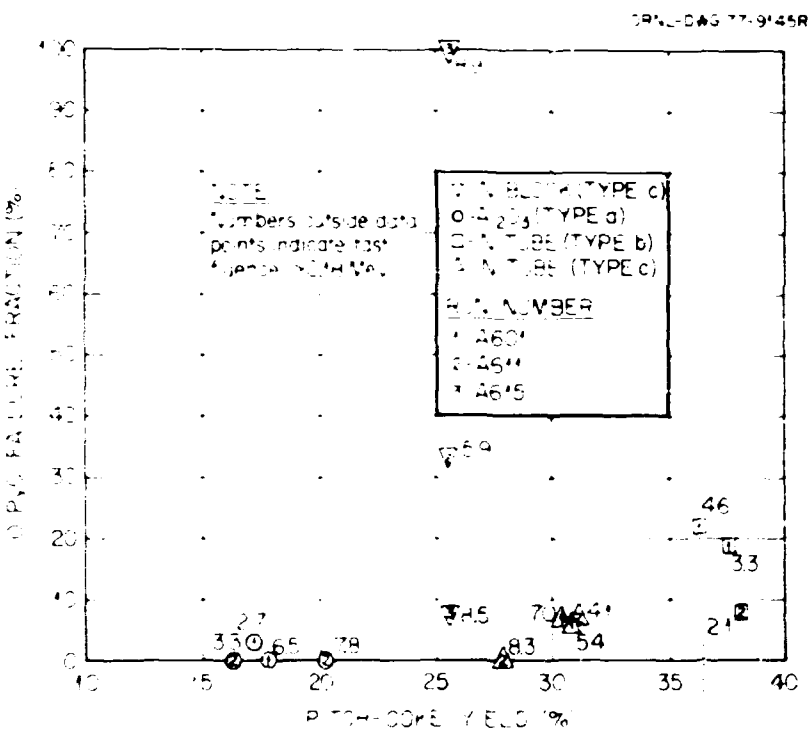

Fig. 3.13. Rate of Irradiation-Induced oLTI Coating Failure for Triso-Coated Fissile Particles in OF-2.

The highest oLTI failure fraction (100%) occurred in fuel rod C-2-1, which contained particles from batch A-615 and was carbonized in-block. This fuel rod also contained Triso-coated inert particles, which also showed 100% oLTI failure. The oLTI coatings on batch A-615 showed a high degree of optical anisotropy, expected because of the high BAF measurements observed before irradiation (Fig. 3.14). Coatings with high optical anisotropy typically have high rates of failure from differential irradiation-induced shrinkage.

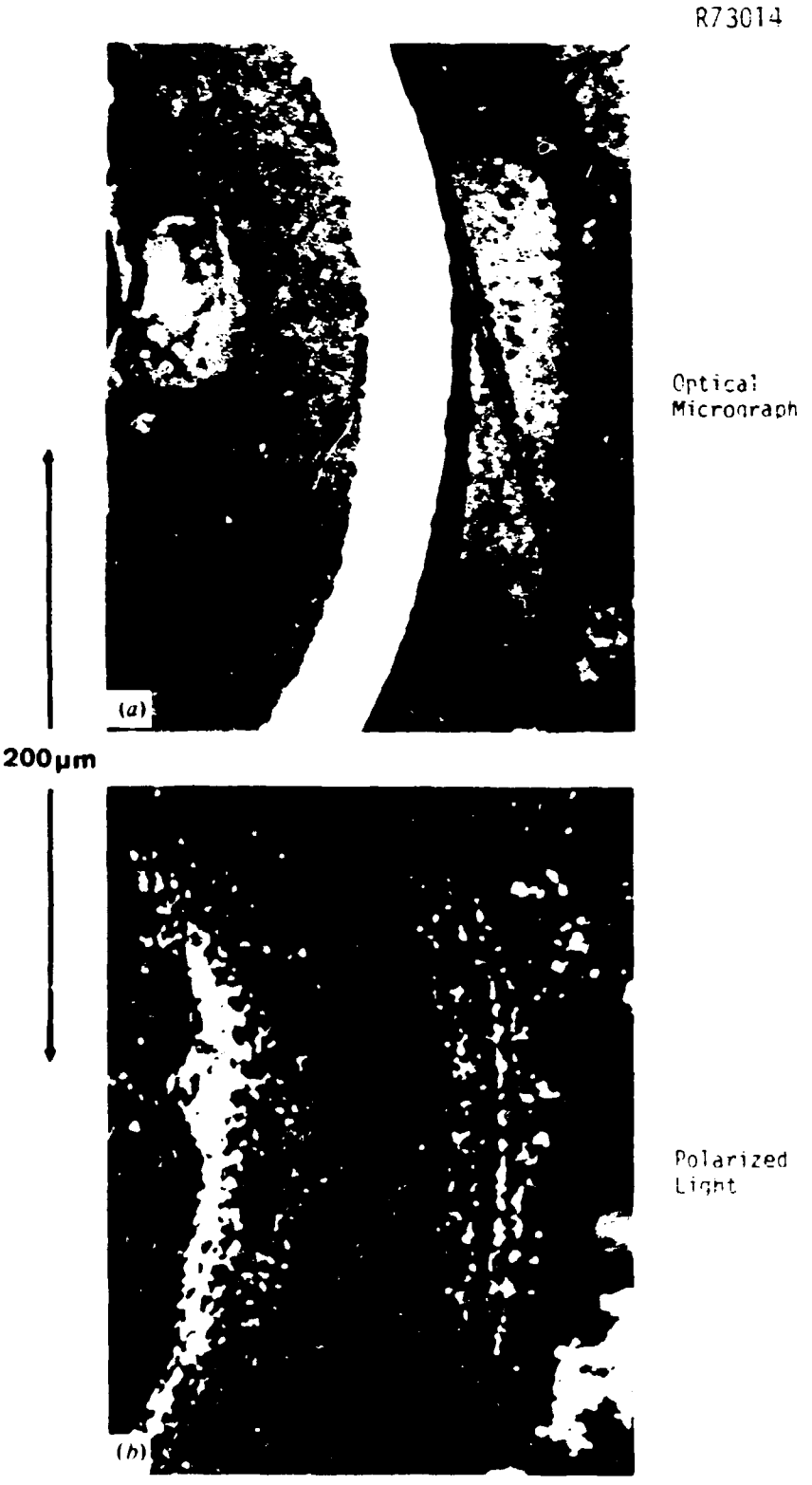

Fig. 5.14. Broken oLTI Coating of Fissile Particle Batch A-oL5 Irradiated in Fuel Rod C-2-1. (a) Under bright field. (b) Under polarized light. Note bands of high optical anisotropy in oLTI coating.

Failure fractions of the oLTI coatings in batches A-601 and -611 ranged from 0 to 33%. The only trend observed was that the rods with higher pitch-coke yields (typically matrix type b) had higher oLTI failure fractions. In addition the oLTI coating of these two particle batches had much open porosity, which probably increased the bonding between the matrix and the particle.

The Biso-coated fertile and inert particles showed no coating failures in any metallographic section. The Biso-coated particles apparently were able to shrink with the matrix during irradiation, so strong interactions were minimized. On the other hand, the SiC coating prevented the Triso-coated particles from shrinking with the matrix, so strong interactions developed. Thus, coating failures were observed in the Triso-coated particles, both fissile and inert, while none were observed in the Biso-coated particles.

The following conclusions about oLTI failure were drawn from these data:

1. The most important property resulting from irradiation of the oLTI coating is optical anisotropy. All oLTIs (100%) failed in particle batch A-615, which had a high BAF_0 (1.069), whereas oLTI coating failures were far fewer in batches A-601 and A-611, which had lower BAF_0s (1.030 and 1.035, respectively).

2. Failure of the oLTI at high pitch-coke yields occurred, even at such relatively low fast-neutron exposures as less than 5×10^{25} n/m^3. A pitch-coke yield of less than 30% is necessary to prevent oLTI failure. The effect of high pitch-coke yield is increased by the great open porosity of the pyrocarbon.

3. In-block carbonization resulted in consistently higher oLTI coating failures.

Other than the oLTI coating failures of the fissile particles from the three batches in Magazine C, the fuel apparently performed very well. No broken SiC coatings and only slight fission product attack ($\leq$ 3 μm) were noted. The performance of the kernels in the three fissile particle batches examined is summarized below. The observations for each batch were virtually identical for all rods.

Fissile Particle Batch A-601: Approximately 75%-Converted WAR. Examples of the metallographic examination of batch A-601 are shown in Fig. 3.15.* As is typical of all WAR particles, during irradiation the kernel and buffer densified, creating a significant void volume. Two kernel phases were dispersed in the densified buffer with no visible metallic inclusions. The dispersion probably resulted from the high conversion level since the metallic fission products are soluble in a high-carbon milieu. In contrast to observations made in previous experiments,[10] the densified buffer was optically isotropic. Localized fission product accumulations, rare earths and palladium, were observed at the SiC coating (Fig. 3.16). These fission products primarily accumulated in the areas adjacent to where the WAR kernels had shrunken and adhered to the iLTI coating. This indicates that rare earth or palladium migration most probably follows a solid diffusion mechanism.

Fissile Particle Batch A-611: Approximately 15%-Converted WAR. Examples of the metallographic examination of batch A-601 from rods in every magazine are shown in Fig. 3.17. Typical densification of kernel and buffer was observed. Like batch A-601, the kernel was dispersed in the densified buffer with no optical anisotropy noted. The dispersed kernel looked much like irradiated UO_2, in which fission gas bubbles and inclusions are visible. Metallic fission product inclusions observed in the kernel phase indicate nonsolubility of those fission products in high oxygen content kernels. These results are similar to previous studies.[11] Very slight fission product accumulations resembling those in Fig. 3.16 were observed on some particles, with no visible attack on the SiC coating. No effects of a thermal gradient were seen; however, the fission products accumulated near the densified kernel.

Fissile Particle Batch A-615: Approximately 75%-Converted WAR. Examples of the metallographic examination of batch A-615 from rods in Magazine C are shown in Fig. 3.18. Typical densification of kernel and buffer was observed. The appearance of the kernel was as in batch A-601, but the

*In the following micrographs of particle metallography, the outer surface of the rod (the "cold" side of the particle) is on the right in the figure.

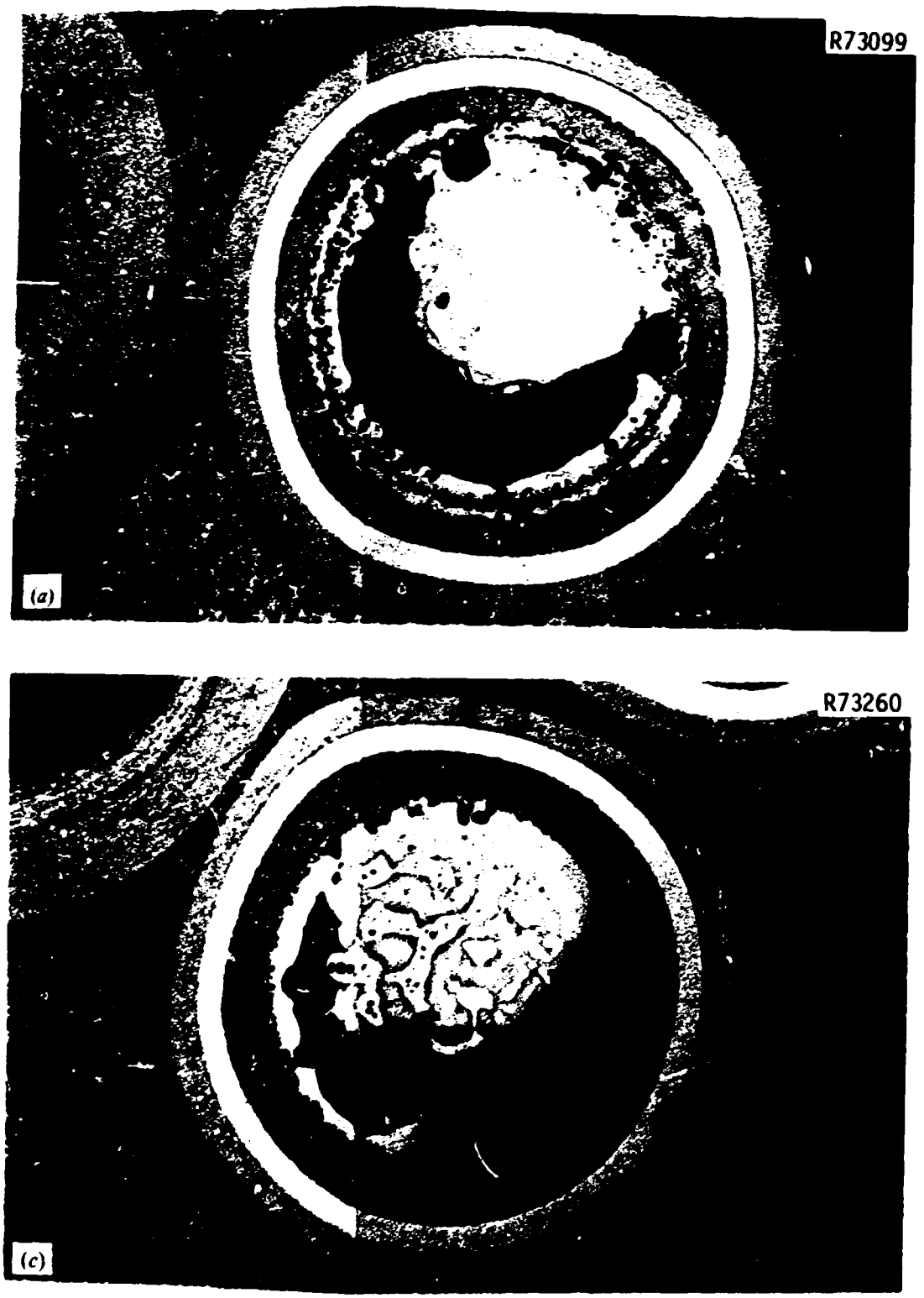

Fig. 3.15. Representative Particles from Fissi
side of micrographs. (a) Irradiated in fuel rod B-1
(b) Same. Polarized light. (c) Irradiated in fuel
oLTI coating failure. (d) Same. Polarized light.

BLANK PAGE

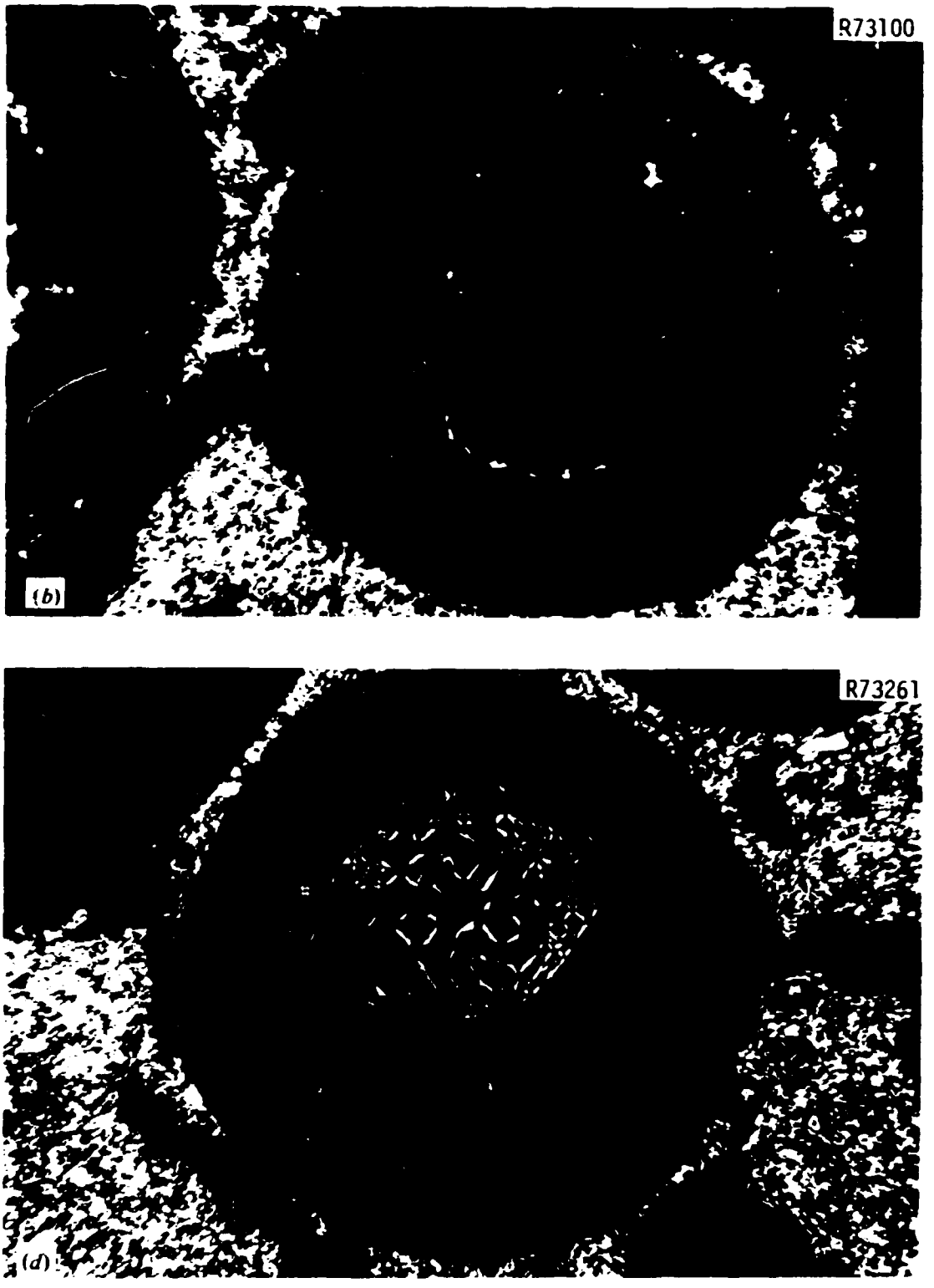

le Batch A-601. 150×. Rod surface is on right
-3, on outer surface of rod. Bright field.
rod A-1-2, near rod center. Bright field. Note

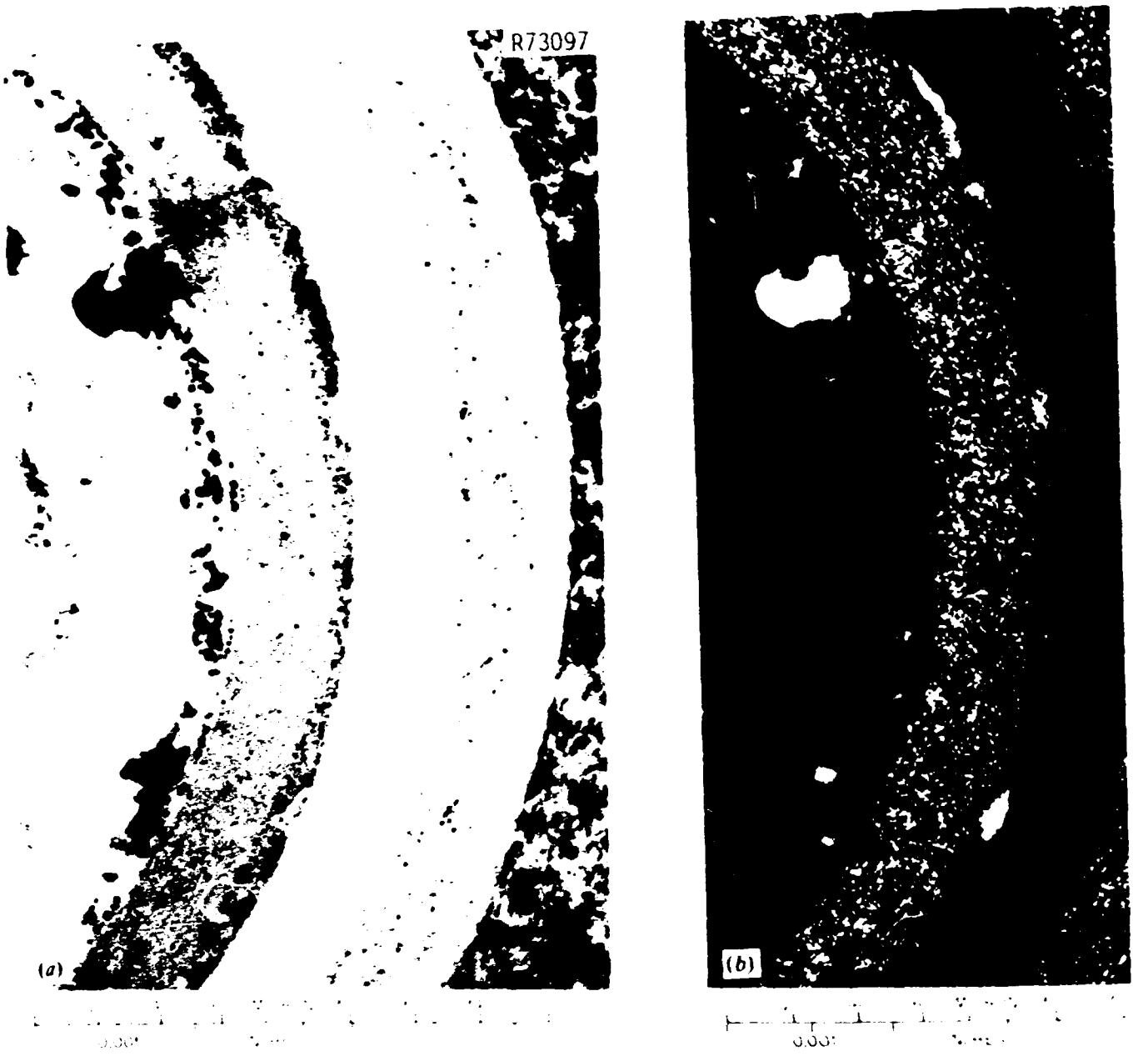

Fig. 3.16. Fission Product Accumulations at SiC-ILTI Coating Interface. From fissile particle batch A-601 irradiated in fuel rod B-1-2. (a) Bright field. (b) Polarized light.

Coating
in fuel rod

BLANK PAGE

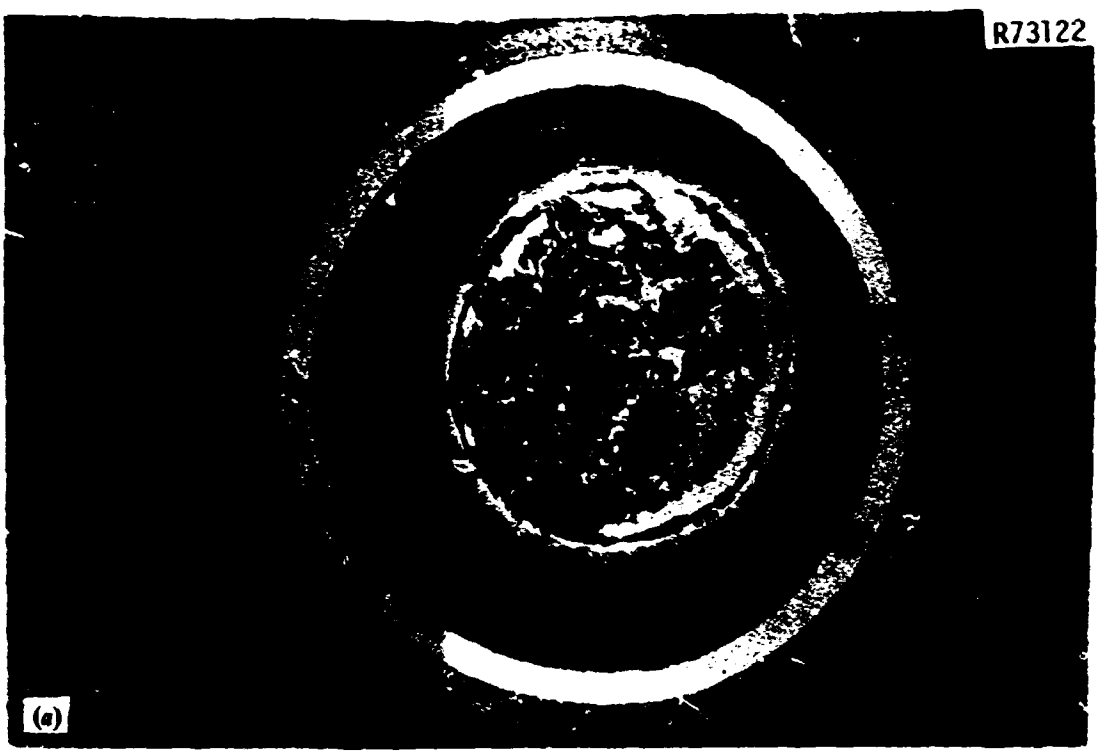

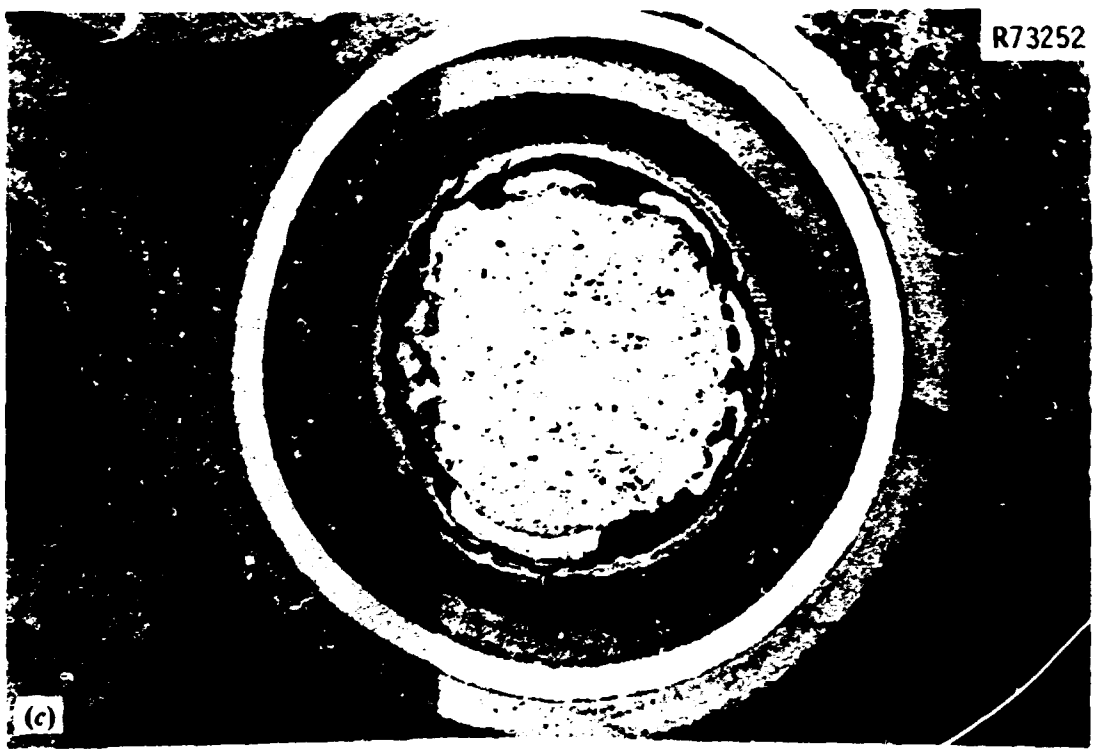

Fig. 3.17. Representative Particles from Fissile
right side of micrographs. (a) Irradiated in fuel rod
field. (b) Same. Polarized light. (c) Irradiated in
(d) Same. Polarized light.

BLANK PAGE

Ba[illegible] A-611. 150×. Rod's outer surface is on B-[illegible] 3560 cm from rod's outer surface. Bright fi[illegible] rod A-1-6, near rod center. Bright field.

Fig. 3.12. Representative [illegible] graphs. 150×. (a) [illegible] radiated in fuel rod C-7-3. [illegible]

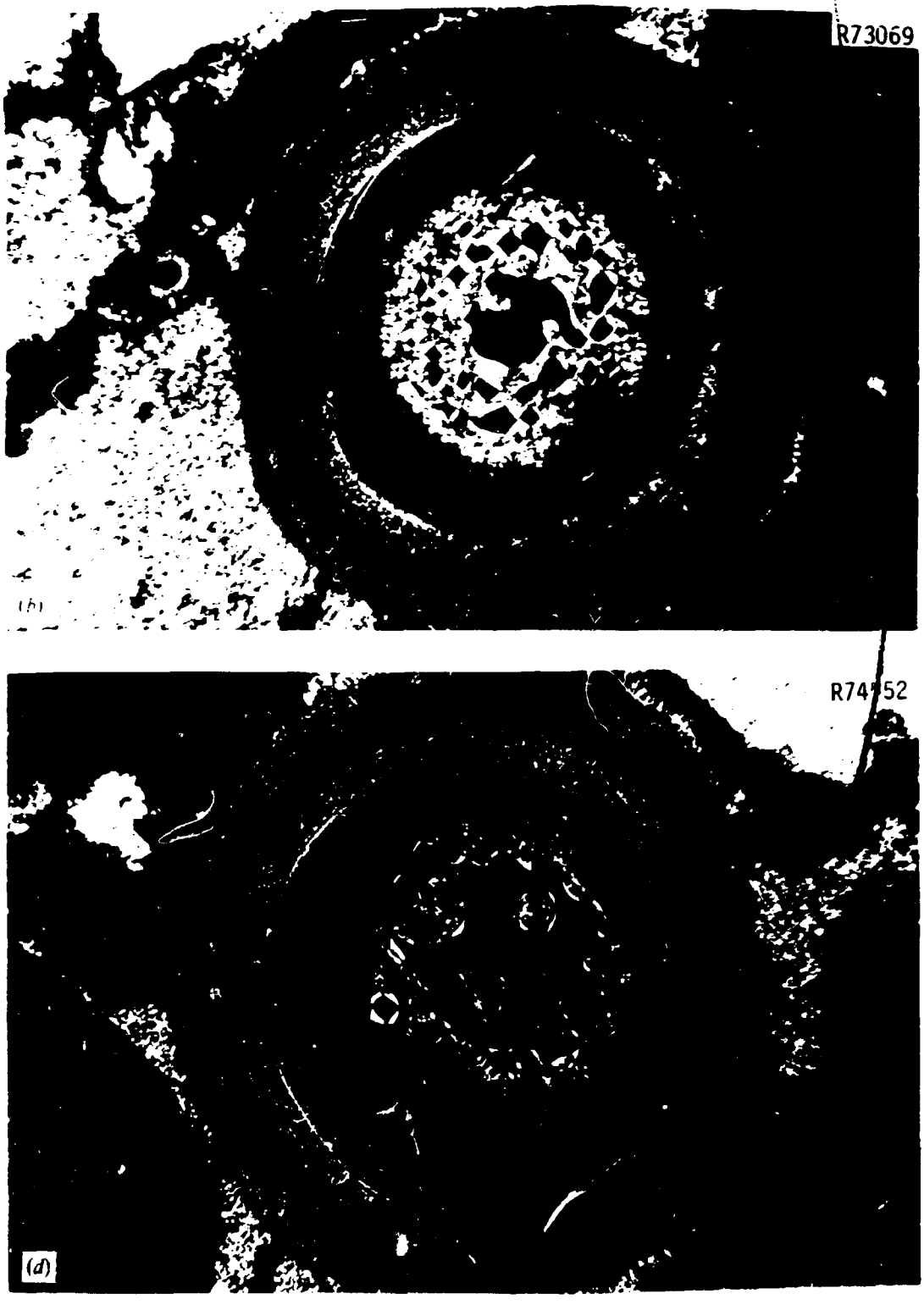

ssile Batch A-615. Rod surface is at right of m.cro- Bright field. (b) Same. Polarized light (c) Ir- ame. Polarized light.

BLANK PAGE

buffer surrounding the dispersed kernel was optically anisotropic. For the same reason as in batch A-601, no metallic fission products were observed in the kernel. Small localized fission products accumulated at the SiC coating. These accumulations resembled those in Fig. 3.16 and had the same relationship to the densified kernel as in A-601 and A-611. Such fission product accumulations had caused the iLTI coating to graphitize and were themselves optically active under polarized light. Many times a gap between the SiC and iLTI coatings had formed where the fission products had accumulated.

3.5.2 Fissile particles made in laboratory coater

Metallography was also performed on selected fuel rods from Magazine A, which contained fissile particles made in the laboratory coater. Metallography of the fuel rods from Magazine B will be performed only after they are examined by the Irradiated Microsphere Gamma Analyzer (IMGA) system.[12] Results of the metallography will be coupled with the gamma analysis so as to better determine fuel performance.[13] The fissile particles examined included WAR particles at various conversion levels, sol-gel $(4Th,U)O_2$ particles, and VSM UC_2 particles.

Metallography was performed on fuel rods A-4-2 and A-4-10, which both contained fissile particles WAR $UC_{5.43}$ $O_{1.95}$ at a nominal conversion of 0%. The two metallographic cross sections display 21 particles in all. Amoeba was observed in 16 and 22% of the particles in A-4-2 and A-4-10, respectively. The maximum migration observed was 10 μm. Representative particles are shown in Fig. 3.19. The kernels and buffers had densified to create a void volume between the kernel and the iLTI coating. This effect is typical of WAR kernels at all conversion levels.[11] The kernel often was dispersed in the densified buffer and in excess kernel carbon [as in Fig. 3.19(a)], instead of agglomerating [as in Fig. 3.19(c)]. As in irradiated UO_2, the kernels were characterized by fission gas bubbles, ceramic inclusions, and metallic inclusions. Under polarized light, most particles showed an optically active layer of carbon on the inner surface of the iLTI coating. Evidently, the oxygen potential was sufficiently high to transport carbon out of the kernel and buffer, the

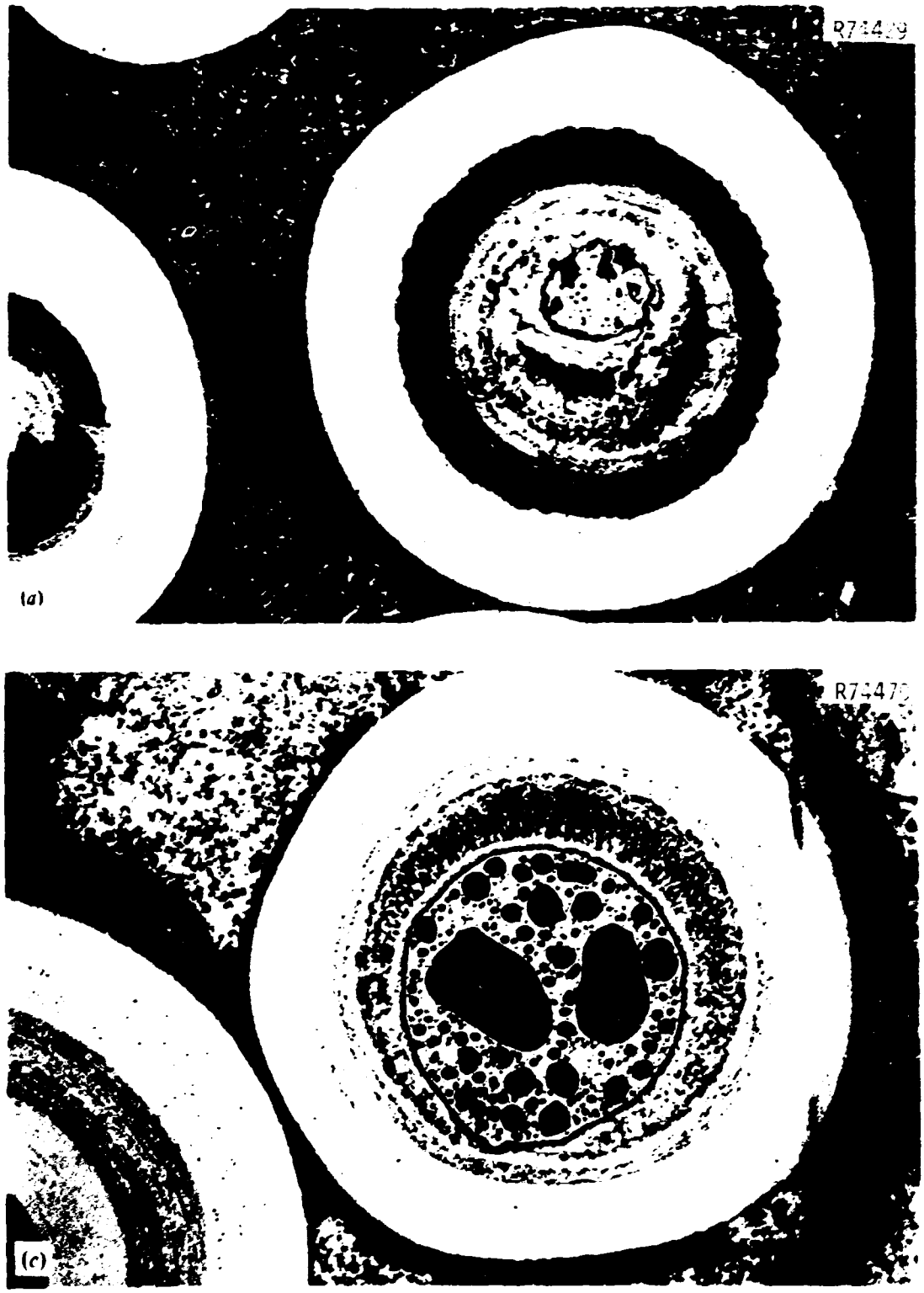

Fig. 3.19. Representative Particles from Fiss
is to the right of the micrographs. 150×. (a) Fr
light. (c) From fuel rod A-4-10. Bright field. (

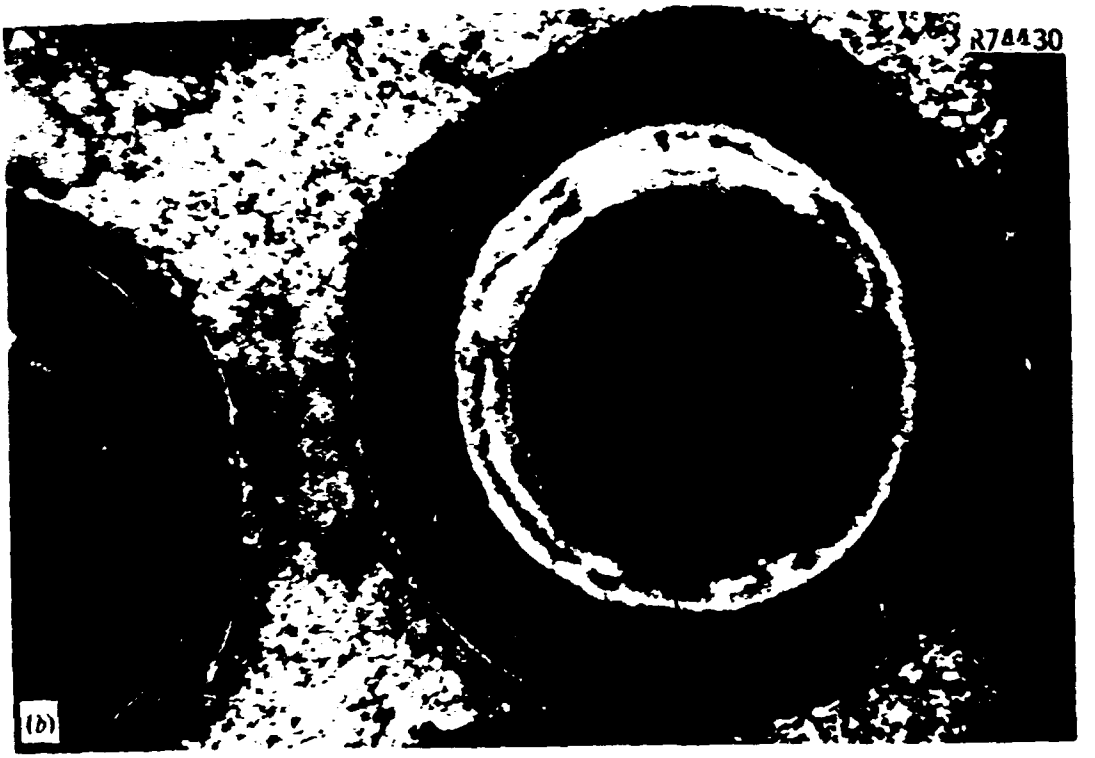

ile $UC_{0.33}O_{1.95}$ Batch OR-2332-H. The rod's surface
m fuel rod A-4-2. Bright field. (b) Same. Polarized
d) Same. Polarized light.

BLANK PAGE

...m the IPyC coating. This agrees with the ...ides with the stoichiometry, $UC_{...}O_{...}$. In ... metallic-looking inclusions, believed to be ... observed at the SiC coating with no apparent ...

... performed on fuel rod A-4-5 containing ... a nominal conversion of 15 . A total of 10 ... with no failures or amoeba. Representative ... Fig. 3.20. The kernel was dispersed in a por... buffer and the excess kernel carbon. In contrast ... the densified buffer was not ... under polarized light. No corrosion of the SiC ...

... in fuel rods A-3-2 and A-3-4 was a KAR ... nominal conversion of 9 . The thickness of the ... fissile particle from the one contained in ... present one had a "thin" buffer of 24.0 μm ... particles were observed in the two ... sections. Amoeba migration was not prevalent, but ... was observed. Representative particles are shown ... In the previous rods, the appearance of the ... were dispersed in the densified buffer and had ... agglomerated. Fission gas bubbles, ceramic ... inclusions were present. In addition, polarized ... showed a layer of vapor-deposited carbon on the ... face, as in rods A-4-2 and A-4-10 (Fig. 3.21). ... shown in Fig. 3.22. Here small parts of the ... IPyC coating on the hot side of the particle. ... amoeba migration. Similar migration of kernel ... in UC$_2$-converted KAR particles with buffer coatings ... metallic inclusions thought to be palladium at ... were observed. These and other results[3] show ... buffer thickness of KAR particles to 23 μm does not ... performance.

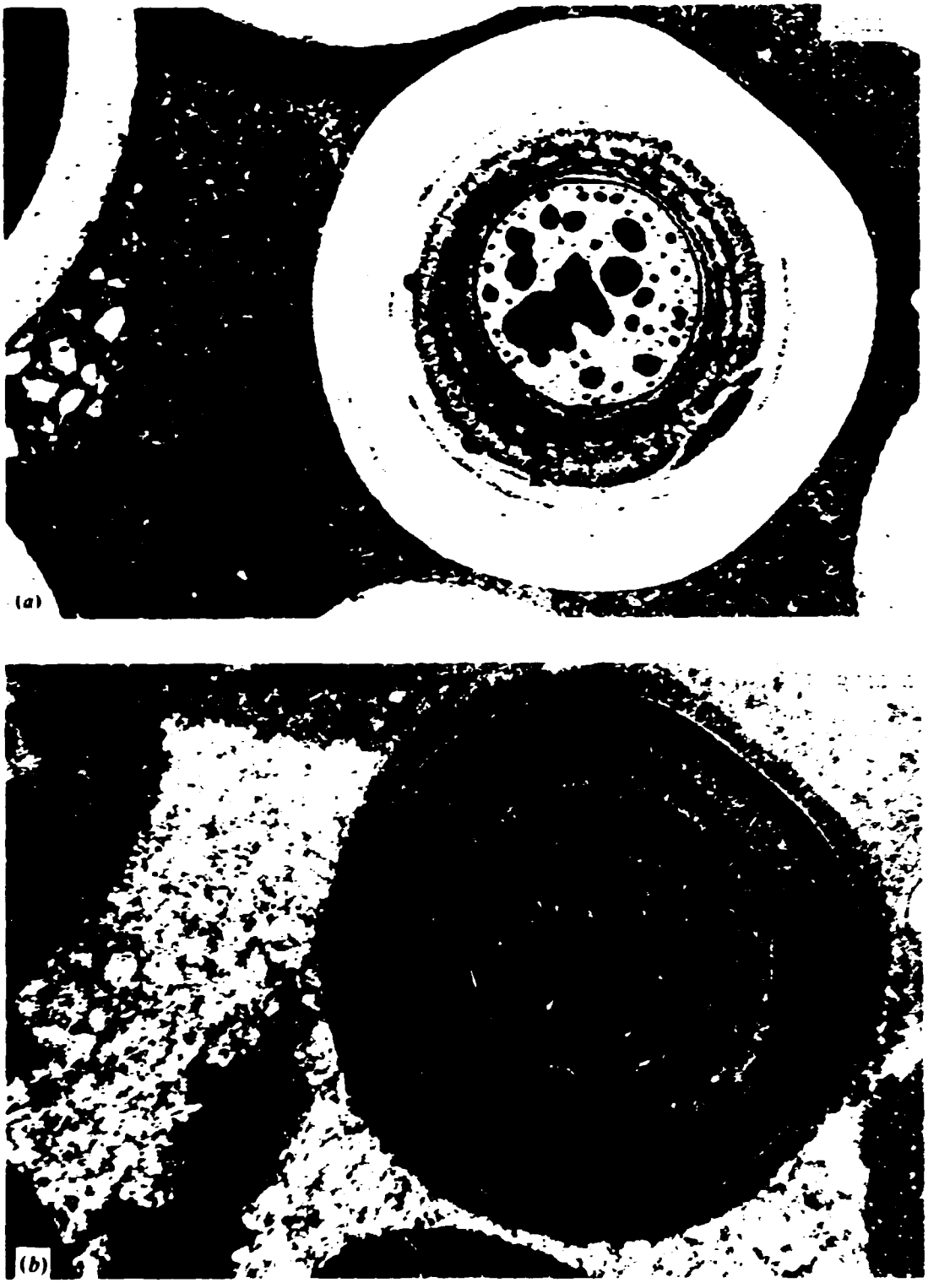

Fig. 3.20. Representative Particle from [illegible] Fissile Fuel ORR-2329-H. The particle had been irradiated in fuel rod [illegible] located 900 μm from the rod's outer surface, which is to the right in the micrographs. 100×. (a) Bright field. (b) Polarized light.

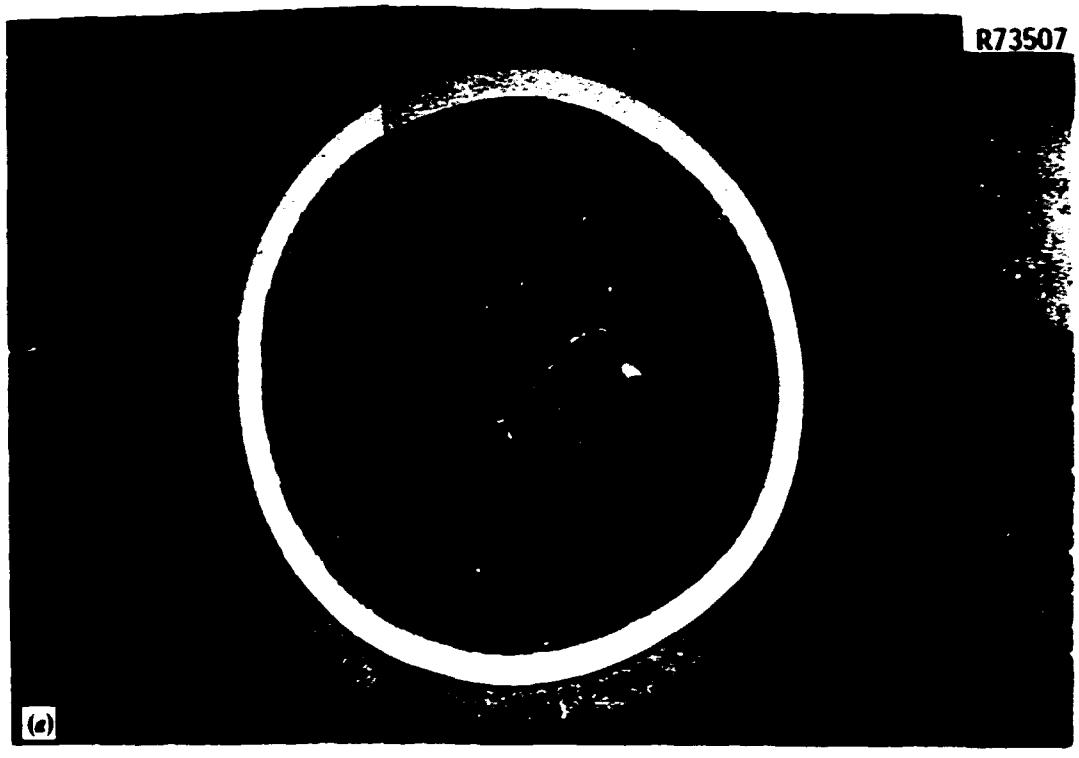

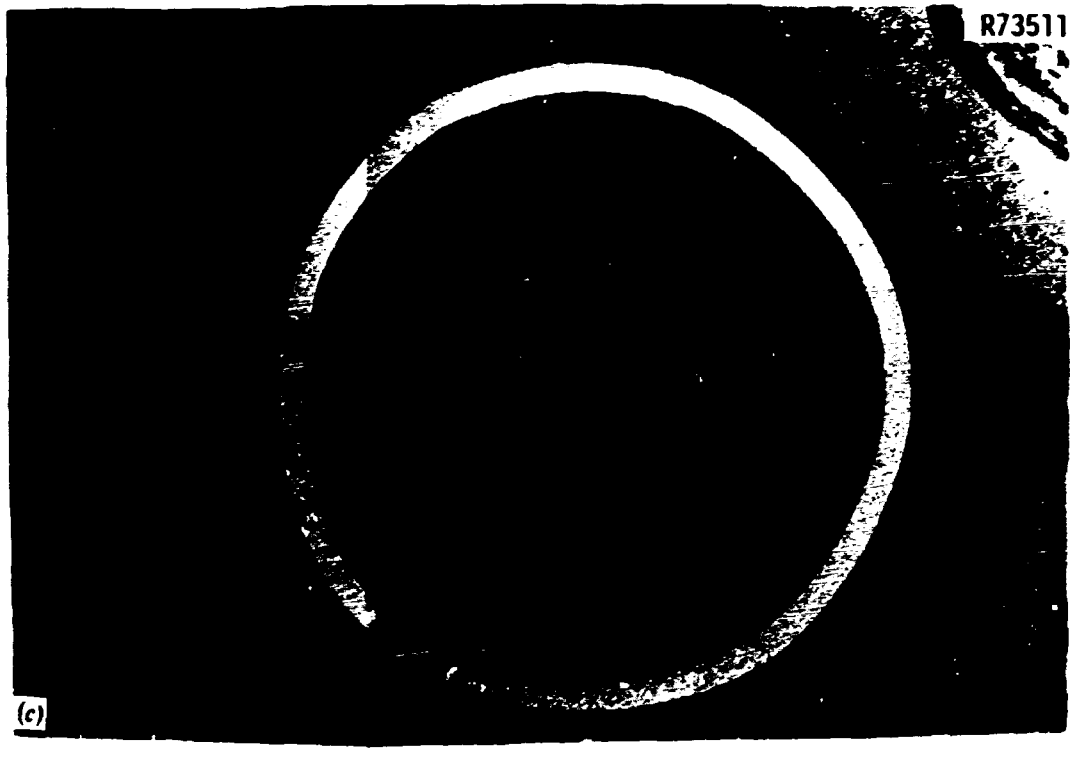

Fig. 3.21. Representative Particles of Fissile
Rod A-3-4. 150×. The outer surface of the rod is t
(c) Bright field. On inner surface of rod. (b) and
surface of rod.

BLANK PAGE

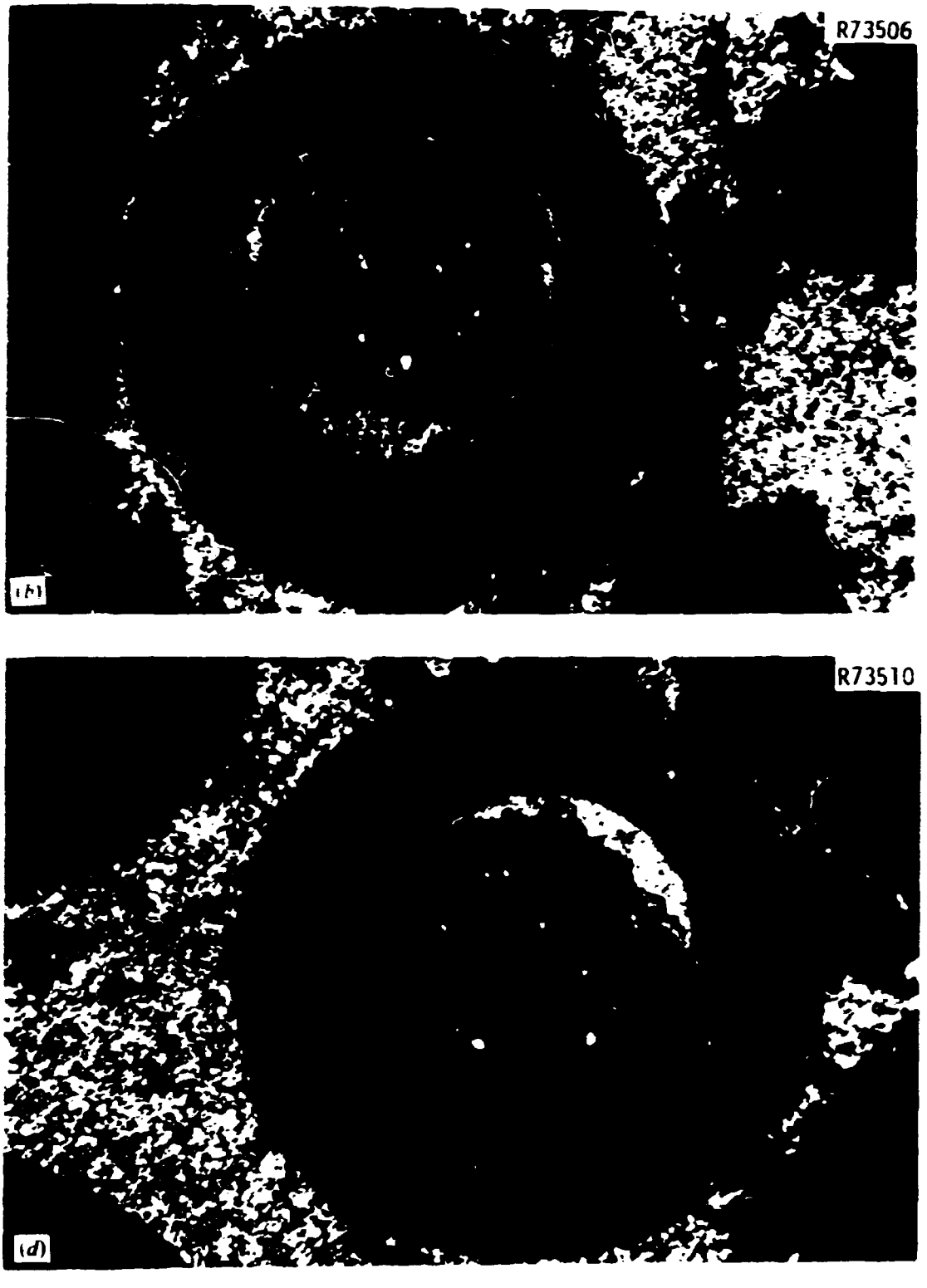

Batch OR-2329-H ($UO_{2.30}O_{1.97}$) Irradiated in Fuel
oward the right of the micrographs. (a) and
(d) Polarized light. At 4200 μm from outer

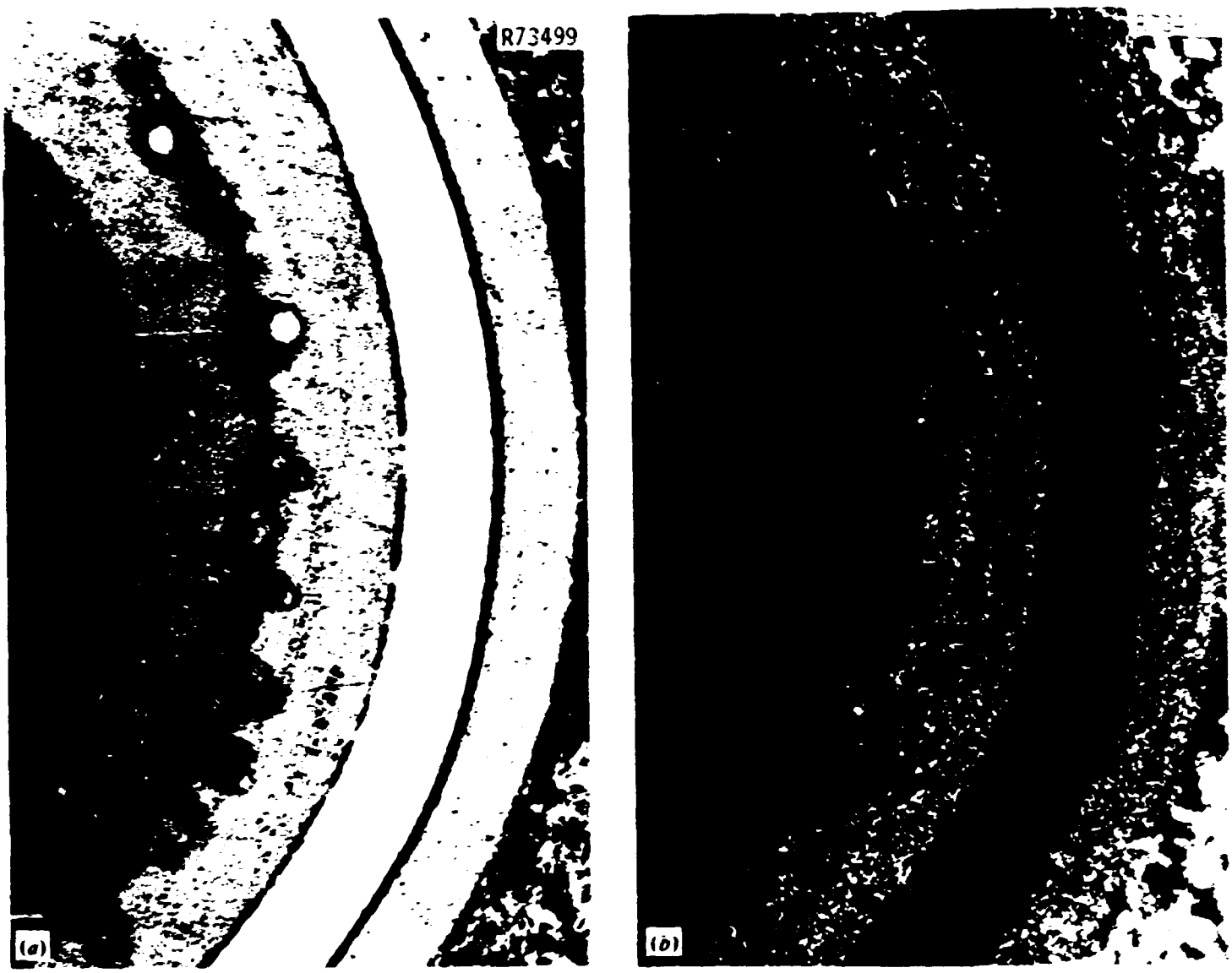

Fig. 3.22. Migration of Parts of the Kernel in the ILTI Coating of a Fissile Particle from Batch OR-2329-H ($UC_{x}O_{y}$). (a) Bright field. (b) Polarized light.

Another WAR particle type with a nominal conversion of 0% was examined in rods A-4-5 and A-4-9. It was carbonized at a very high rate (see Tables 1.1 and 1.4) and thus had a composition of $UC_{4.58}O_{2.24}$. A total of 11 particles were observed with no amoeba of the kernel readily apparent. Representative particles are shown in Fig. 3.23. Deposition of carbon was seen on the surfaces of the void volume, as in the previous two particle batches. The kernels resembled those of irradiated UO_2, as fission gas bubbles, ceramic inclusions, and metallic inclusions were present. The metallic-appearing palladium inclusions at the SiC were also observed.

Metallography was performed on fuel rod A-3-5 containing WAR $UC_{5.58}O_{1.63}$ with a nominal conversion of 15%. A total of 10 particles were observed with no failures or amoeba. Representative particles are shown in Fig. 3.24. The kernel was dispersed in a portion of the densified buffer and in the excess kernel carbon. In contrast to results from recent tests,[11,17,18] the densified buffer was not optically anisotropic under polarized light. No corrosion of the SiC was observed.

The fissile particle in fuel rod A-4-6 was a WAR $UC_{5.12}O_{1.54}$ particle with a nominal conversion of 25%. No failures were seen in the ten particles examined. Representative particles are shown in Fig. 3.25. The kernel and buffer had densified as the other WAR particles had. The kernels had two main phases, which were dispersed together in the densified buffer and excess kernel carbon. No fission gas bubbles or inclusions were observed in the kernel. Small fission product accumulations — most likely palladium[15,16] — were seen at the SiC coating, penetrating it about 1–3 μm.

Another WAR particle with composition $UC_{4.63}O_{0.97}$ and a nominal conversion of 50% was contained in rod A-3-6. A total of only four particles were observed in the metallographic cross section. Representative particles are shown in Fig. 3.26. The kernel had two main phases dispersed in the densified buffer, as in the 25%-converted WAR particles in rod A-4-6. Fission product accumulations were seen at the SiC coating with penetrations of about 3 μm in particles at the outer surface, and 15 μm in particles near the inner surface. The fission product

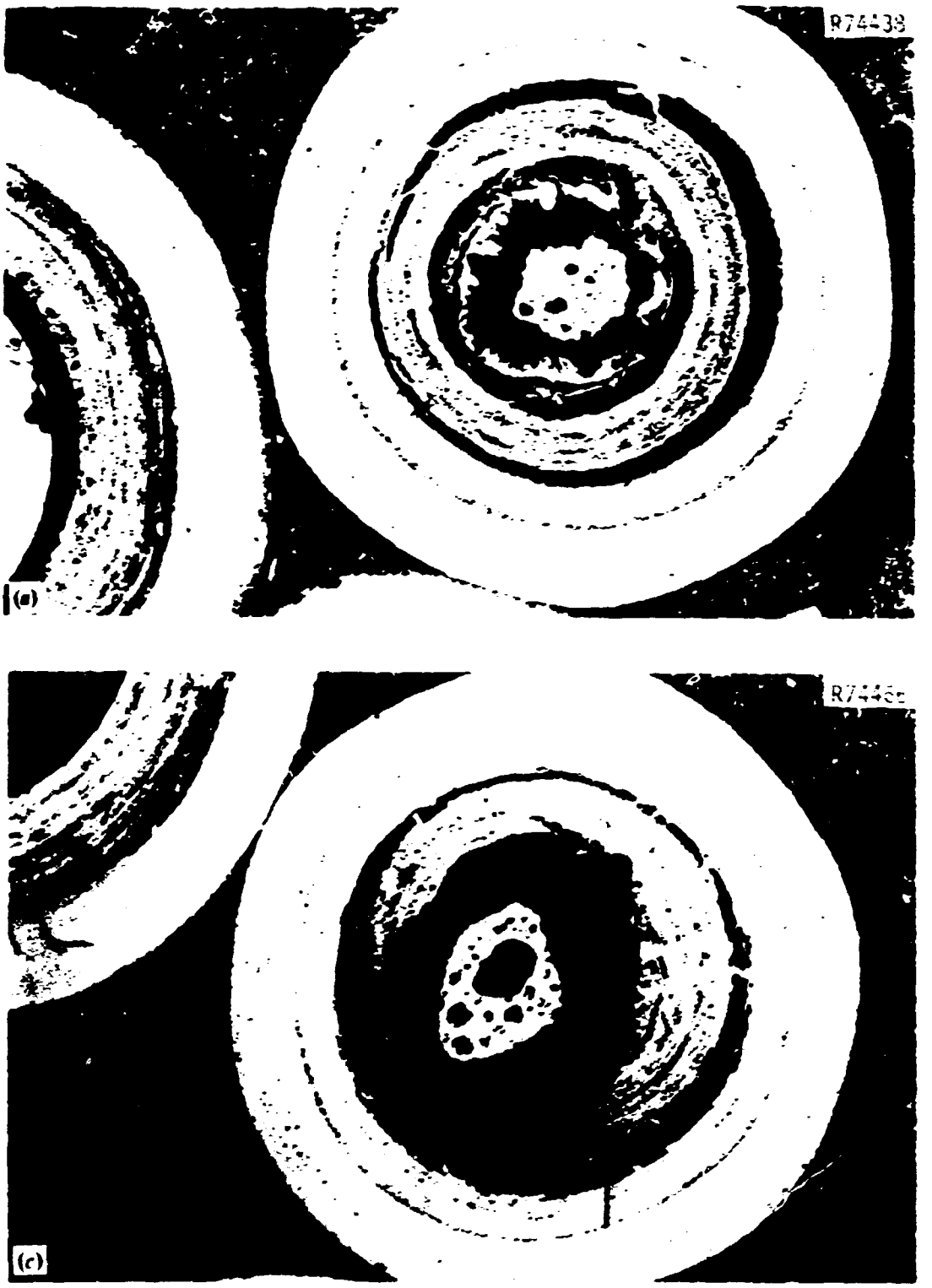

Fig. 3.23. Representative Particles of Fi
is to the right side of micrographs. 150×. (a)
field. (b) Same. Polarized light. (c) From
Bright field. (d) Same. Polarized light.

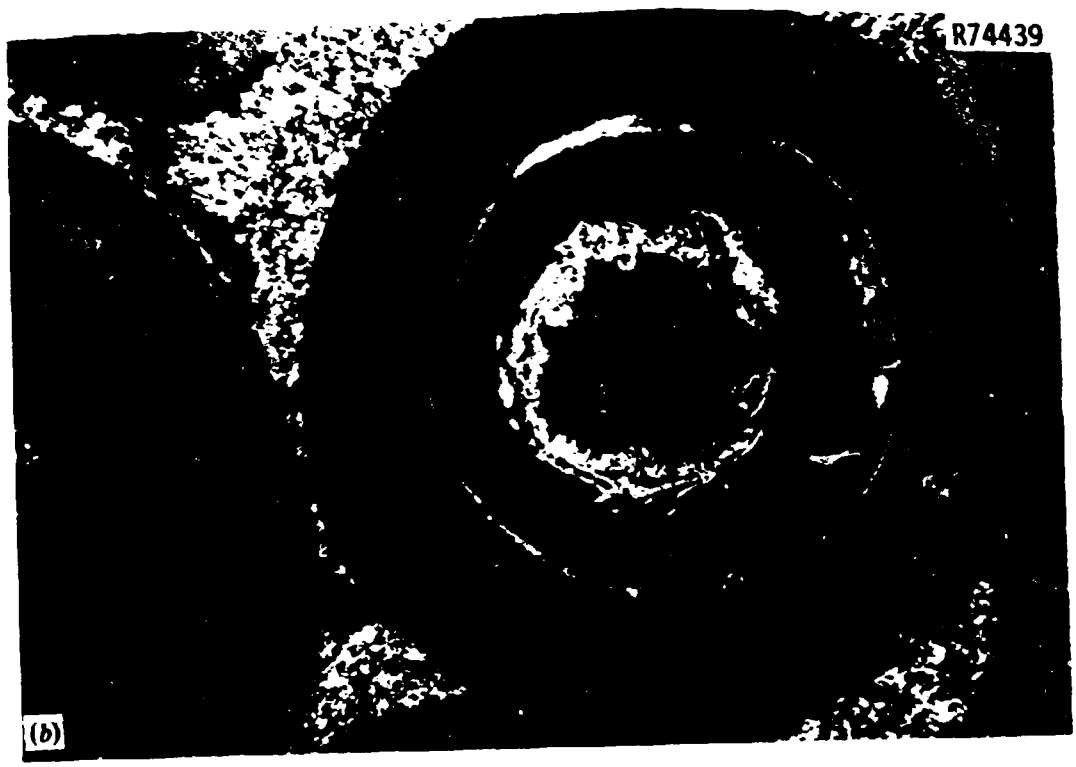

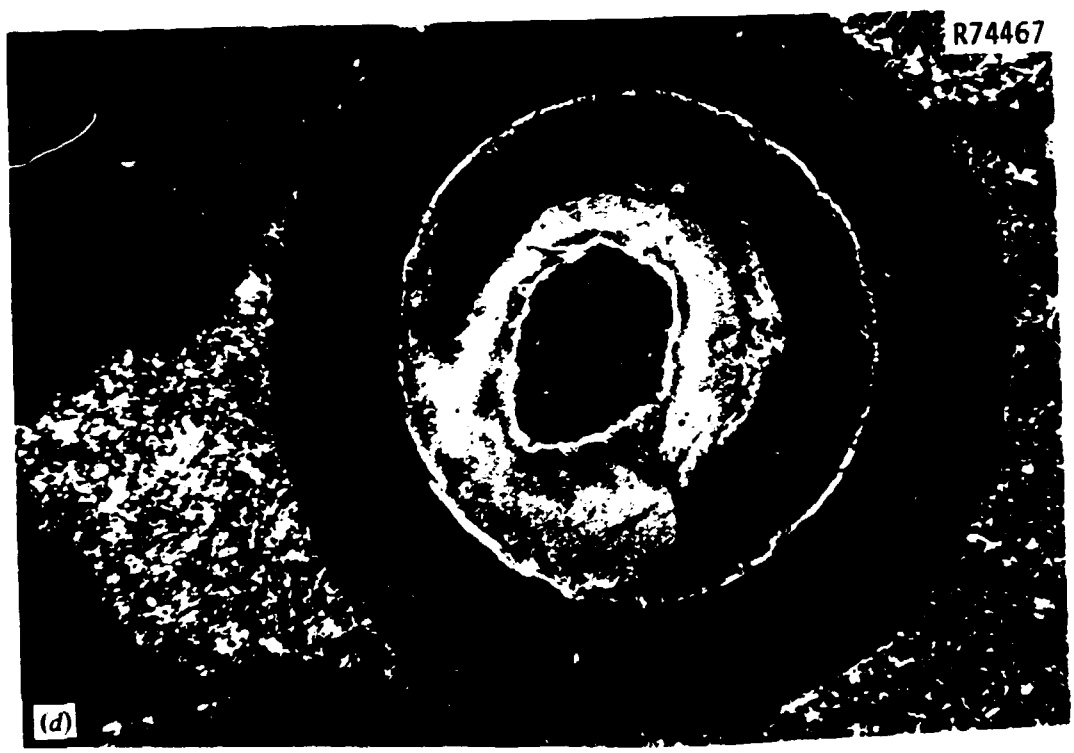

le $UC_{4.58}O_{2.04}$ Batch OR-2218-H. Rod's outer surface
rom fuel rod A-4-5, on rod's outer surface. Bright
rod A-4-9, at 2100 μm from rod's outer surface.

BLANK PAGE

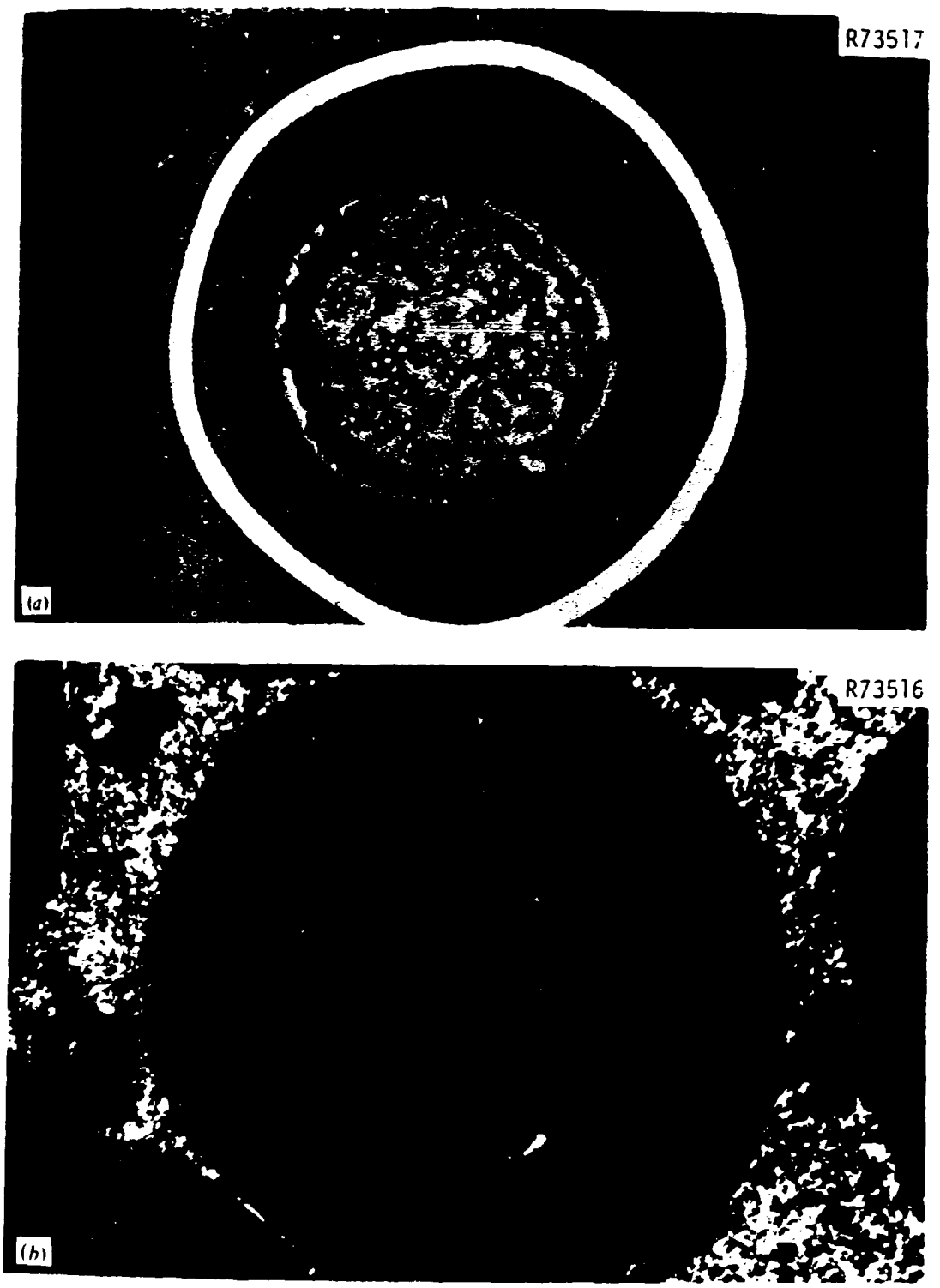

Fig. [illegible]. Representative Particle of Fissile Batch OR-2322-H [illegible] Irradiated in Fuel Rod A-3-5. 150×. The rod's outer [illegible] toward the right side of micrographs. (a) Bright field. (b) Polarized light. The particle was located 1800 μm from the rod's outer surface.

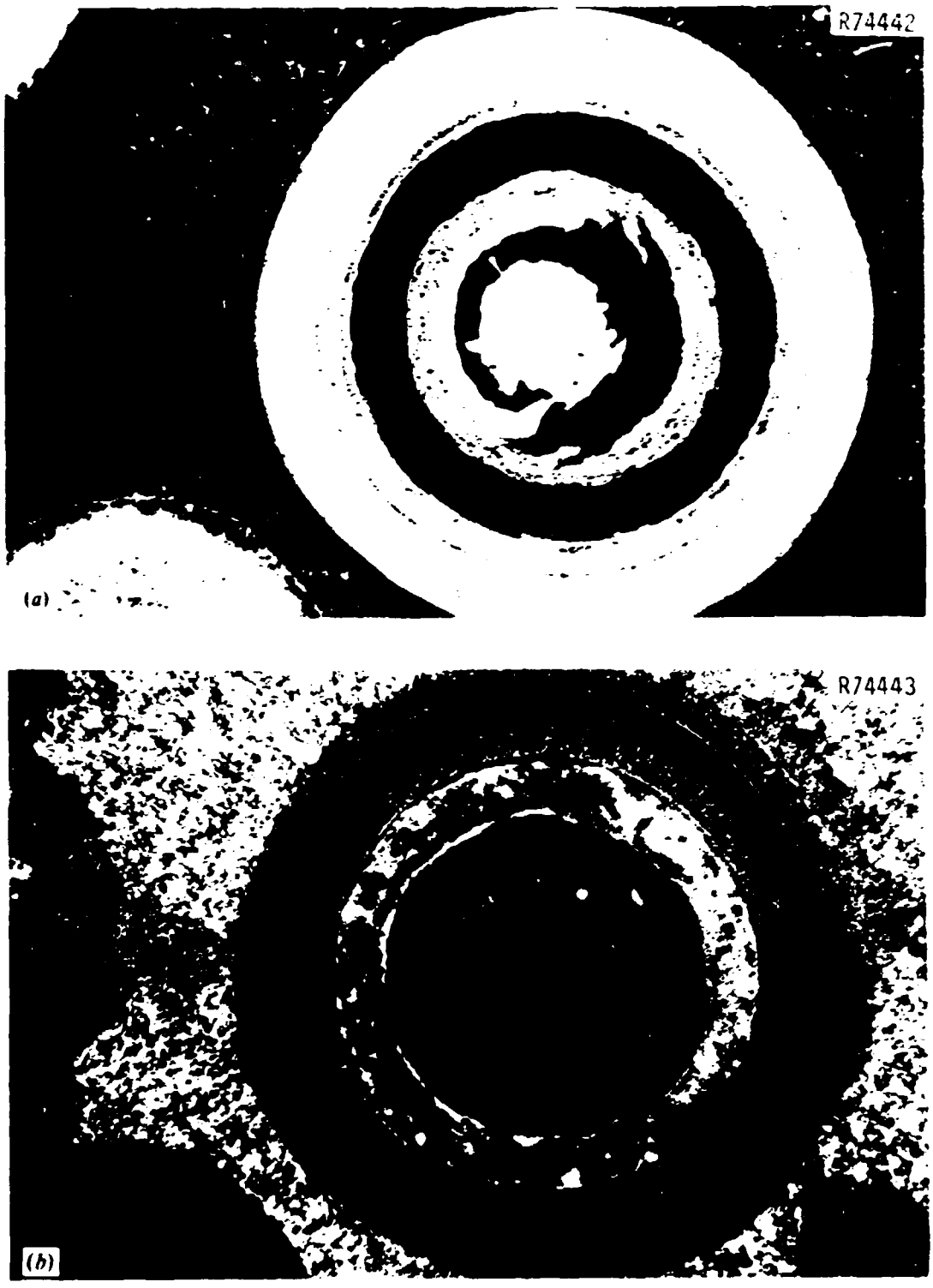

Fig. 3.25. Representative Particle from Fissile $UC_{1.12}O_{1.88}$ Batch OR-2320-H. The particle had been irradiated in fuel rod A-4-6 and was located 900 μm from the rod's outer surface, which is to the right of these micrographs. 150×. (a) Bright field. (b) Polarized light.

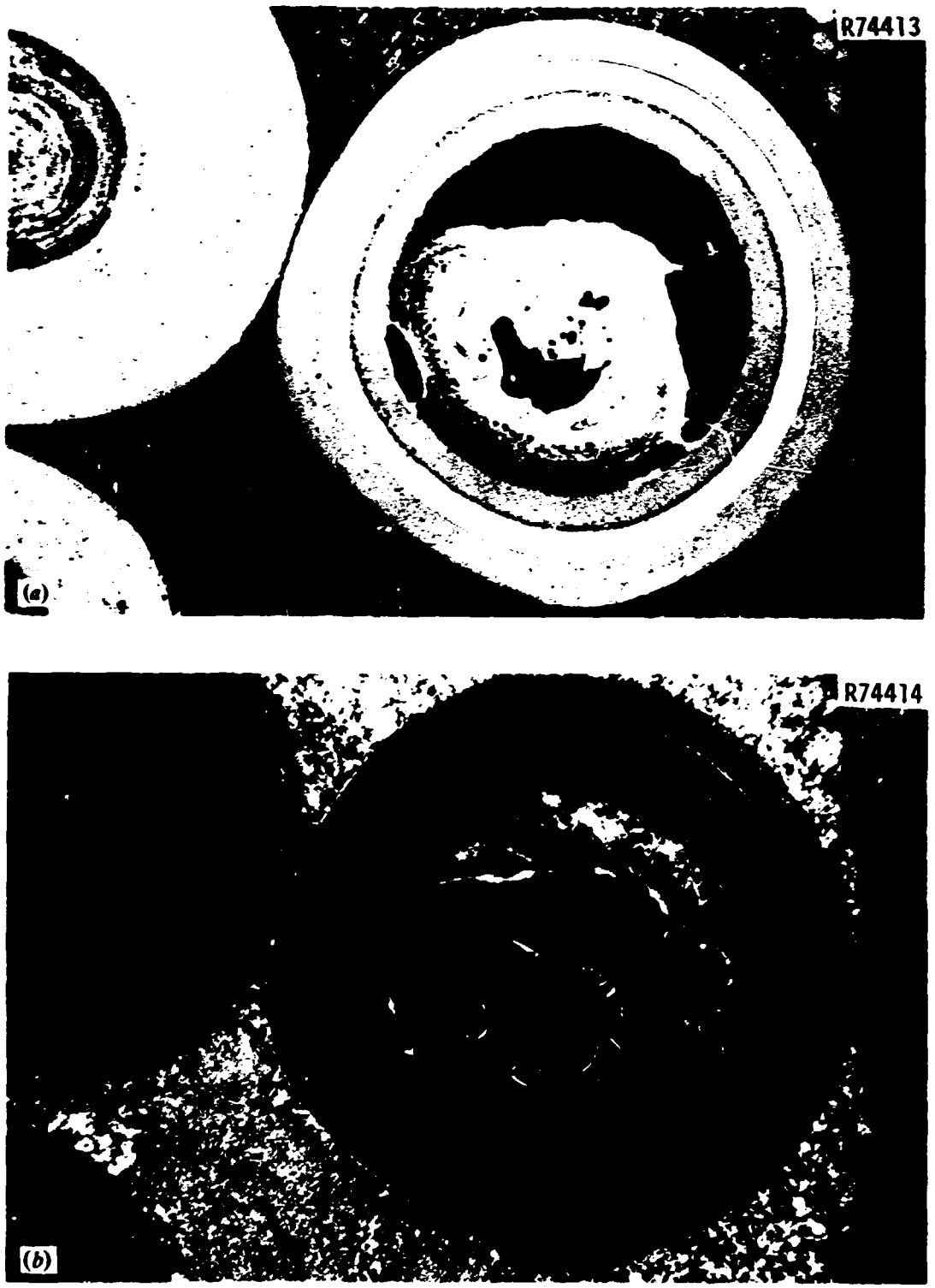

Fig. 3.26. Representative Particle from Fissile $UC_{4.63}O_{0.97}$ Batch OR-2211-H. Particle has been irradiated in fuel rod A-3-6. The particle was located on the rod's outside surface which is to the right of the micrograph. 150×. (a) Bright field. (b) Polarized light.

accumulations and SiC corrosion did not always depend on the radial position of the particle in the rod, but rather on how the kernel had densified. Most accumulations appeared on the SiC adjacent to the densified kernel. While palladium may contribute to it, much of the corrosion is believed attributable to the rare earth fission products. This same batch of particles was irradiated in HRB-9 and -10 tests[18] and examined extensively by the electron microprobe. The results of the study[11] showed that although most rare earths are retained in the kernel, an appreciable amount migrate to the SiC. In addition, chlorine, known to affect the behavior of the rare earths as well as SiC corrosion,[19] was observed in the particles.

Fuel rod A-4-7 was metallographically examined; it contained WAR $UC_{4.14}$ $O_{0.53}$ with a nominal conversion of 75%. Among the twenty particles observed no failures were seen. Typical particles are shown in Fig. 3.27. Kernels resembled the previous two rods discussed. Small fission product accumulations at the SiC coating were observed; however, the maximum penetration was less than 2 μm. The electron microprobe study[11] of this particle batch had also shown considerable rare earth migration (as well as chlorine in some particles), so the discrepancy in SiC penetration probably arose from factors other than the kernel composition.

Fuel rod A-3-7 containing WAR $UC_{3.68}$ $O_{0.01}$ particles with nominal conversion of 100% was examined. Twenty-seven particles were observed; 16 had cracked SiC coatings, but they were artifacts of the polishing. The kernel was dispersed in the densified buffer and in excess kernel carbon. Representative particles are shown in Fig. 3.28. As shown, the densified buffer was optically anisotropic under polarized light. Fission product accumulations were observed on the cold side of the particles, as was corrosion, which penetrated about 5 μm. Other results[11] indicate that rare earth fission products corroded the SiC.

Another 100%-converted WAR particle type with a stoichiometry of $UC_{2.61}$ $O_{0.16}$ was contained in fuel rod A-4-1. It differed from the previous 100%-converted WAR particle in that its kernel density was higher (see Tables 1.1 and 1.4). Only three particles were observed in which

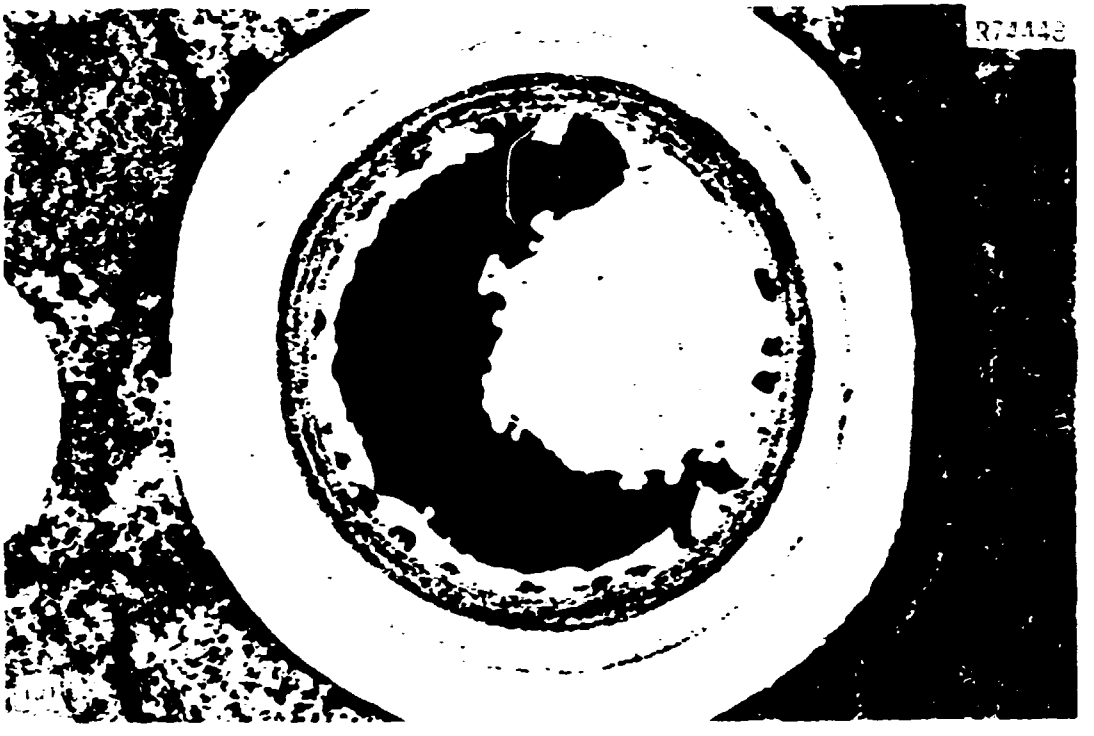

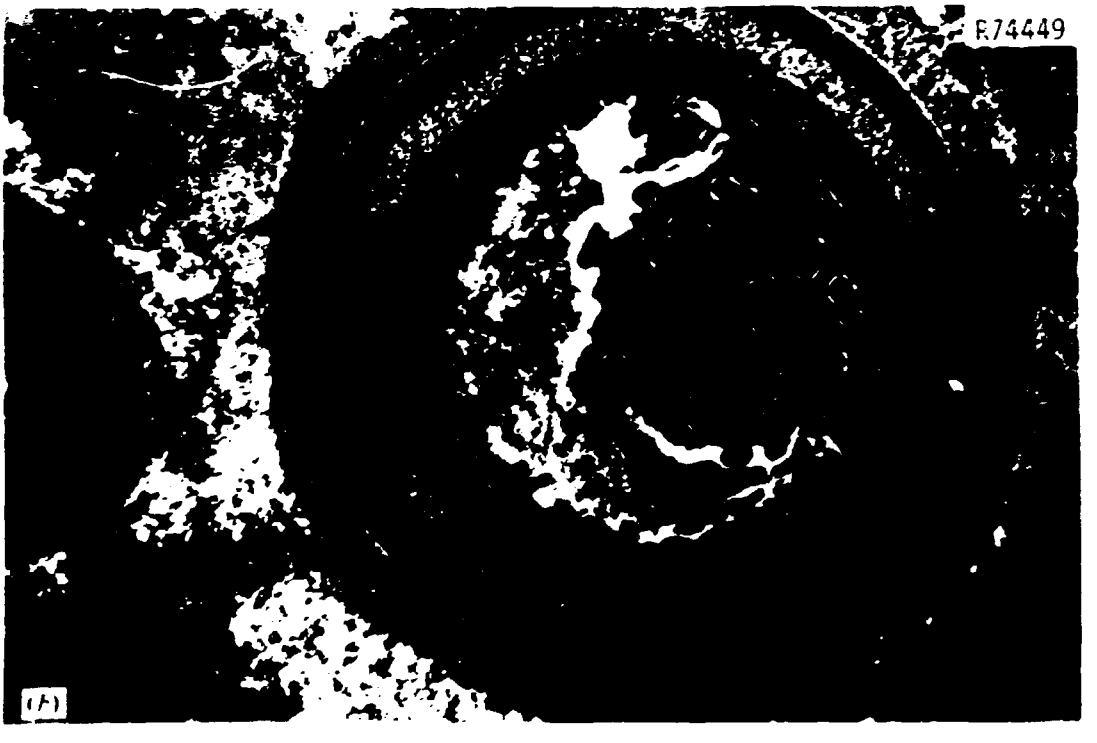

Fig. 5.27. Representative Particle from Fissile $(U_{0.15}Th_{0.85})O_{1.95}$ Batch [illegible]. The particle was irradiated in test rod A-5-7. The [illegible] is on the rod's outer surface, which is to the right of the [illegible]. (A) Bright field. (B) Polarized light.

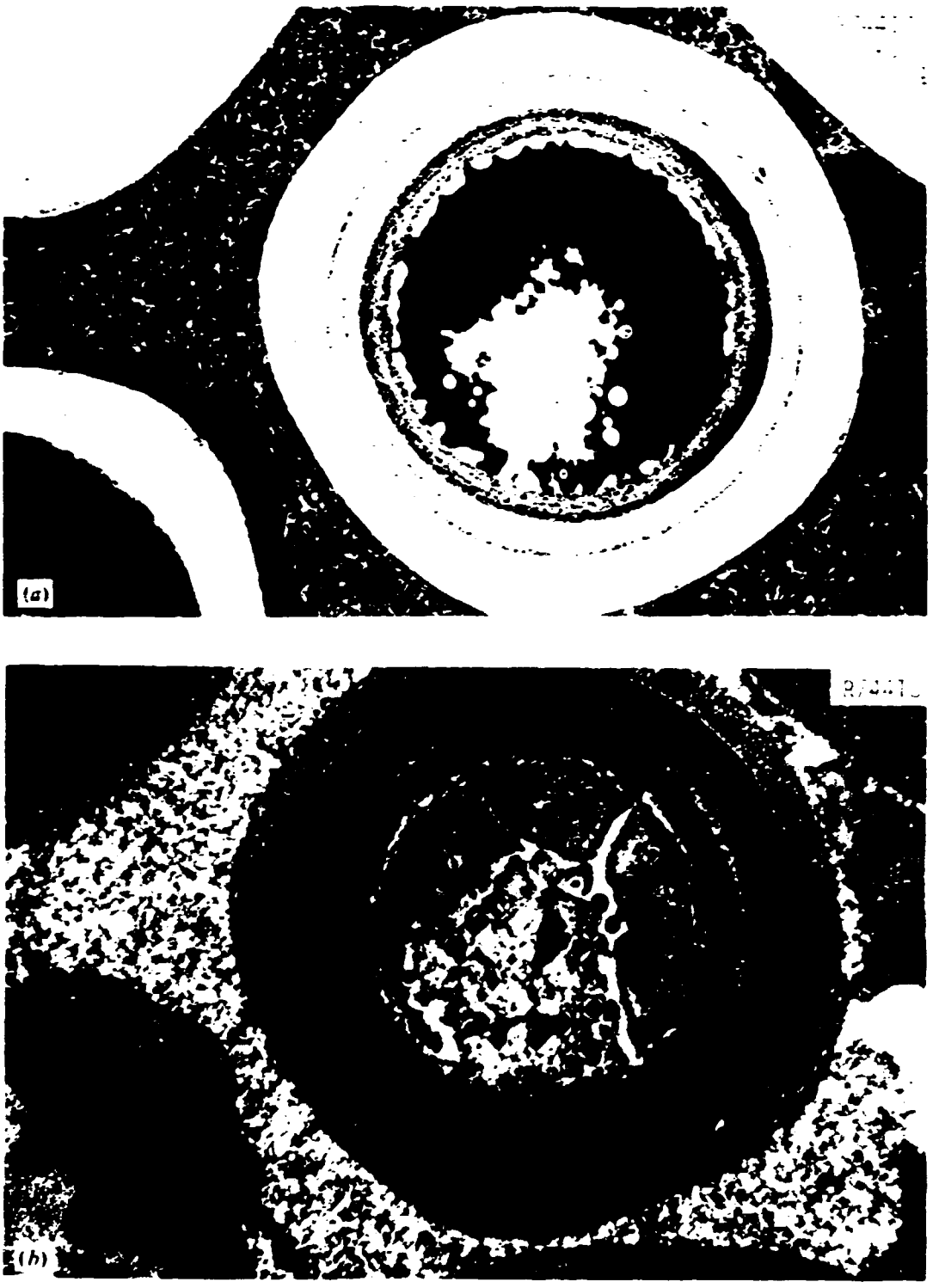

Fig. 3.28. Representative Particle from Fissile [illegible] Batch OR-2208-H. Particle had been irradiated in rod [illegible] from the rod's outer surface, which is to the right of these micrographs. 150×. (a) Bright field. (b) Polarized light.

[illegible] not fallen out during metallographic preparation. Representative particles are presented in Fig. 3.29. All the particles examined appeared to be in excellent condition with no apparent SiC [illegible] or fission product accumulations. This same particle batch, [illegible] irradiated in HRB-9 and -10 showed massive rare earth fission product migration and high failure fractions. We should point out that this rod was at the very end of the capsule; there the operating temperatures were rather low. Evidently they were low enough that the rare earth fission products did not corrode the SiC coating. The performance of these and other 100%-converted WAR particles did not appear to differ, save the kernels were denser.

A metallographic examination was made of fuel rod A-4-8 containing [illegible] (Th,U)O_2 fissile particle. A total of 32 particles were observed in the sample; no broken SiC coatings — no failures — were seen. A typical particle is shown in Fig. 3.30. Eight particles had observable [illegible] with a maximum migration of 10 μm. The kernel had a typical [illegible] appearance with fission gas bubbles and metallic inclusions present. No fission product accumulation or SiC corrosion was observed.

A VSM UC$_2$ particle from fuel rod A-3-1 was examined. Of the thirty-eight particles observed, no broken SiC coatings — no failures — were seen. A typical particle is shown in Fig. 3.31. The kernels resembled typical UC$_2$ with some indications of plasticity during irradiation. Graphitization of the iLTI coating on the cold side was observed in 15 particles, which were always located on the inner half of the rod that is, in areas of higher temperature. Very slight corrosion — less than 2 μm — of the SiC coating was seen where iLTI graphitization had occurred. We should point out that this rod, like A-4-1 previously discussed, was at the very end of the capsule, where the operating temperatures are typically lower.

Metallography was also performed on fuel rod A-3-8, which contained WAR fissile particles with a composition of $UC_{1.71}N_{0.14}$. A typical particle is shown in Fig. 3.32. We believe that lack of oxygen in the kernel inhibited any amoeba migration. However, this particle type

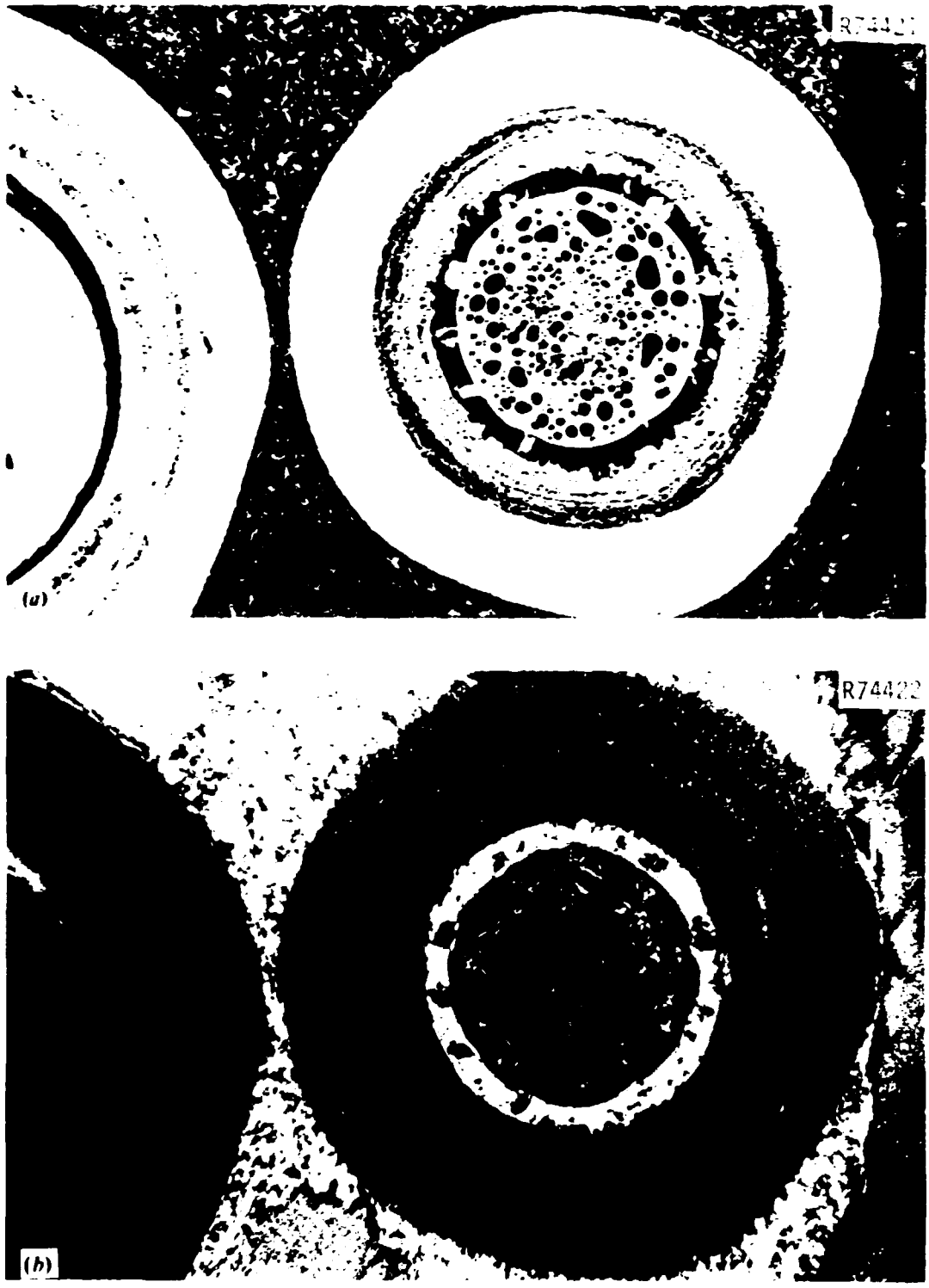

Fig. 3.29. Representative Particle from Fissile UC$_{1.90}$ Batch OR-2121-H. Particle had been irradiated in fuel rod A-4-1. The particle was located on the rod's outer surface, which is to the right of these micrographs. 150×. (a) Bright field. (b) Polarized light.

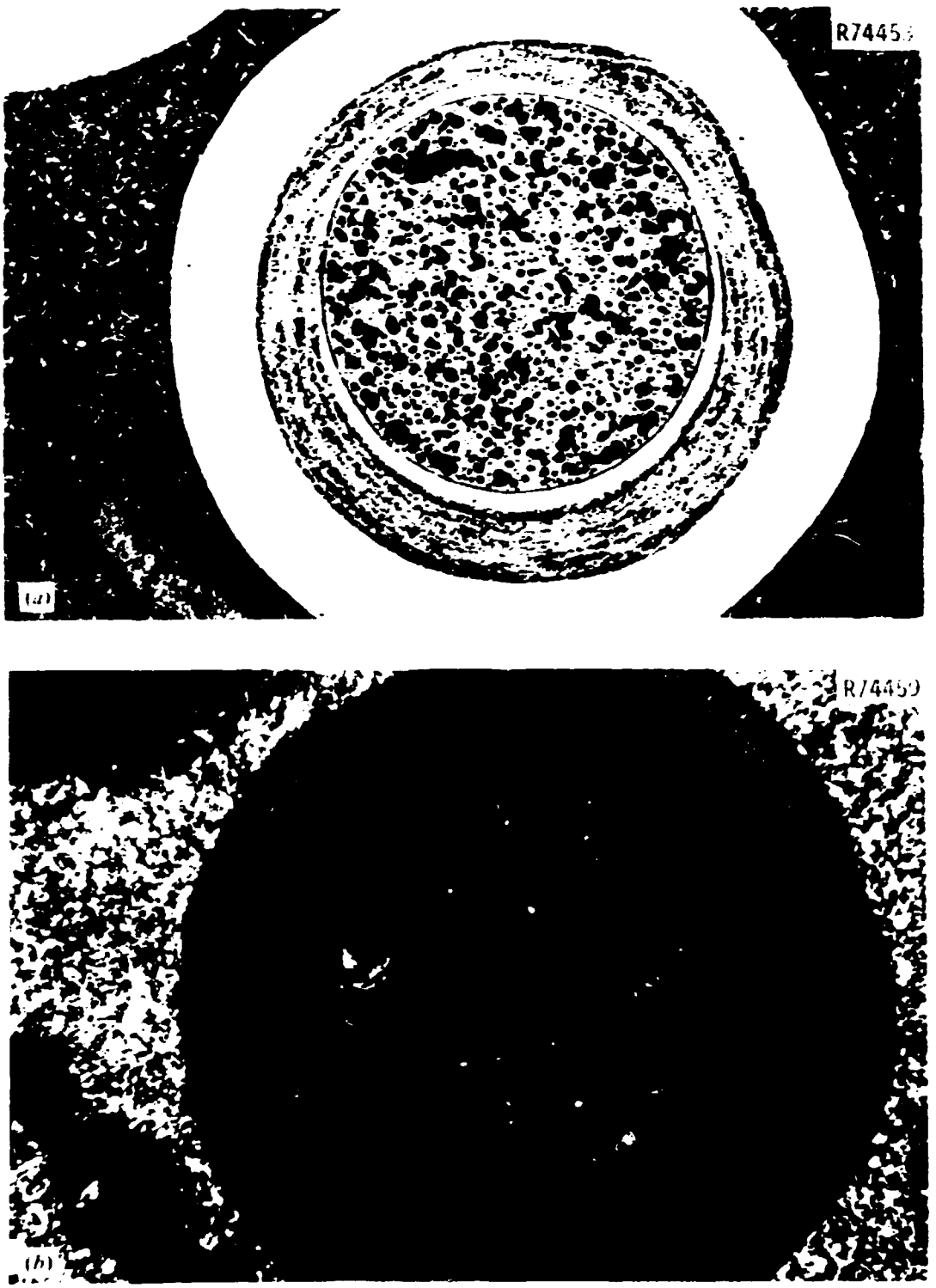

Fig. 3.30. Representative Particle from Fissile Batch OR-2321-H, Which Consisted of Sol-Gel ($Th_{.}U_{.}$)O_2. The particle had been irradiated in fuel rod A-4-3 and was located on the rod's outer surface. The rod's outer surface is to the right of these micrographs. Note the amoeba of the kernel up the temperature gradient. 100×. (a) Bright field. (b) Polarized light.

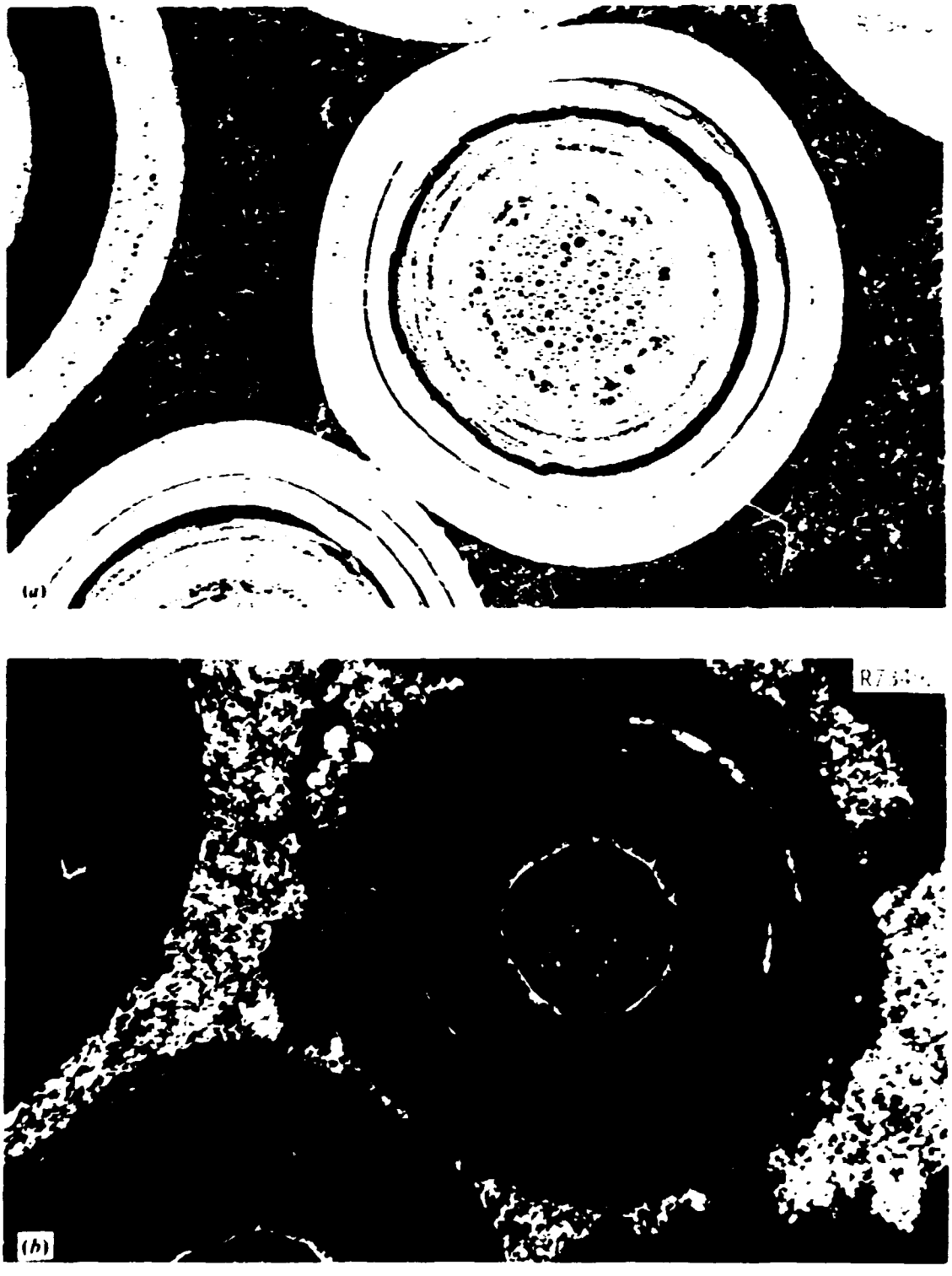

Fig. 3.31. Representative Particle from Fissile Particle Irradiation Experiment (FSM FC-1) Irradiated in Fuel Rod X-3-L. [illegible] located 3600 μm from the rod's outer surface. Note the graphitization of the IPyC on the cold side of the particle. The rod's outer surface is toward the right side of micrographs. (a) Cr Bright Field. (b) Polarized Light.

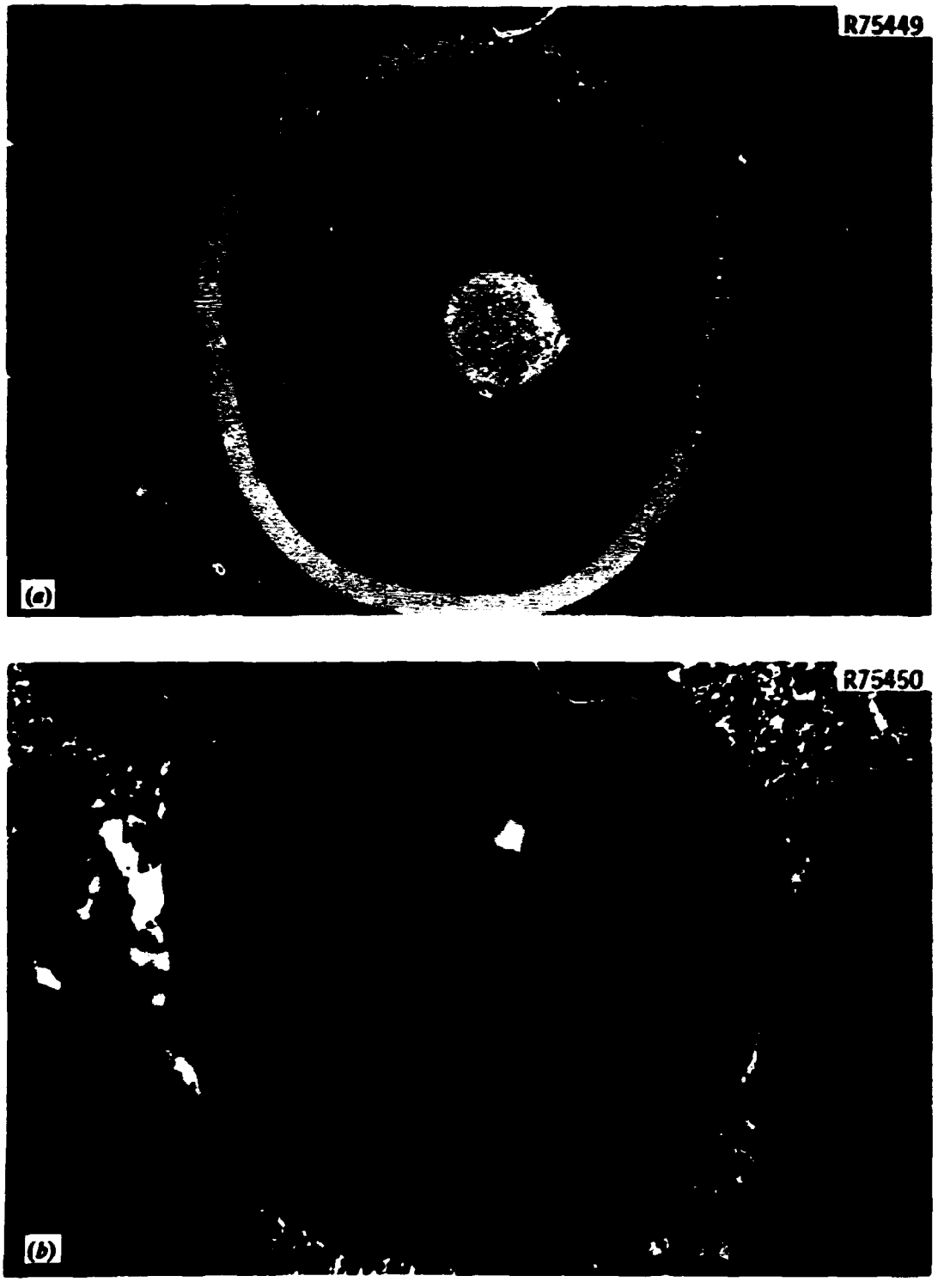

Fig. 3.32. Representative Particle from Fissile Batch OR-2219-H ($UC_{3.68}N_{0.53}$). Irradiated in fuel rod A-3-8. The particle was located 1600 μm from the rod's outer surface. The rod's outer surface is to the right of the micrographs. 150×. (a) Bright field. (b) Polarized light.

suffered from the same problem as does a 100%-converted WAR particle — fission product migration down the temperature gradient with subsequent accumulation at the SiC. Of twelve particles observed, accumulations located on the inner half of the rod were visible in about half of the particles. Penetrations of the SiC, possibly by rare earth fission products or by palladium, appeared to be 1–2 μm. In HRB-9 and -10, these same particles exhibited massive rare earth fission product migration down the temperature gradient and, in some cases, subsequent SiC failure. We expect that analysis of the rods from the high-temperature region, Magazine B, will show similar results.

3.5.3 Fertile particles

Nearly all the Biso-coated ThO_2 fertile particles (see Table 1.2) were examined metallographically, with the exception of batch OR-1849-HT. This batch was contained in fuel rod B-3-7 only, and we decided to do an IMGA analysis and perform metallography on the loose particles from this rod later. Typical particles from each batch are presented in Figs. 3.33 through 3.47. Generally, the metallographic examination revealed very few microstructural differences among the particle batches, although their coating properties varied. All the particle types appeared to have performed well, with one exception.

In particle batch J-481, examined in fuel rod A-3-1, 9% of the particles lacked a buffer coating (Fig. 3.48). Evidently this problem had occurred during the coating process. In addition, in 4% of the particles the coatings had cracked and the kernels appeared to have converted to carbide (Fig. 3.49).

While these results indicate a poorly coated batch of particles, other results show that the bad particles were not representative of batch J-481. The bad particles were observed in one metallographic cross section only. On the other hand, eight other rods containing batch J-481 particles were metallographically examined and no bad particles were observed. In addition, seven more rods, which contained batch J-488 particles, were examined and no bad particles were observed. Batches J-481 and J-488 were coated together, but J-488 was annealed while

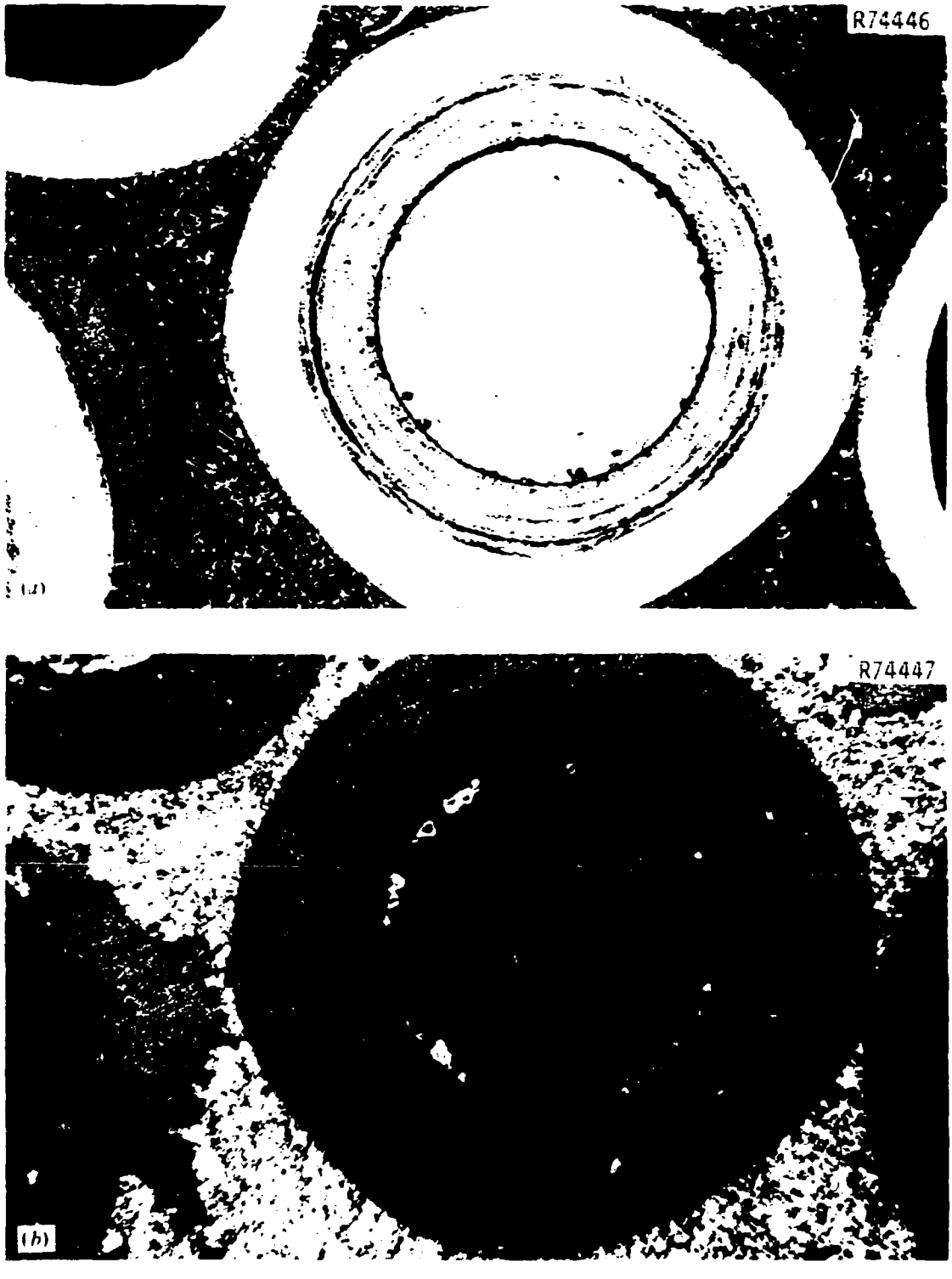

Fig. 3.33. Typical Biso-Coated ThO Particle from Batch ORNL-2265-III Irradiated in Fuel Rod A-5-6. 125×. (a) Bright field. (b) Polarized light.

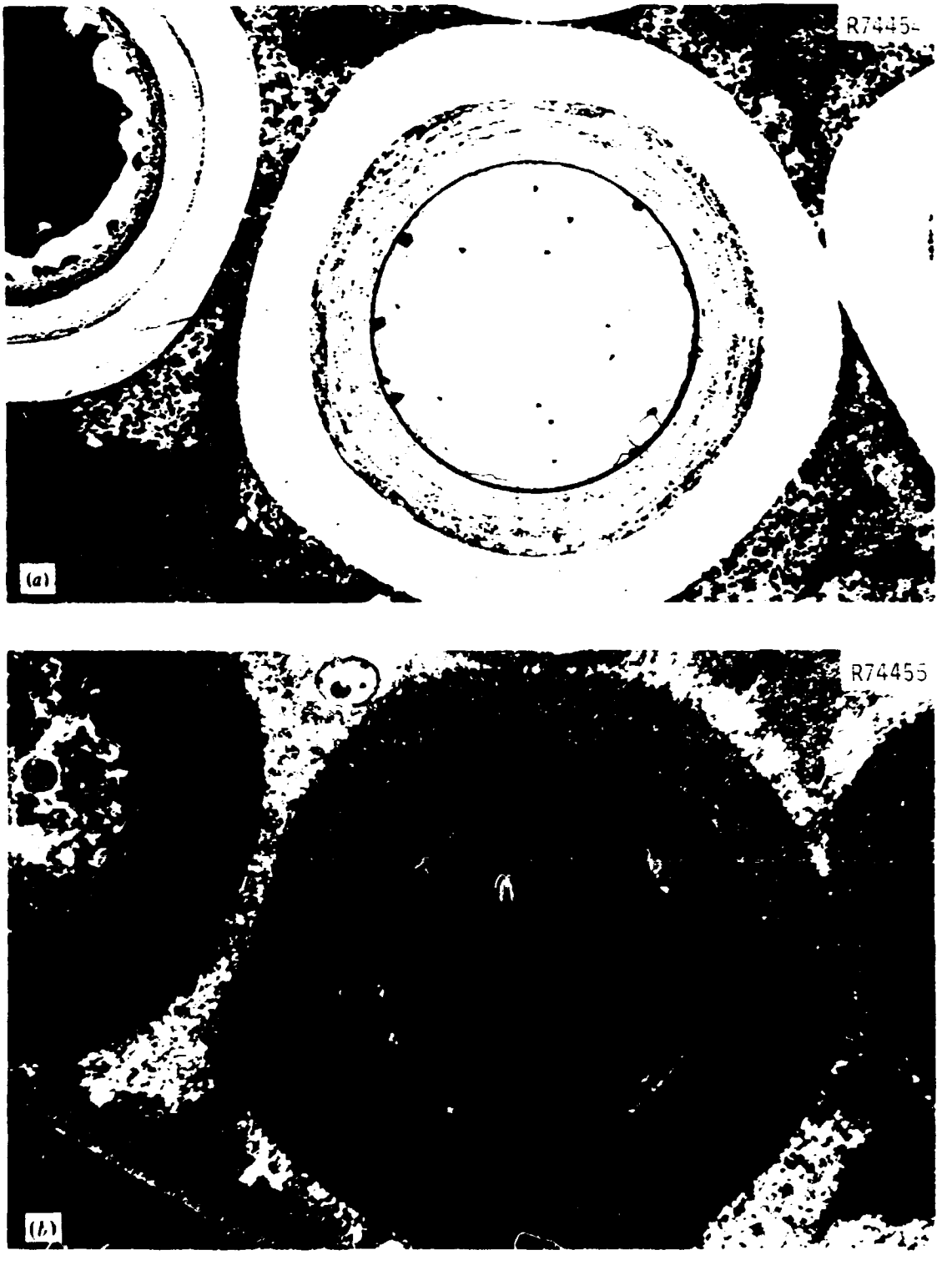

Fig. 3.34. Typical Biso-Coated ThO$_2$ Particle from Batch OR-2262-BT Irradiated in Fuel Rod X-[illegible]. 125×. (a) Bright Field. (b) Polarized Light.

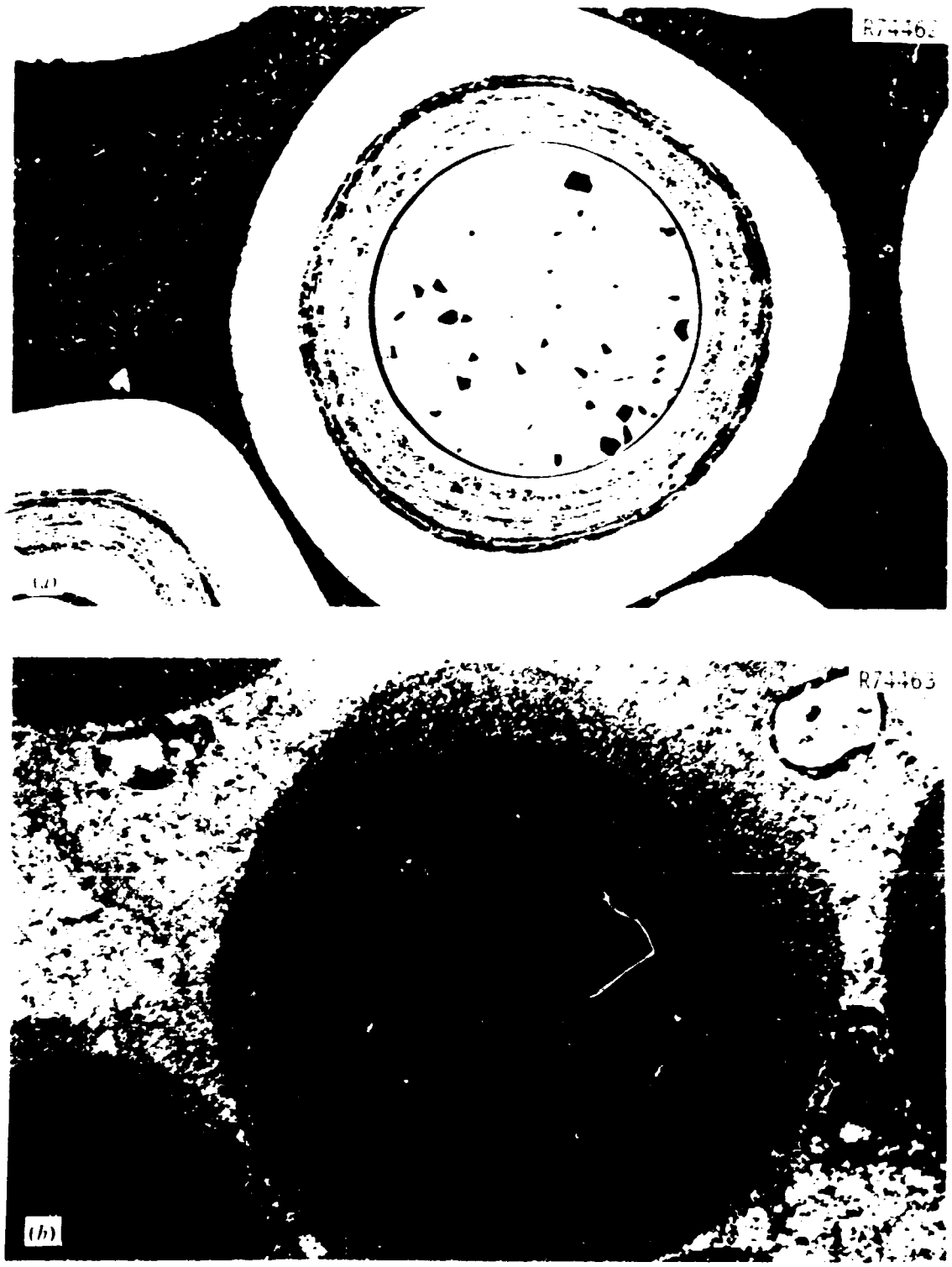

Fig. 3.3. Typical Biso-Coated ThO Particle from Batch ORNL-1261-III Irradiated in Fuel Rod A-1-8. Exp. (a) Bright Field, (b) Polarized Light.

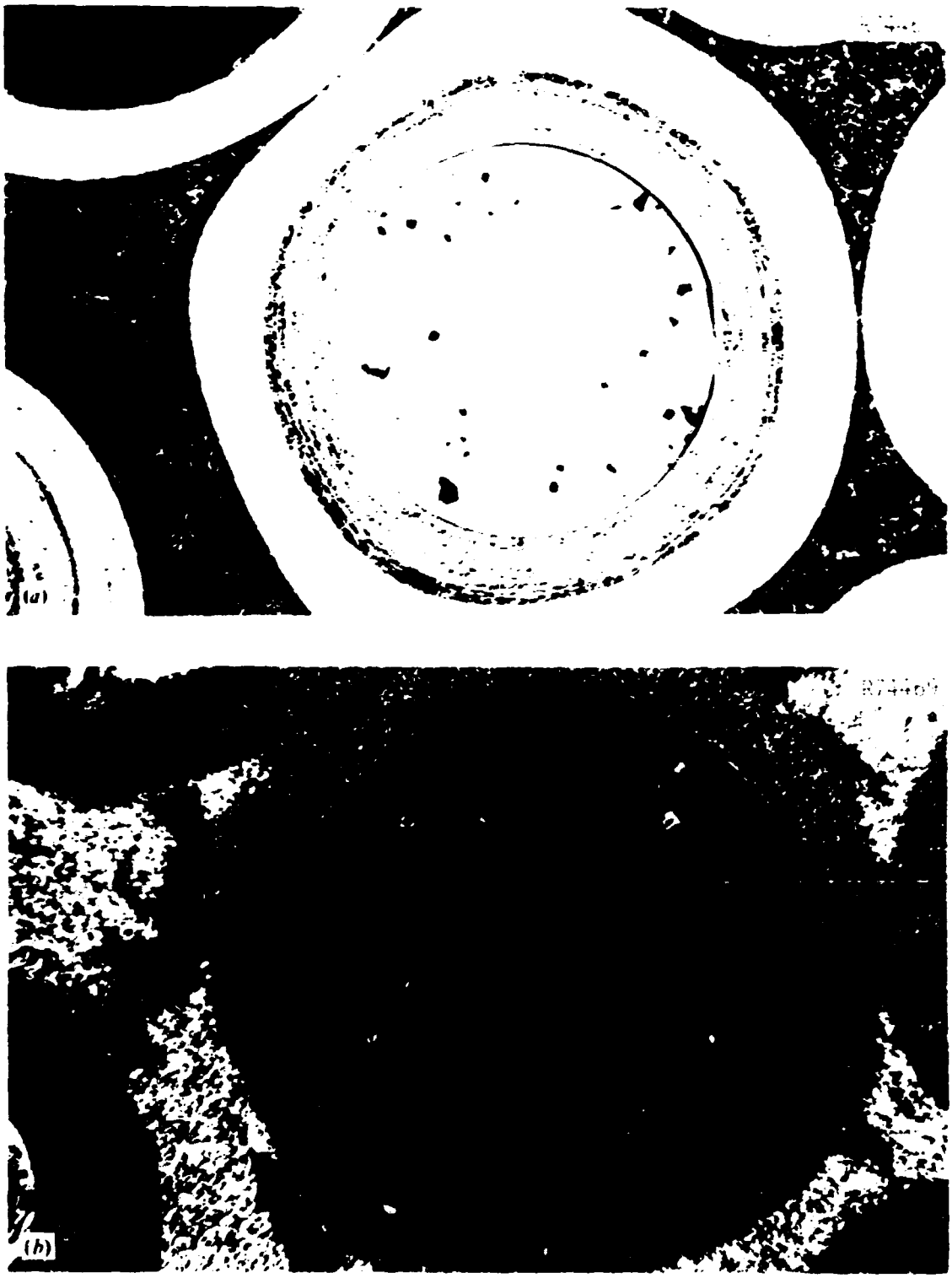

Fig. 3.86. Typical Biso-Coated UO2 Particle from Batch ORNL-2264-67 Irradiated in Fuel Rod Y-[illegible]. (a) Bright Field. (b) Polarized Light.

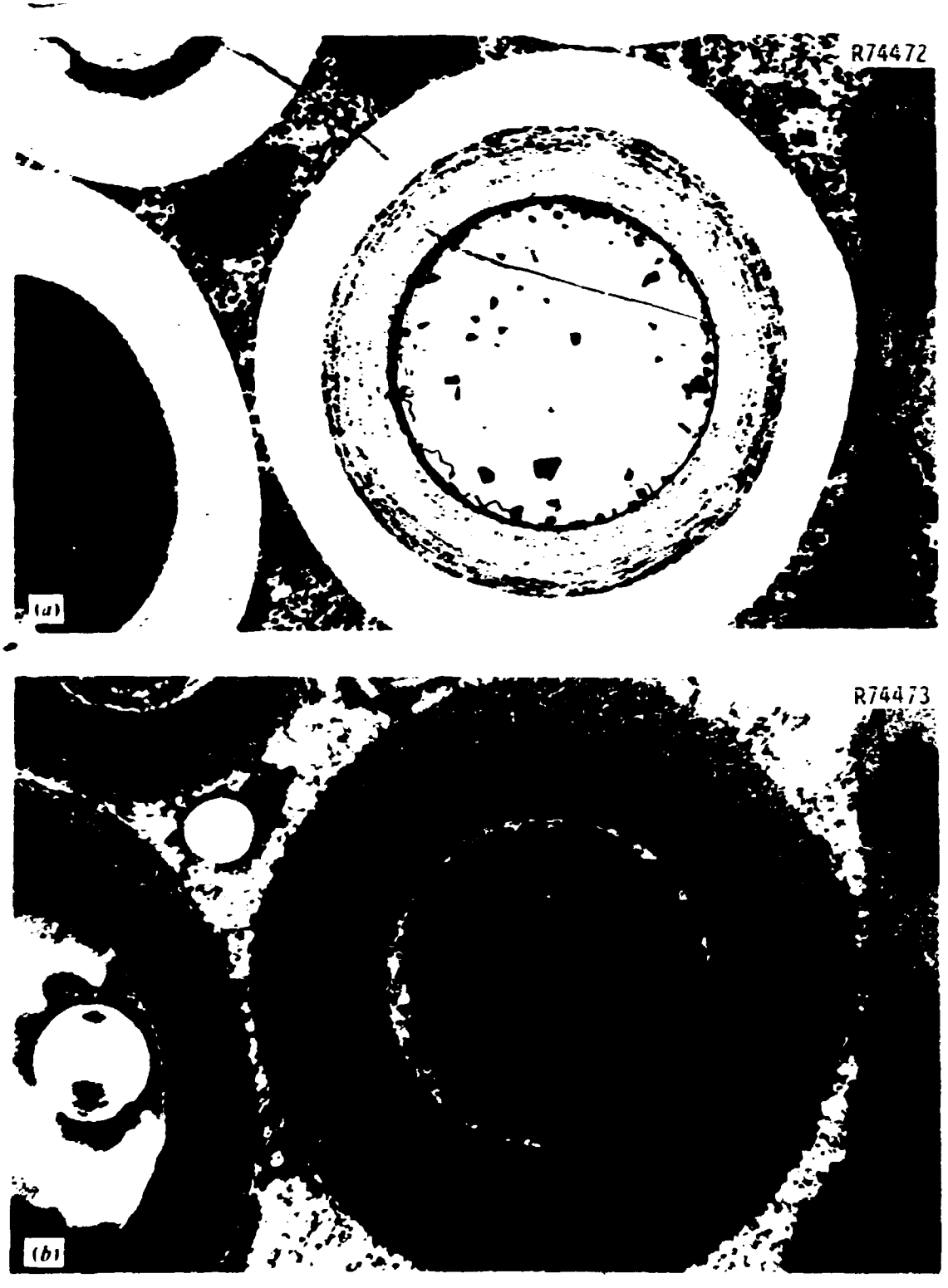

Fig. 3.5. Typical Biso-Coated ThO Particle from Batch OR-3263-81 Irradiated in Fuel Rod A-4-10. 125×. (a) Bright Field. (b) Polarized Light.

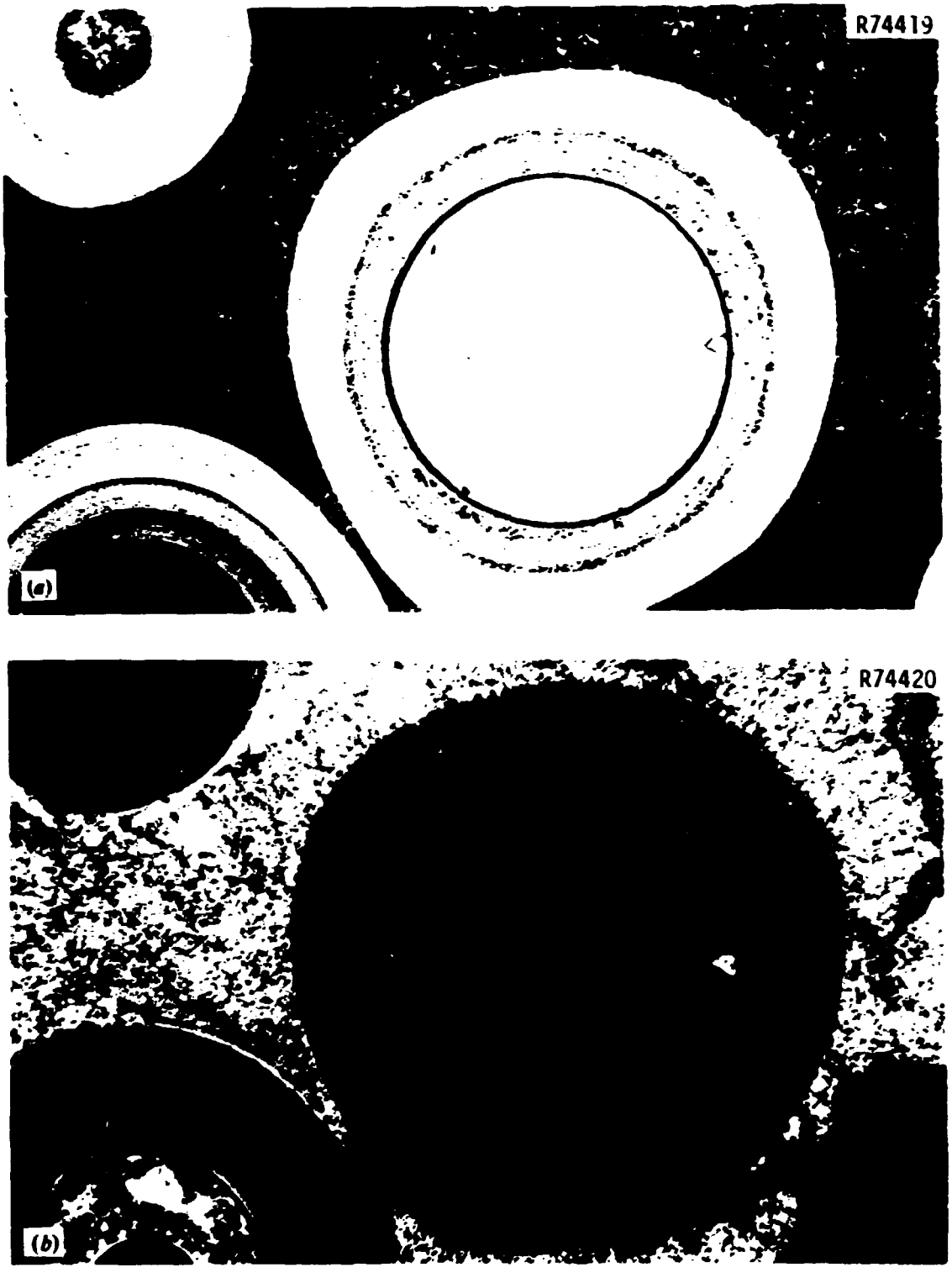

Fig. 3.38. Typical Biso-Coated ThO_2 Particle from Batch J-488 Irradiated in Fuel Rod A-3-7. 125×. (a) Bright field. (b) Polarized light.

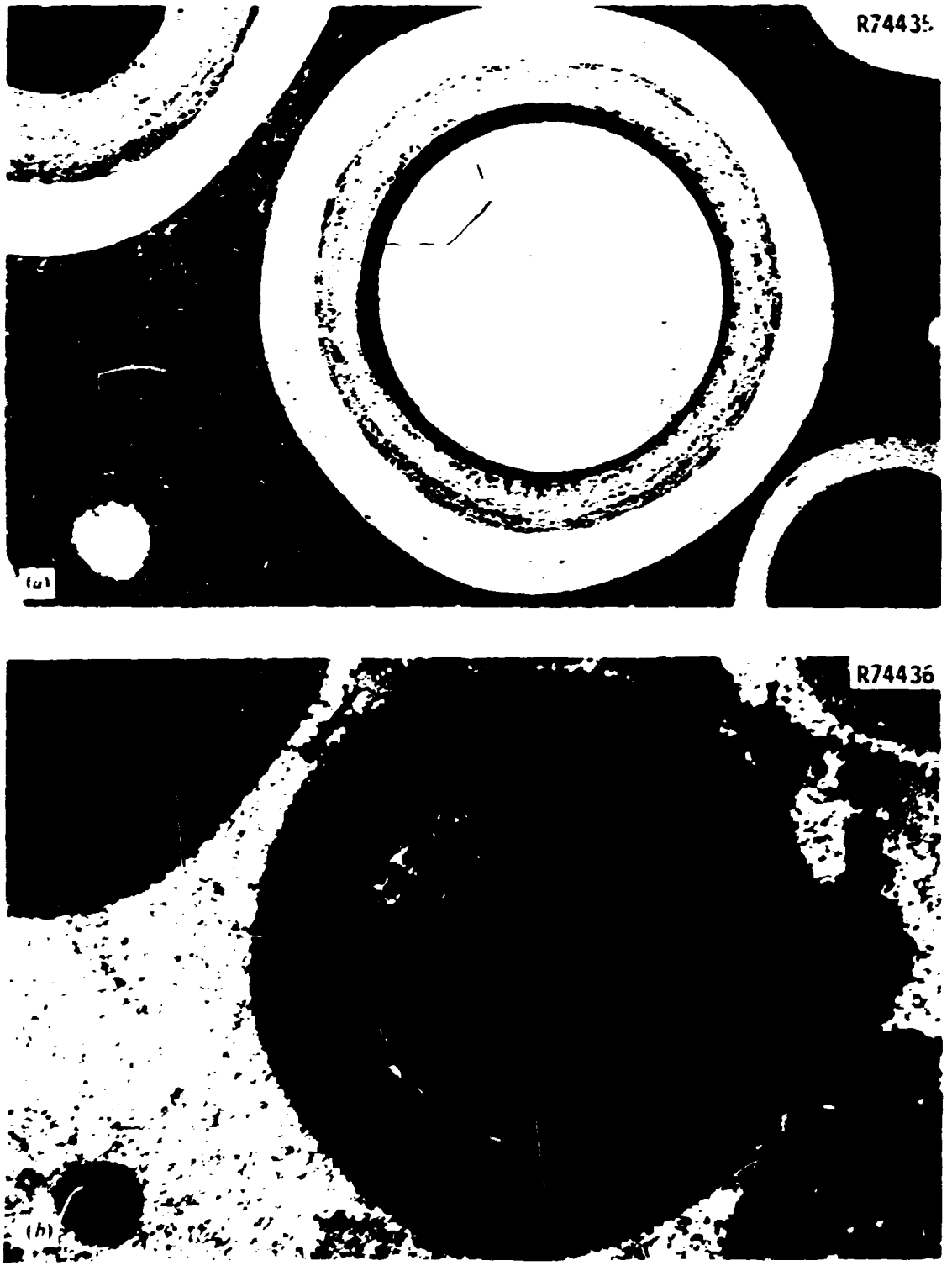

Fig. 3.39. Typical Biso-Coated ThO$_2$ Particle from Batch J-489 Irradiated in Fuel Rod A-4-2. 1250×. (a) Bright field. (b) Polarized light.

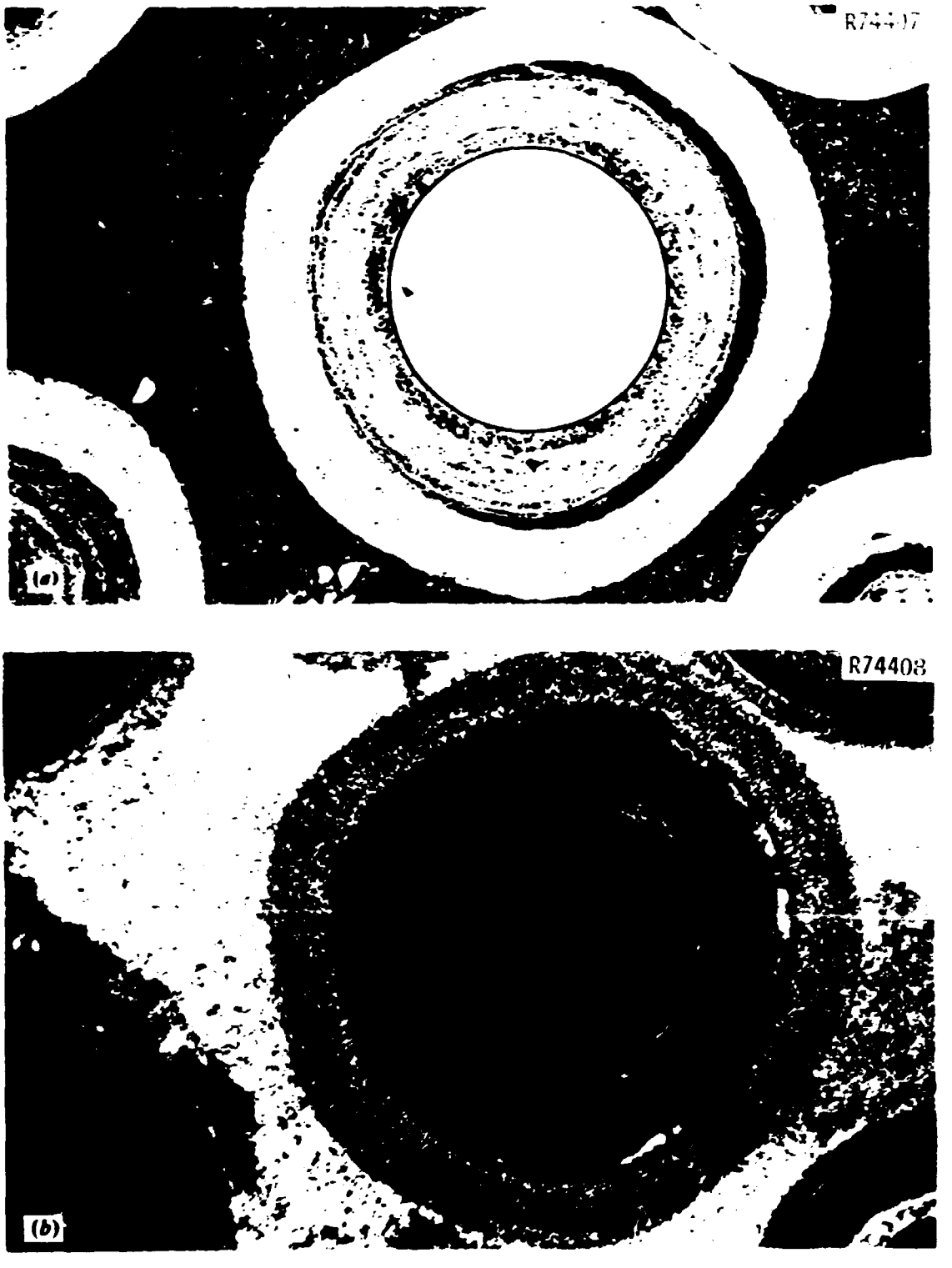

Fig. 3.40. Typical Biso-Coated ThO Particle from Batch 4590 Irradiated in Fuel Rod A-3-2. 125×. (a) Bright field. (b) Polarized light.

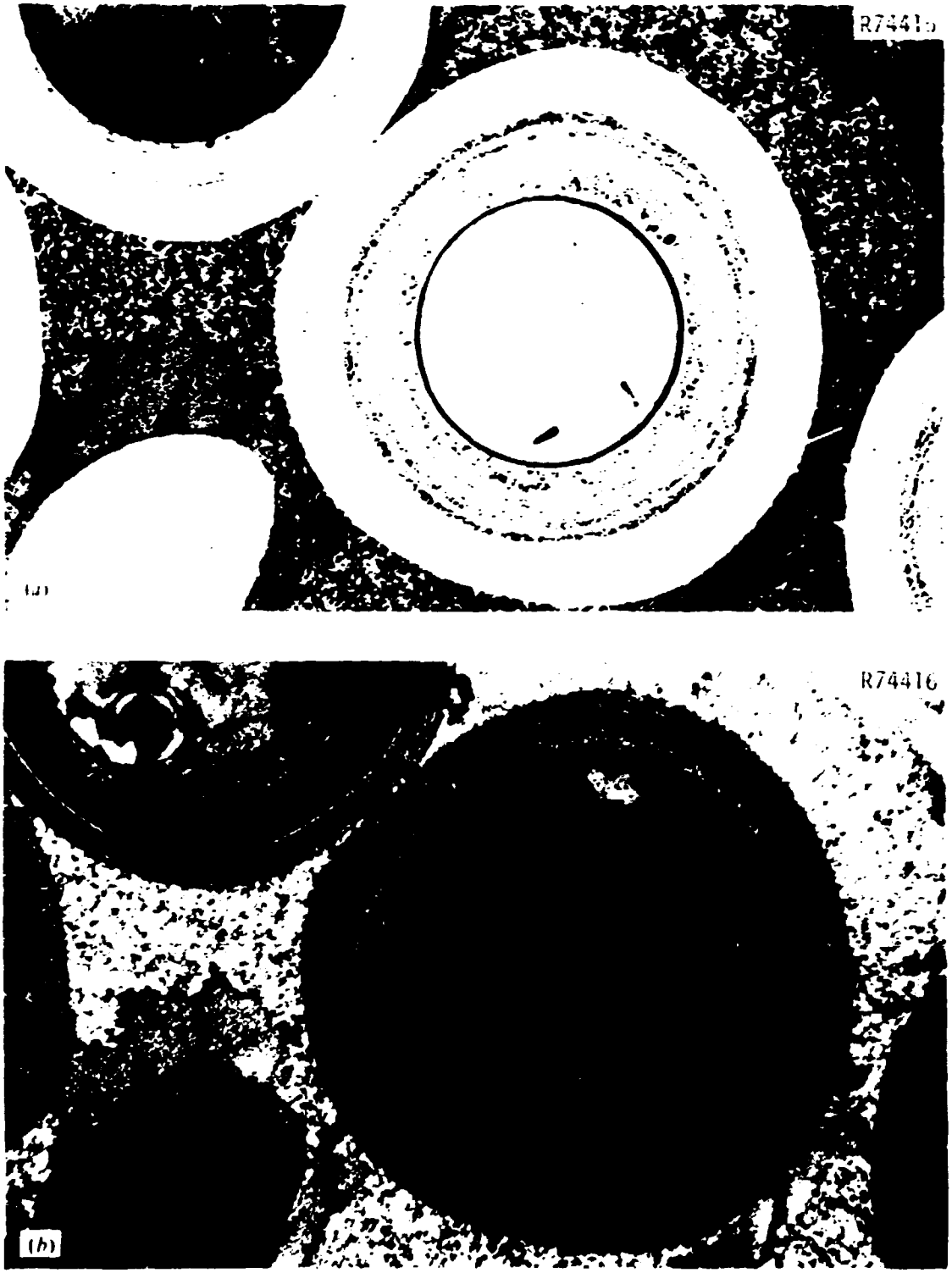

Fig. A.11. Typical Bias-Coated TRO Particle from Batch J-491 Irradiated in Run [illegible]. 125×. (a) Bright Field. (b) Polarized Light.

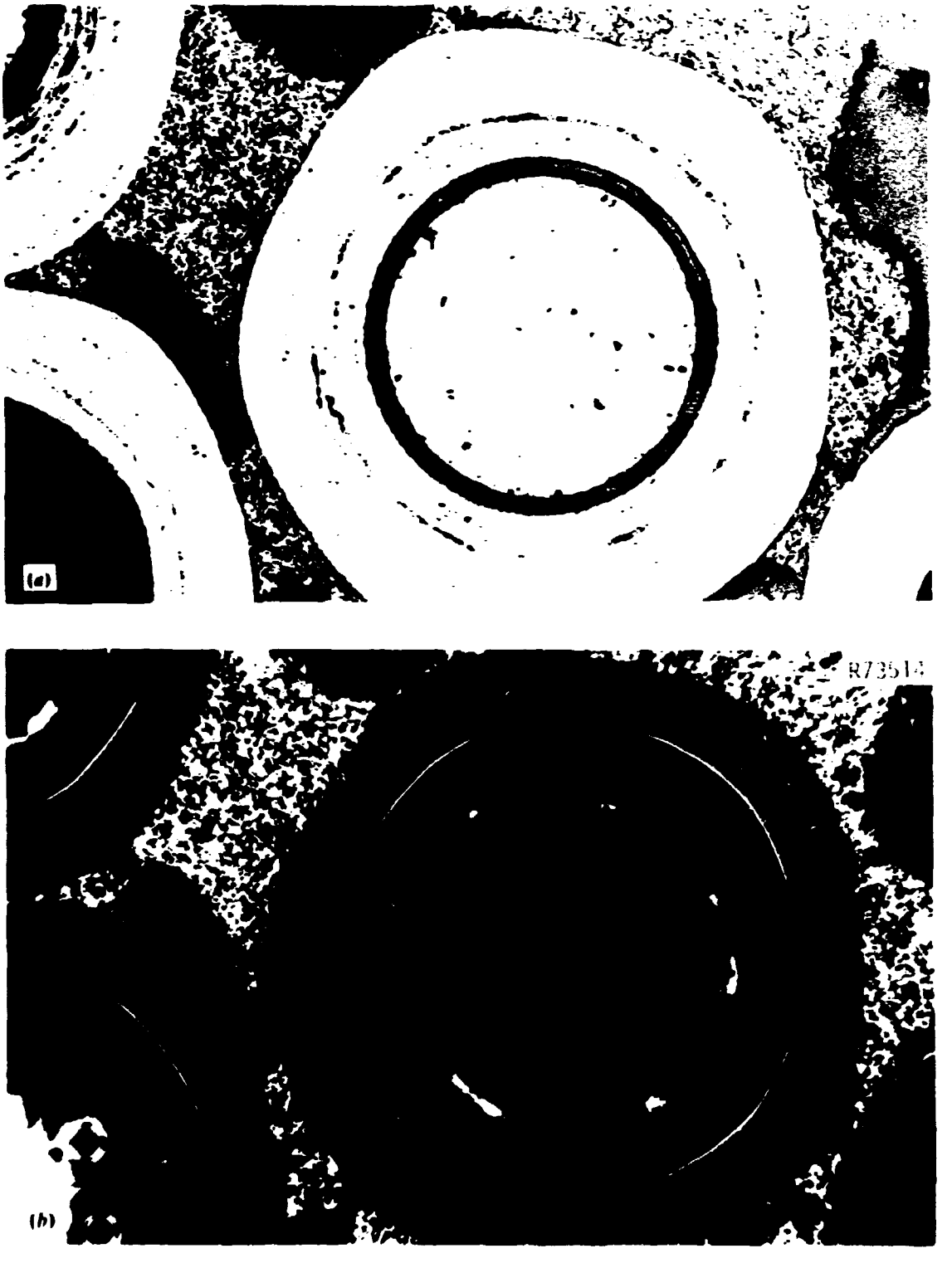

Fig. 3.6?. Typical Biso-Coated ThO Particle from Batch [illegible] Irradiated in Fuel Rod A-3-5. 1?5×. (a) Bright Field. (b) Polarized Light.

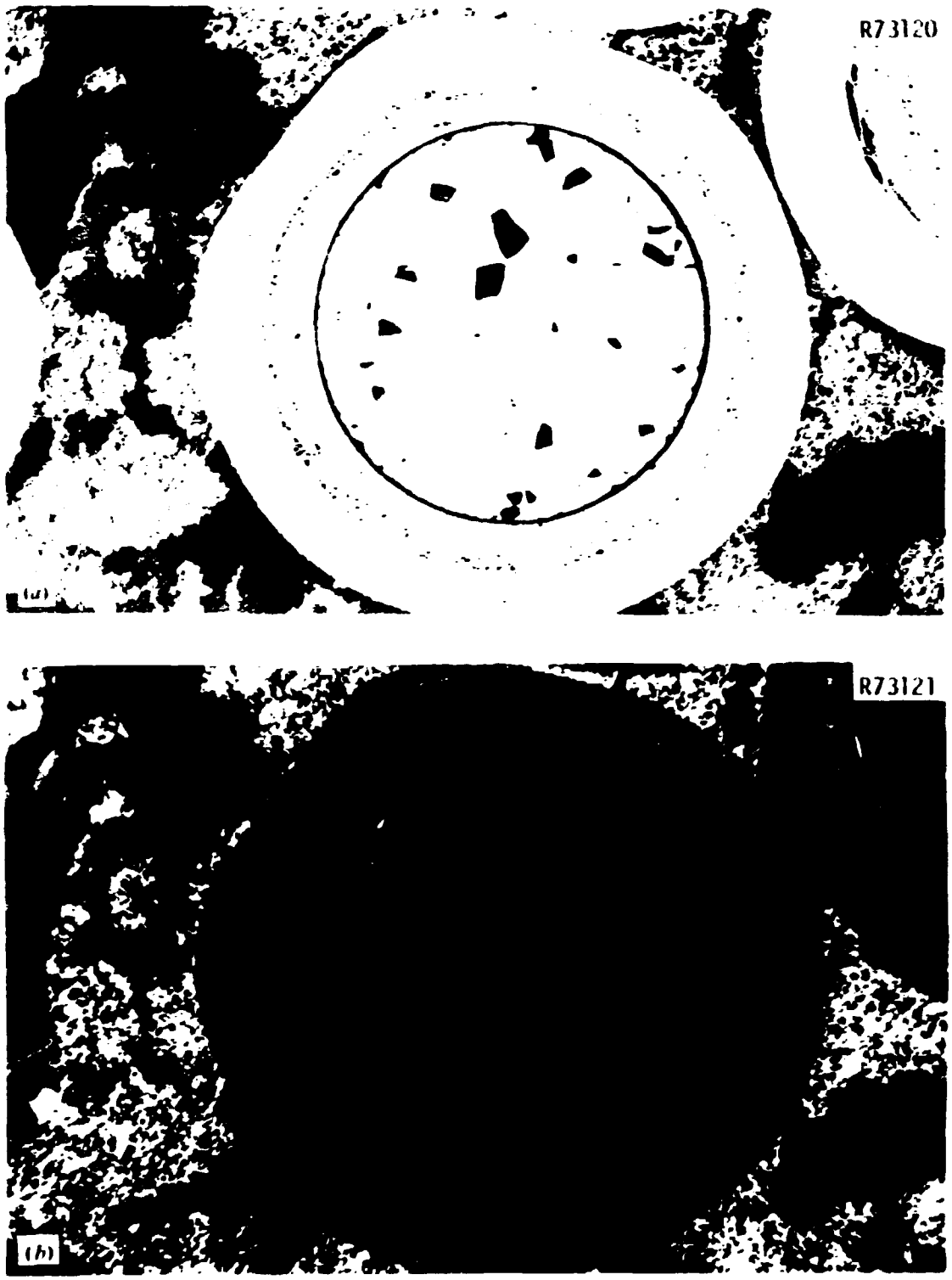

Fig. 3.43. Typical Biso-Coated ThO Particle from Batch J-681 Irradiated in Fuel Rod B-1-6. 1750×. (a) Bright Field. (b) Polarized Light.

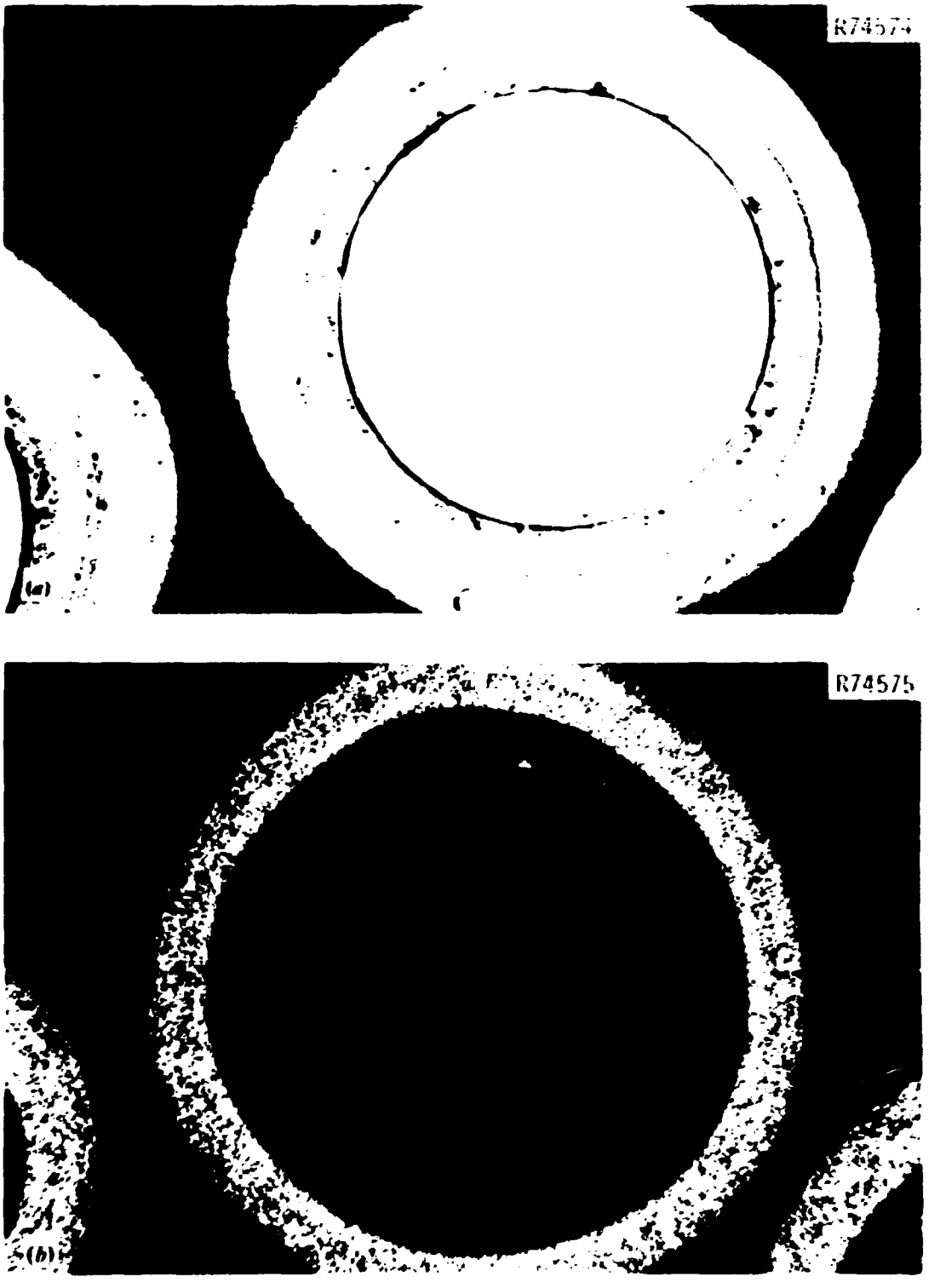

Fig. 3.44. Typical Biso-Coated ThO_2 Particle from Batch J-66 Irradiated in Fuel Rod C-1-1. The rod was deconsolidated to obtain loose particles. 150×. (a) Bright field. (b) Polarized light.

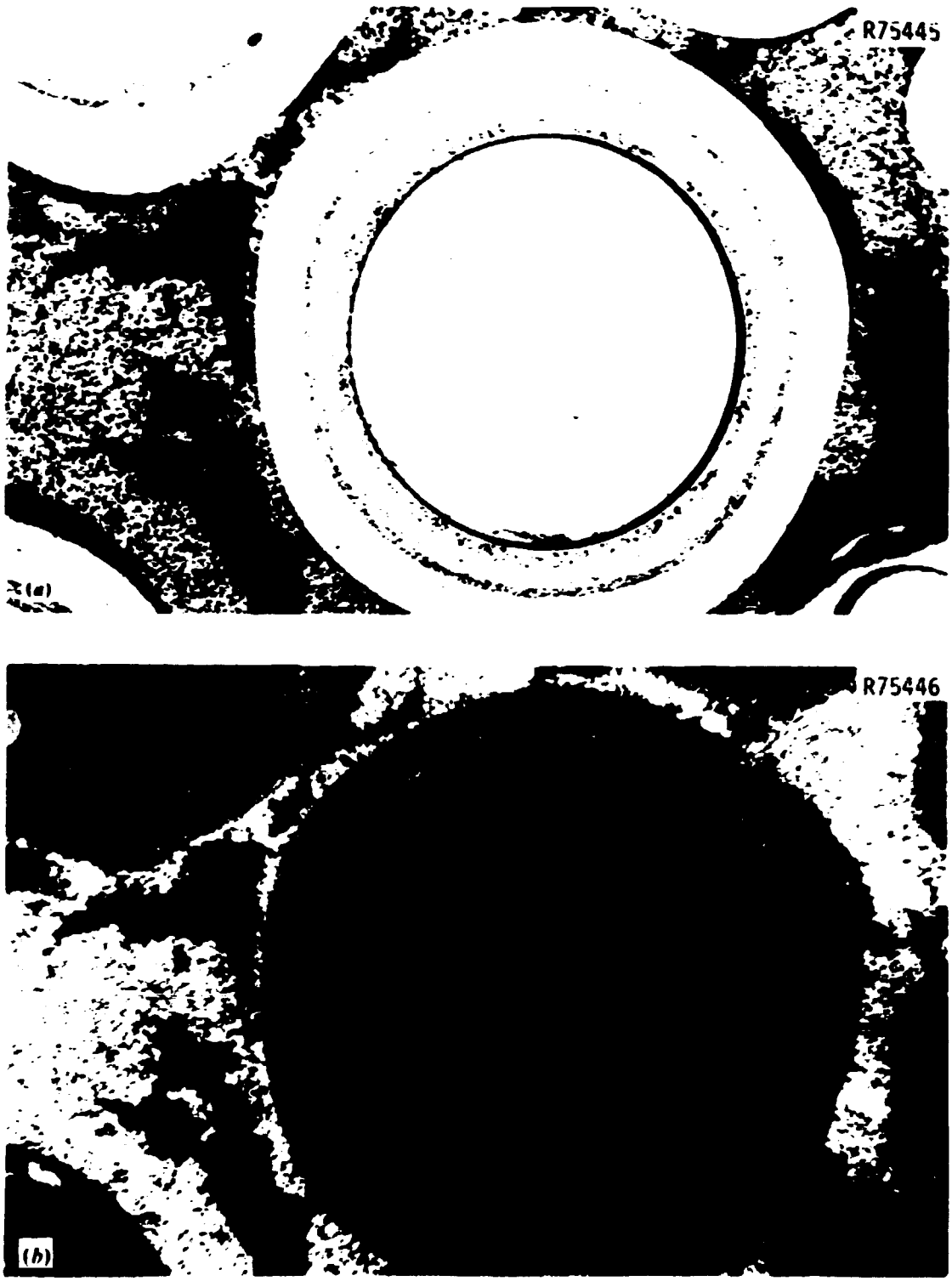

Fig. 3.45. Typical Biso-Coated ThO$_2$ Particle from Batch J-482 Irradiated in Fuel Rod C-2-1. 125×. (a) Bright field. (b) Polarized light.

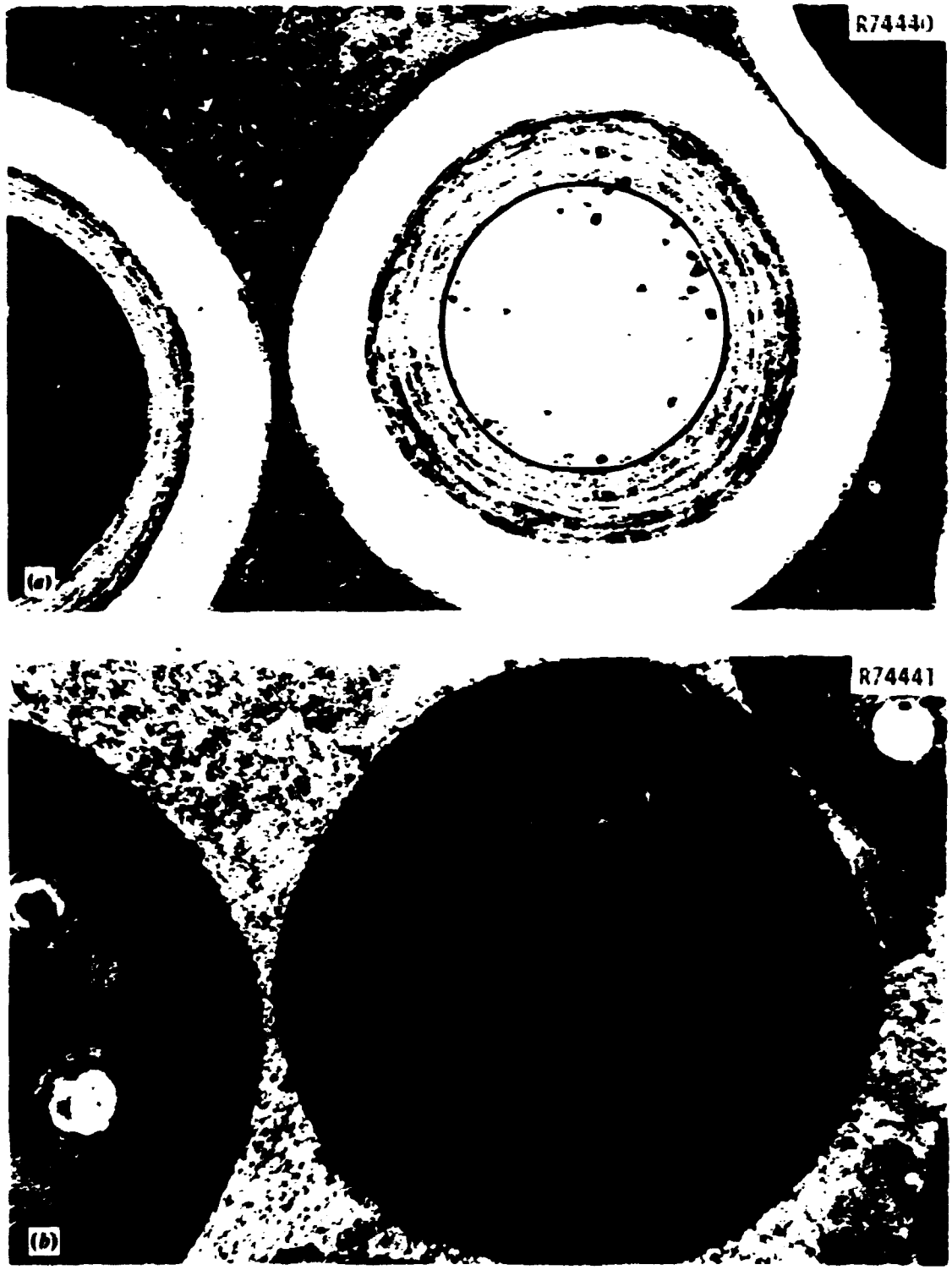

Fig. 3.46. Typical Biso-Coated ThO Particle from Batch OR-2266-HT Irradiated in Fuel Rod A-4-5. 125×. (a) Bright field. (b) Polarized light.

Fig. 3.47. Typical Biso-Coated ThO_2 Particle — from Batch J-487 — Irradiated in Fuel Rod C-2-4. 125×. (a) Bright field. (b) Polarized light.

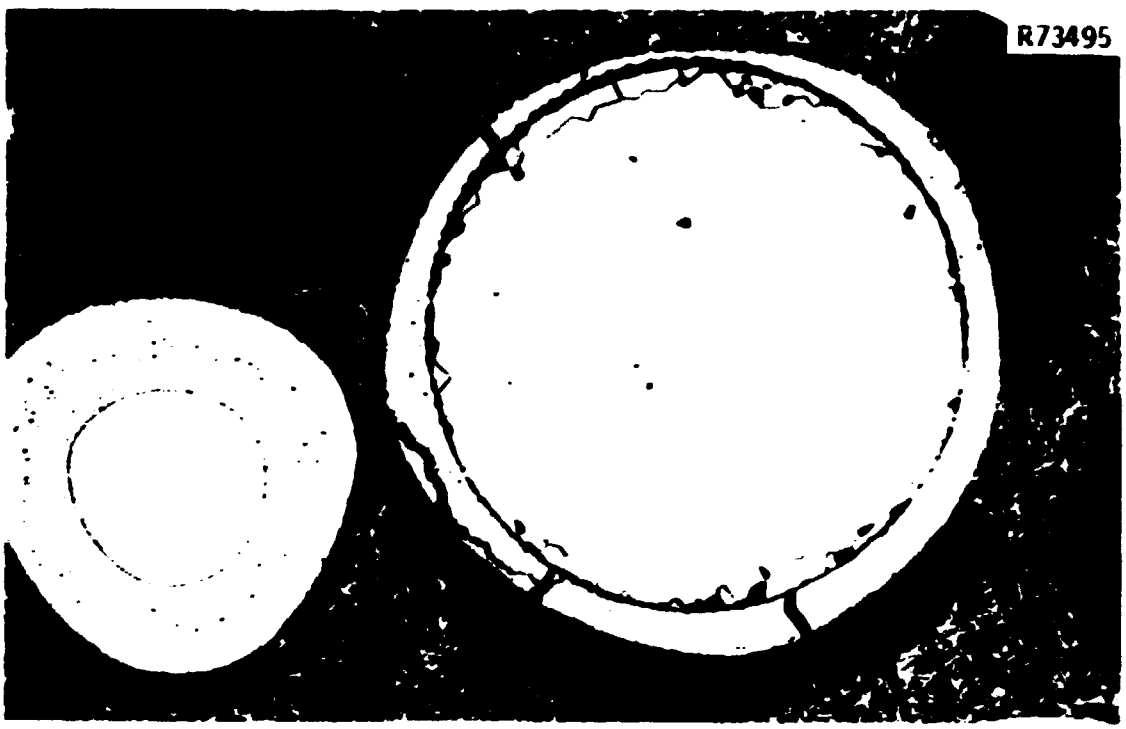

Fig. 3.48. ThO_2 Kernel from Batch J-481 with No Buffer Coating. Irradiated in fuel rod A-3-1. 125×.

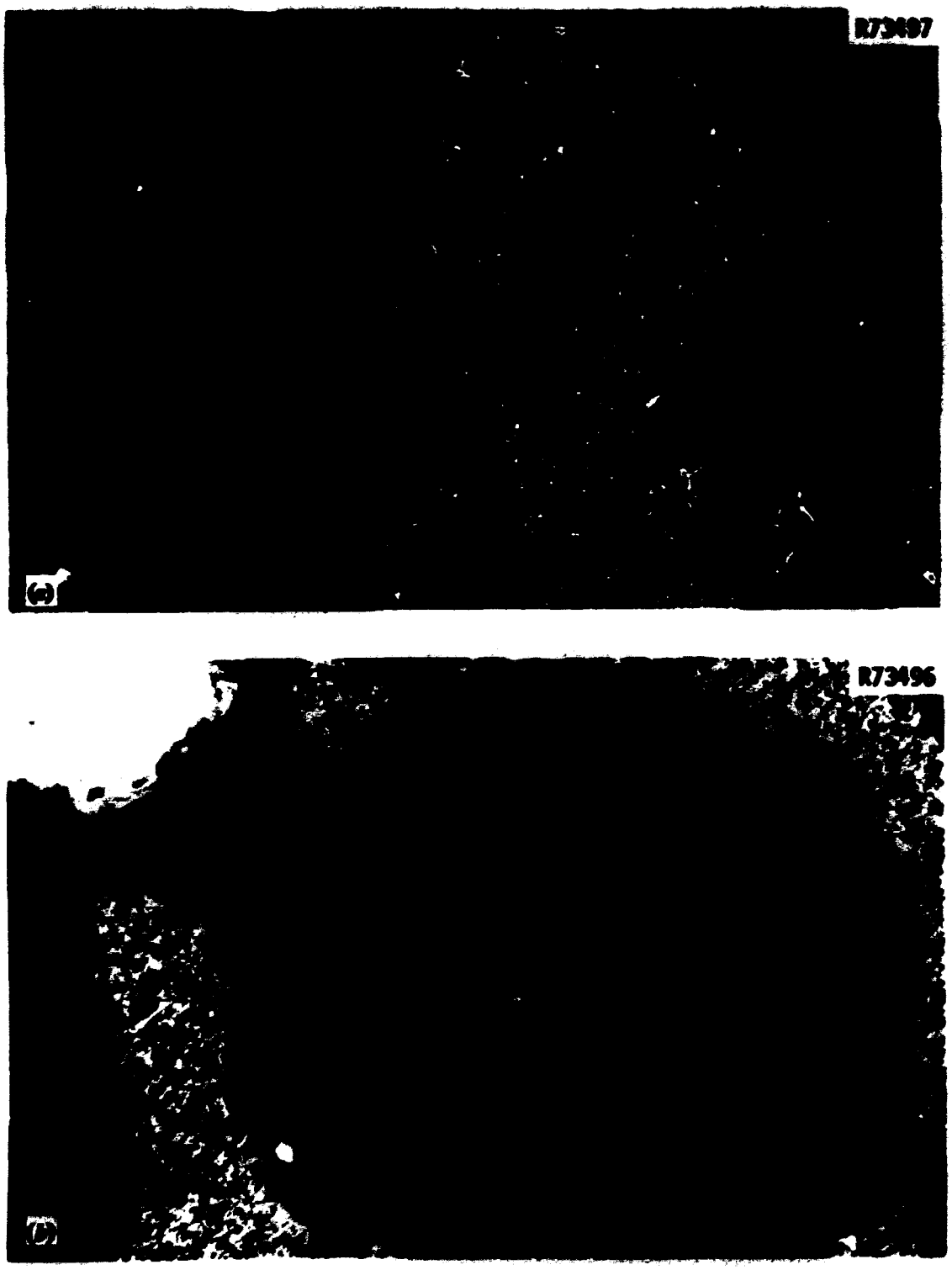

Fig. 3.49. Biso-Coated ThO_2 Particle — from Batch J-481 — with Cracked Coatings. Irradiated in fuel rod A-3-1. Note kernel appears to have converted to a carbide. 125x. (a) Bright field. (b) Polarized light.

J-481 was not. Also, preirradiation radiographs of these batches showed that all (100%) of the particles were good. Thus, the presence of fertile particles with no buffer layers in rod A-3-1 cannot be explained at this time. We are continuing to investigate this problem.

Since the metallography provided no definitive information on the performance of fertile particles under irradiation, conclusions must be drawn after analyses by the IMGA system, now in progress, are completed.[13] Other studies have shown that BISO-coated ThO_2 particles, which appeared to be intact, had permeable coatings that released fission gases.[20,21]

3.5.4 Matrices

Five matrices were used in the fabrication of the fuel rods for the OF-2 capsule. They are described in Table 1.3. The effect of irradiation on the appearance of the matrices is shown in Figs. 3.50 through 3.54. The influence of the matrices on fuel rod integrity and particle performance have been discussed in Sects. 3.3 and 3.5.1, respectively.

The matrix shown in Fig. 3.50 was made from 71 wt % Ashland A-240 pitch and 29 wt % Asbury 6353 filler, and was carbonized in packed Al_2O_3. This combination resulted in low coke yields (average - 18.3%) for the fuel rods. The individual filler particles were discernible.

In contrast, the matrix shown in Fig. 3.51 was also made from 71 wt % Ashland A-240 pitch and 29 wt % Asbury 6353 filler, but was carbonized in a graphite tube to simulate in-block carbonization. The result was a high-coke-yield matrix (average - 37.3%), which appeared "blocky"; the individual filler particles were not discernible.

The matrices shown in Figs. 3.52 and 3.53 both used GA's proprietary matrix composition and used similar carbonization modes — in-block and in-tube, respectively. Their appearances and coke yields, as expected, were quite similar. The individual filler particles were not discernible, and the coke yields were in medium range (25-30%).

The matrix shown in Fig. 3.54 was made from 71.5 wt % Ashland A-240 pitch and 28.5 wt % Asbury 6353 filler, and was carbonized in packed graphite flour. The result was a low-coke-yield matrix (average - 15.6%), the filler particles of which were barely discernible.

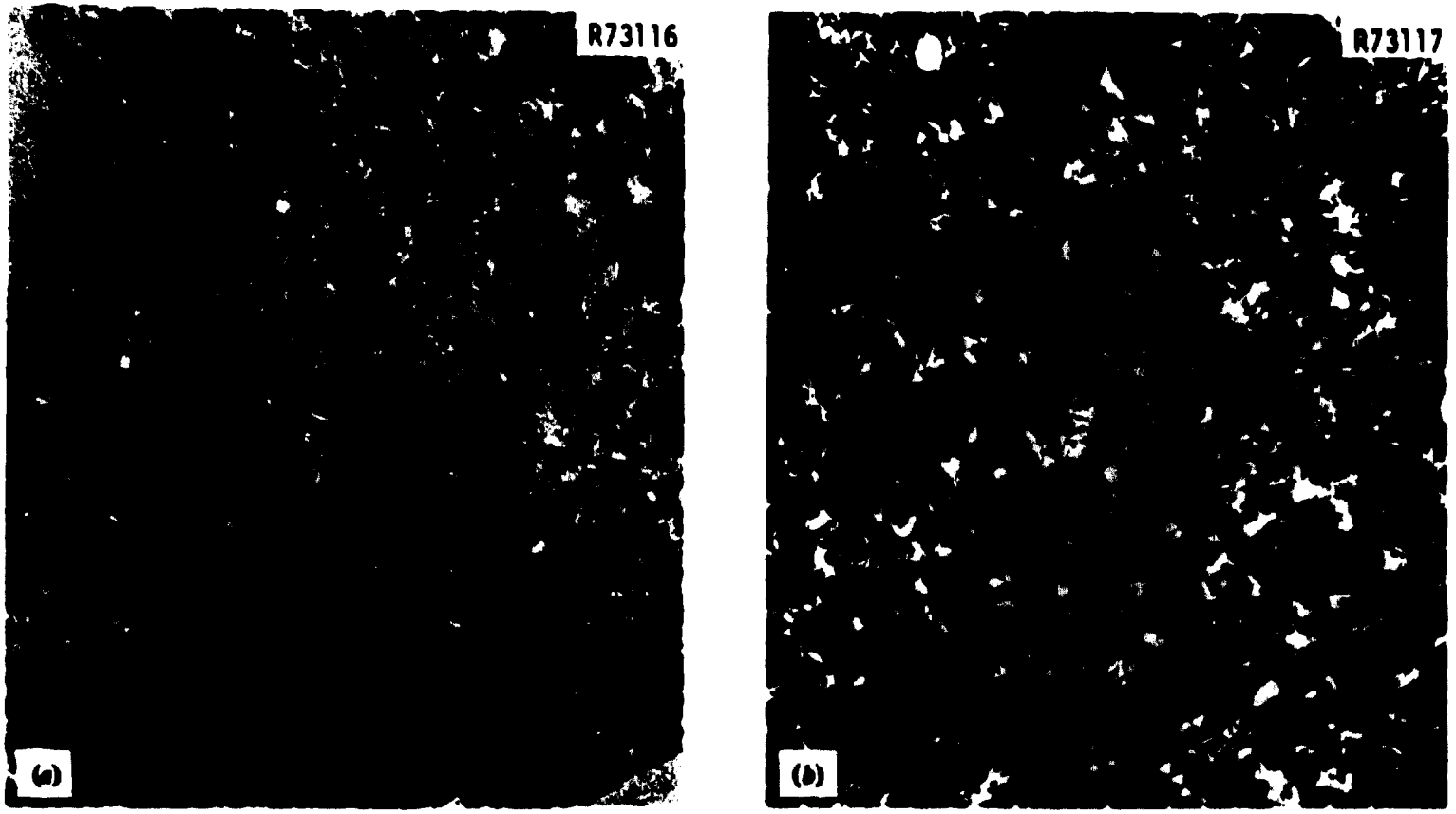

Fig. 3.50. Representative Area of Matrix — After Irradiation — Made from 71 wt % Ashland A-240 Pitch, 29 wt % Asbury 6353 Filler and Carbonized in Packed Al_2O_3. This sample is from fuel rod B-1-4. 500×. (a) Bright field. (b) Polarized light.

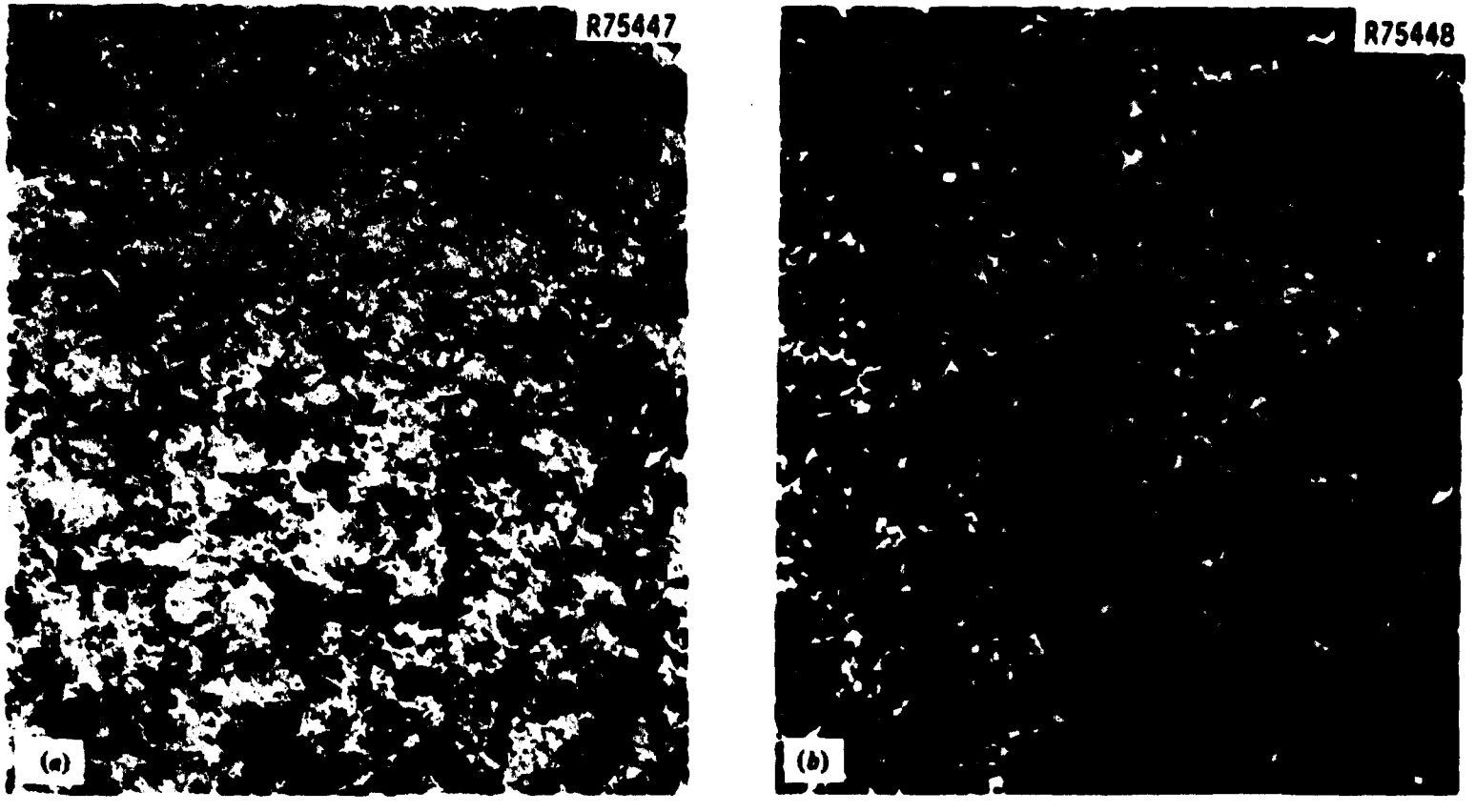

Fig. 3.51. Representative Area of Matrix After Irradiation. Matrix is made from 71 wt % Ashland A-240 pitch, 29 wt % Asbury 6353 filler and carbonized in a graphite tube. Sample is from fuel rod A-2-3. 500×. (a) Bright field. (b) Polarized light.

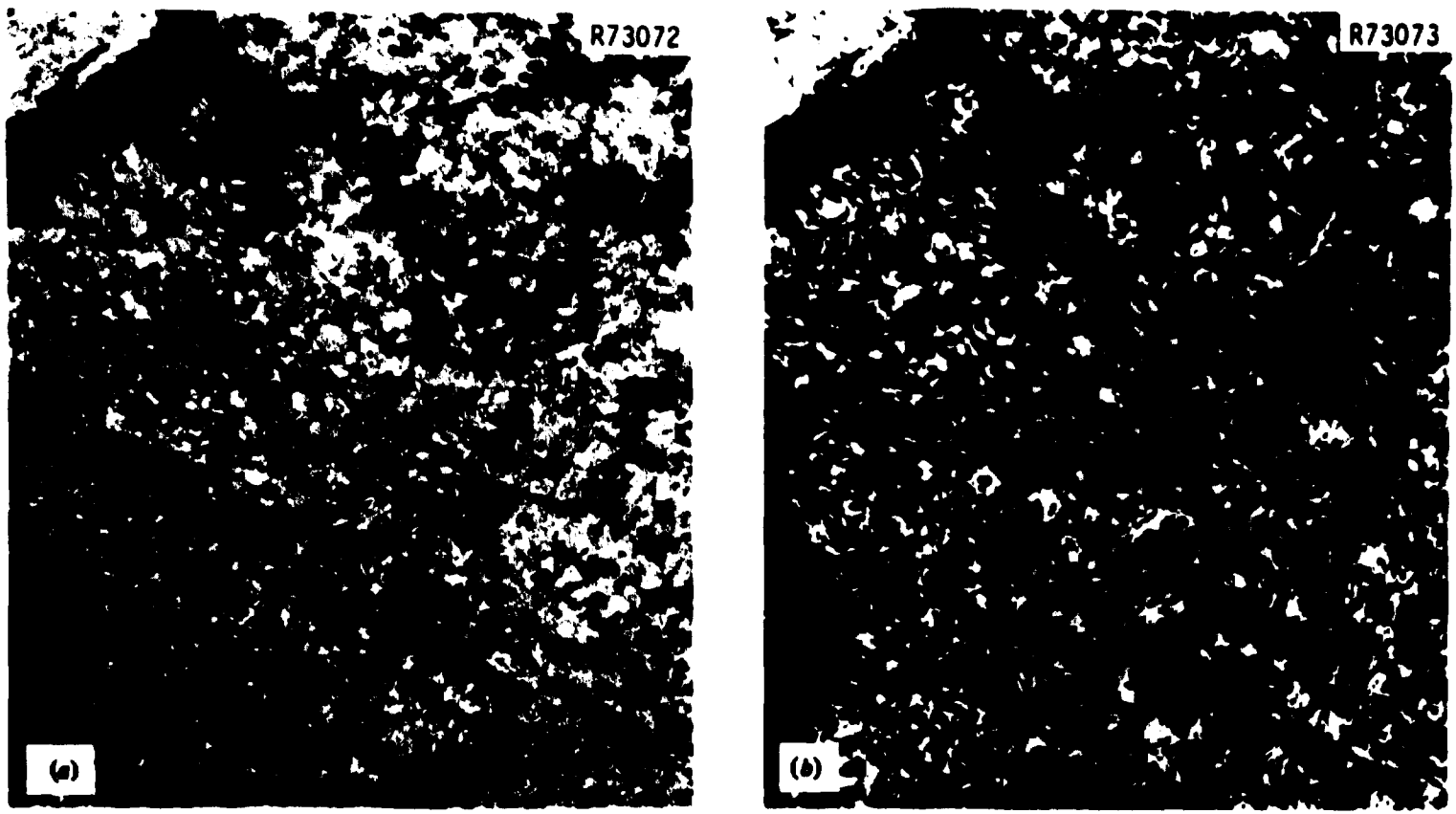

Fig. 3.52. Representative Area of Matrix — After Irradiation — Made from General Atomic Company Proprietary Composition and Carbonized in Magazine C. Sample from fuel rod C-2-1. 500×. (a) Bright field. (b) Polarized light.

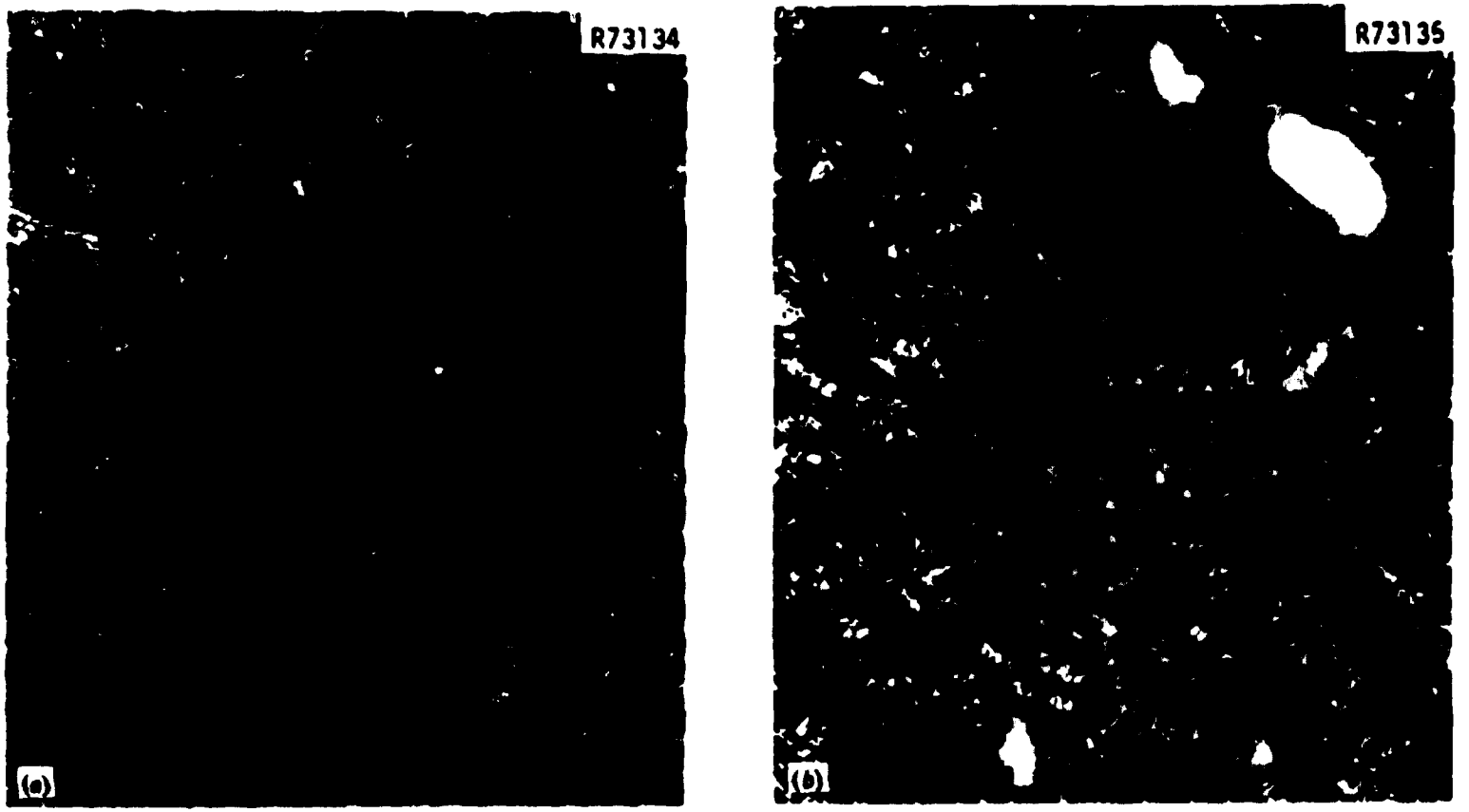

Fig. 3.53. Representative Area of Matrix — After Irradiation — Made from a Proprietary Composition from General Atomic Company and Carbonized in a Graphite Tube. Sample is from fuel rod B-1-6. 500×. (a) Bright field. (b) Polarized light.

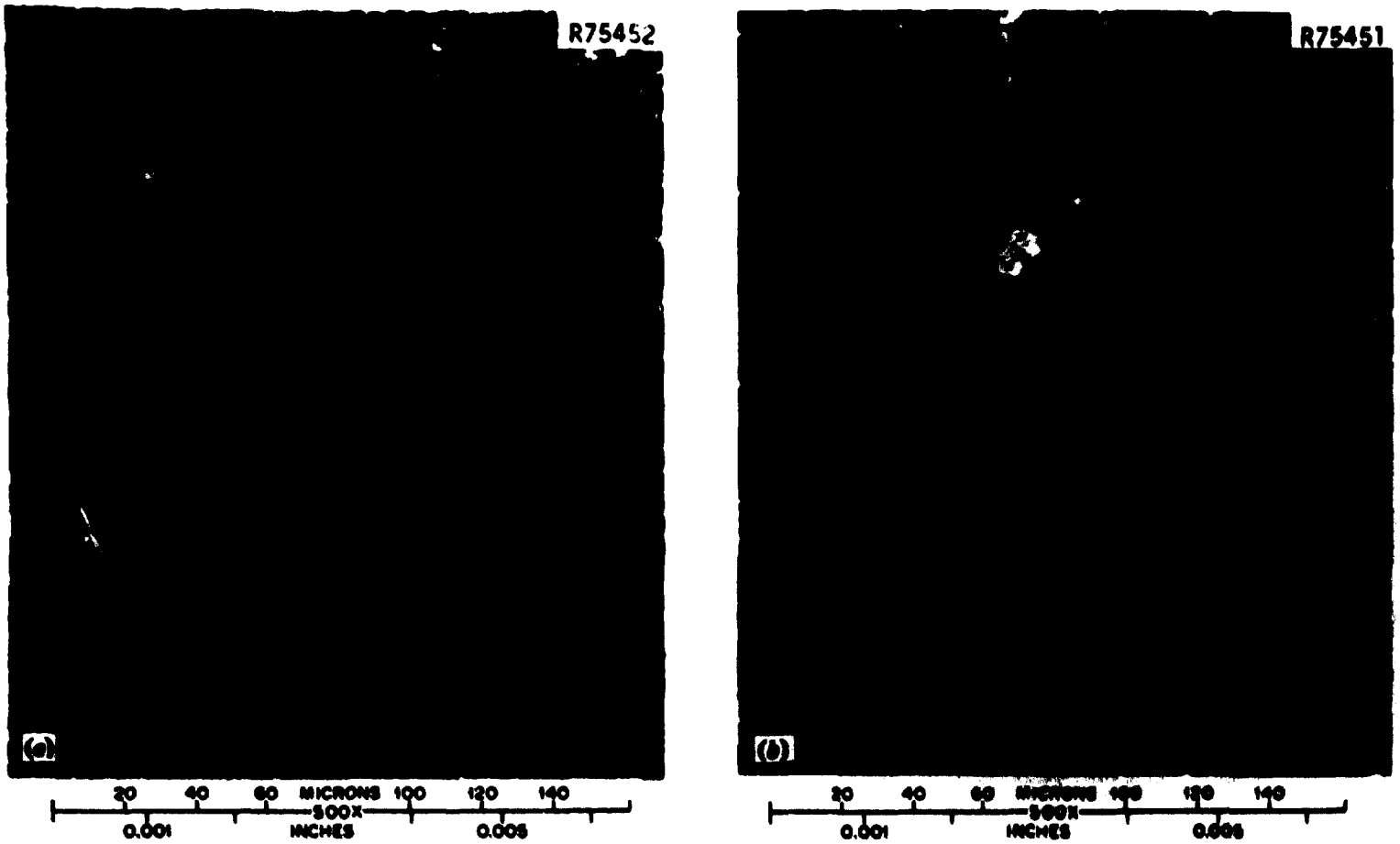

Fig. 3.54. Representative Area of Matrix — After Irradiation — Made from 71.5 wt % Ashland A-240 Pitch, 28.5 wt % Asbury 6353 Filler and Carbonized in Packed Graphite Flour. Sample is from fuel rod A-3-8. (a) Bright field. (b) Polarized light.

3.6 Electron Microprobe Examination

The electron microprobe was used to determine the behavior of fission products from fissile particles from batches A-601 and A-611. As previous studies[11] had investigated the fission product behavior of WAR particles made in the small laboratory coaters, we needed to know whether that information applies to particles made in the 0.13-m-diam coater.

3.6.1 Fissile particle batch A-601

A fissile particle from batch A-601 and which was examined metallographically is shown in Fig. 3.55. It was irradiated in fuel rod C-3-3 and its appearance was typical of the particles from batch A-601 described earlier.

The backscattered electron image and the distributions of uranium and chlorine are presented in Fig. 3.56. As shown, the uranium was located in the main kernel phase and in the densified buffer. The highest concentrations were in the main kernel phase, but some accumulations were localized in the densified buffer. Chlorine, believed to aggravate fission product behavior and SiC corrosion,[19] was also observed in the particle. However, because of the relatively low concentration of chlorine and the associated high background of the irradiated sample, the chlorine x-ray display was not as distinct as the others. The chlorine was located in the kernel and along the inner surface of the iLTI coating. Previous results[11] have shown that the chlorine is associated with the rare earth fission products Nd, Ce, La, and Pr.

The distributions of the rare earth fission products Nd, Ce, La, and Pr are shown in Fig. 3.57. They were observed in the kernel, the densified buffer, along the inner surface of the iLTI coating, and at the SiC coating on the cold side of the particle. These results agree with those of previous studies,[11,14] which showed that the retention of the rare earth fission products depended on the initial oxygen content of the kernel.

The distributions of zirconium, strontium, and barium are shown in Fig. 3.58. Most of the zirconium was located in the main kernel phase,

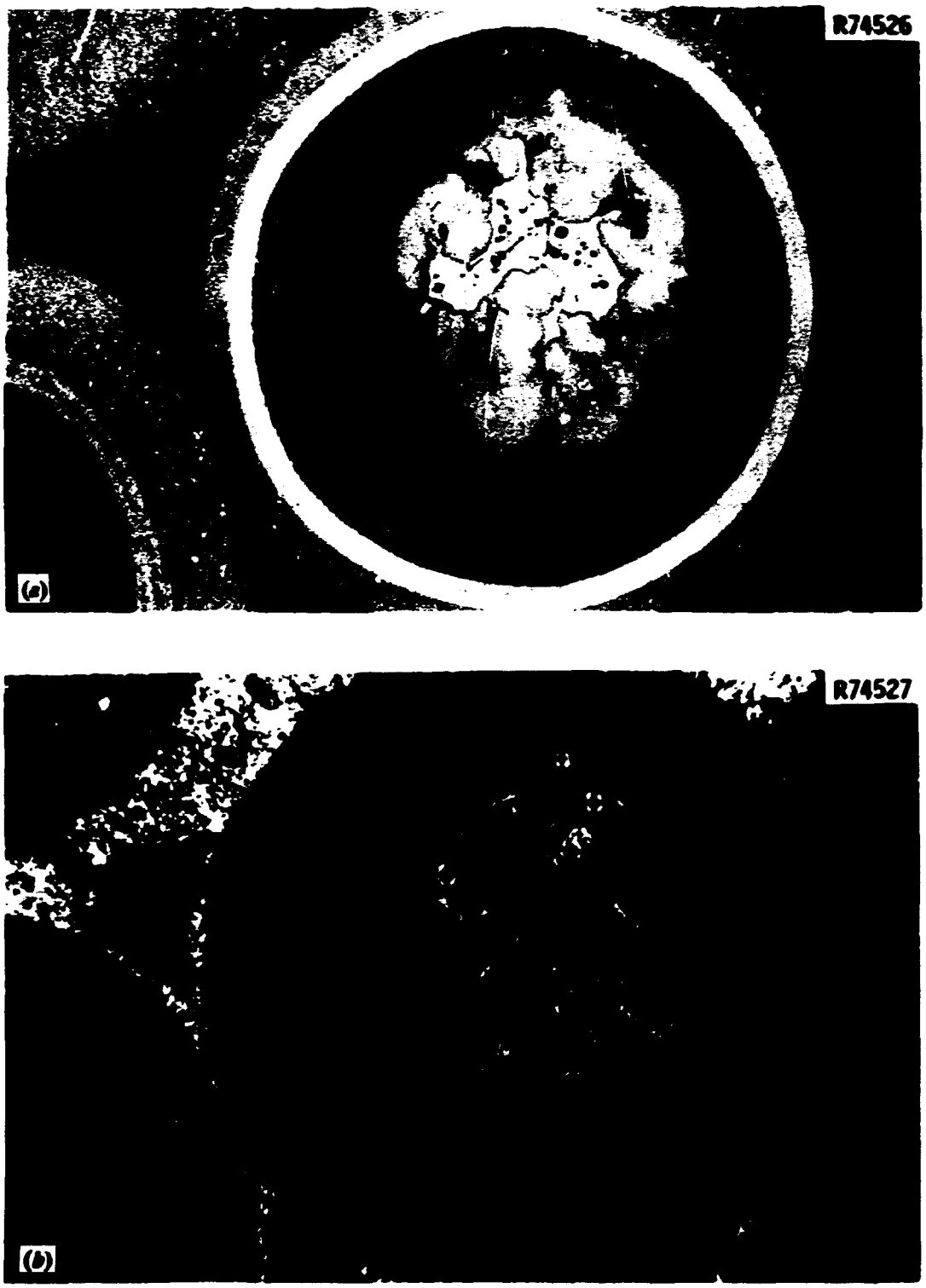

Fig. 3.55. Batch A-601 Fissile Particle Examined with Electron Microprobe. The particle was irradiated in fuel rod C-3-3 and was located on the outer surface of the rod. The rod's outer surface is to the right of the micrographs. 150×. (a) Bright field. (b) Polarized light.

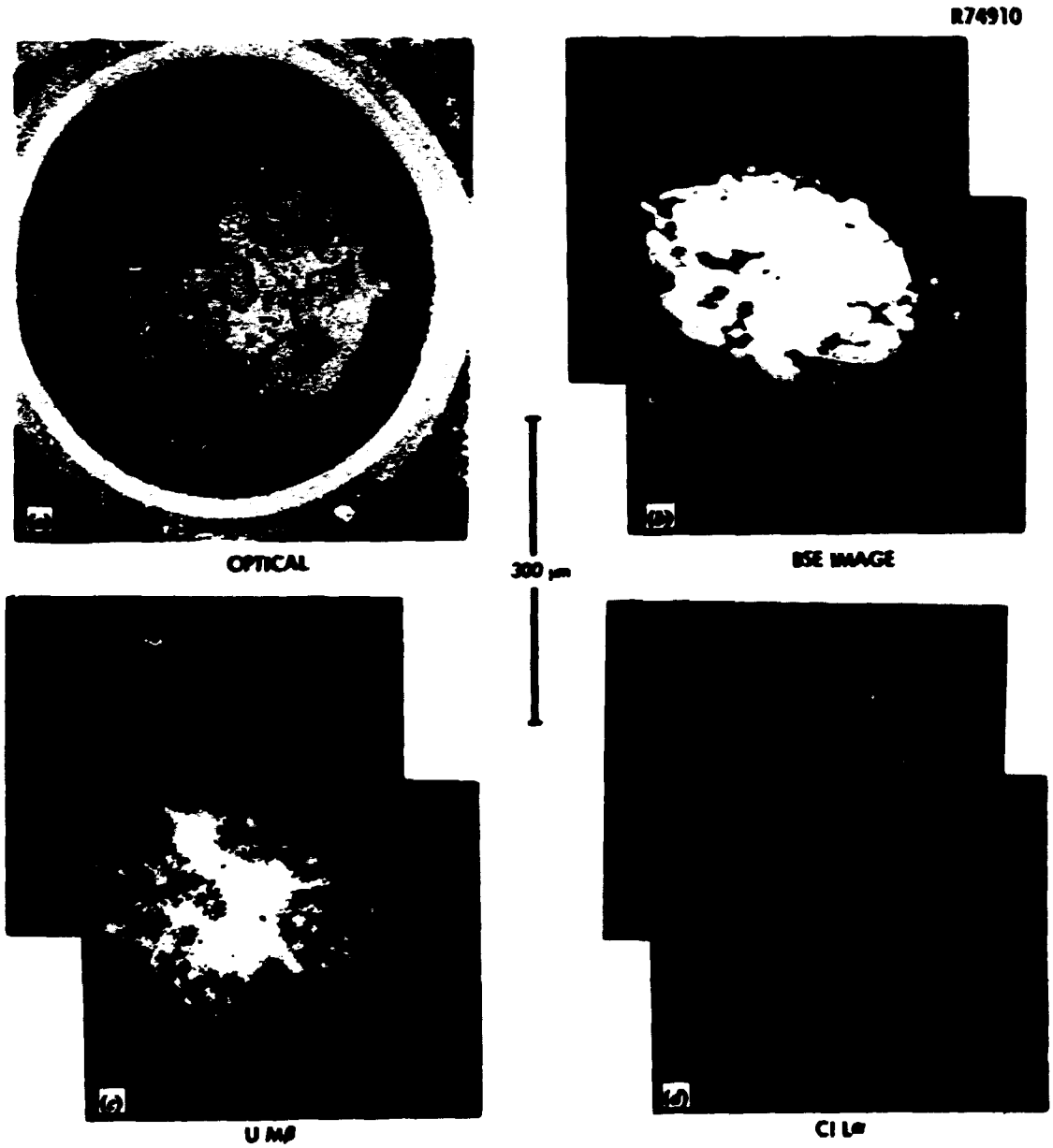

Fig. 3.56. Particle from Fissile Batch A-601. Cold side of particle located at bottom of photographs. (a) Optical. Bright field. (b) Backscattered electron image. (c) U Mβ x-ray display. (d) Cl Lα x-ray display.

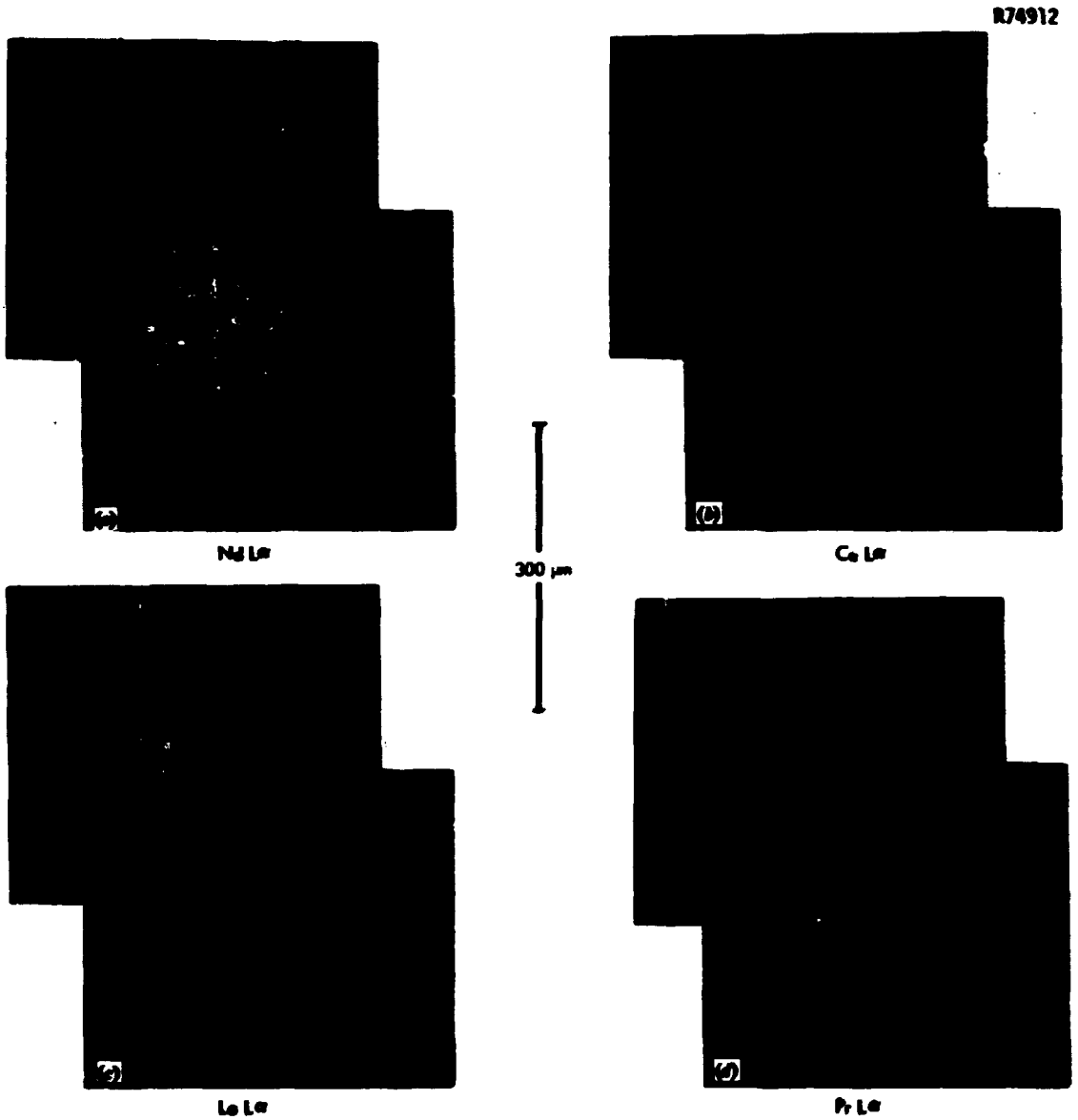

Fig. 3.57. Particle from Batch A-601. Orientation identical to that of Fig. 3.56. X-ray displays of (a) Nd Lα, (b) Ce Lα, (c) La Lα, and (d) Pr Lα.

but concentrations were also in the densified buffer and iLTI coating. On the other hand, strontium had migrated out of the kernel and had concentrated in the densified buffer. Strikingly, the x-ray display also shows strontium in the iLTI and SiC coatings. Previous studies have also detected strontium in the SiC coating,[22] but its migration mechanism through the SiC coating is not known. Also there is some question as to the validity of this observation because of the interference between the strontium and silicon characteristic x rays.[11] The barium, like strontium, had migrated out of the kernel and had concentrated in the densified buffer with a lower concentration in the iLTI coating. However, the SiC coating apparently stopped further migration.

The distributions of the volatile fission products cesium and xenon are presented in Fig. 3.59. The cesium, like the barium just discussed, migrated out of the kernel into the densified buffer and iLTI coating. The SiC coating stopped further migration. The xenon also migrated out of the kernel, but it concentrated on the periphery of the densified buffer with very small concentrations in the iLTI. We believe that much of the xenon was present in the large void volume created by the kernel and buffer densification.

Molybdenum and ruthenium were concentrated in the main kernel phase, while lower concentrations of them were found in the densified buffer (Fig. 3.59). No migration of these fission products into the iLTI coating was detected. Since no metallic inclusions were present in the kernel phases, we expected the molybdenum and ruthenium to be evenly distributed in the kernel.

Palladium had migrated out of the kernel and had accumulated at the SiC coating on the cold side of the particle (Fig. 3.60). These accumulations were identified in the metallographic examination described earlier. The rare earth fission products Nd, Ce, La, Pr were also associated with the palladium accumulations.

3.6.2 Fissile particle batch A-611

The fissile particle examined from batch A-611 is shown in Fig. 3.61. It was irradiated in fuel rod C-1-3 and its appearance was typical of particles from that batch.

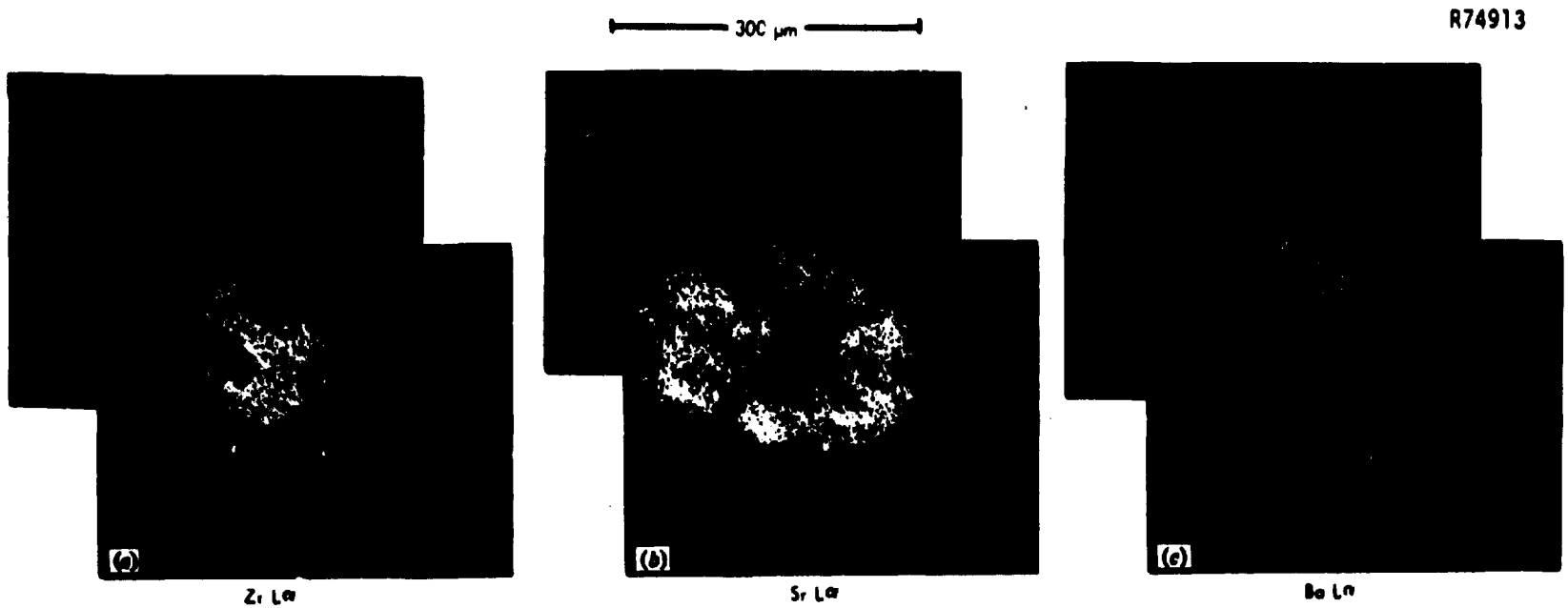

Fig. 3.58. Particle from Batch A-601. Orientation identical to that of Fig. 3.56. X-ray displays of (a) Zr Lα, (b) Sr Lα, and (c) Ba Lα.

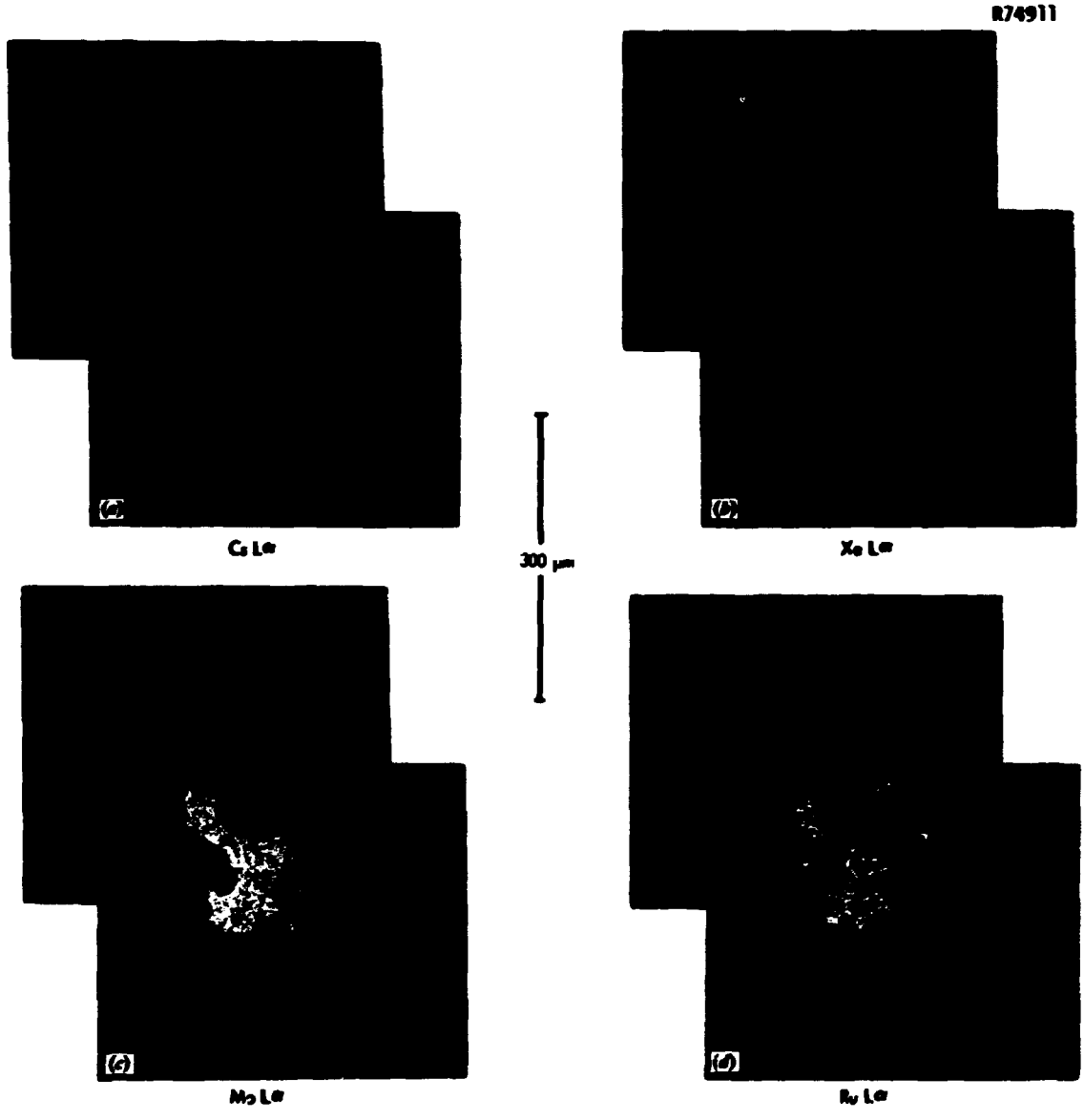

Fig. 3.59. Particle from Batch A-601. Orientation identical to that of Fig. 3.56. X-ray displays of (a) Cs Lα, (b) Xe Lα, (c) Mo Lα, and (d) Ru Lα.

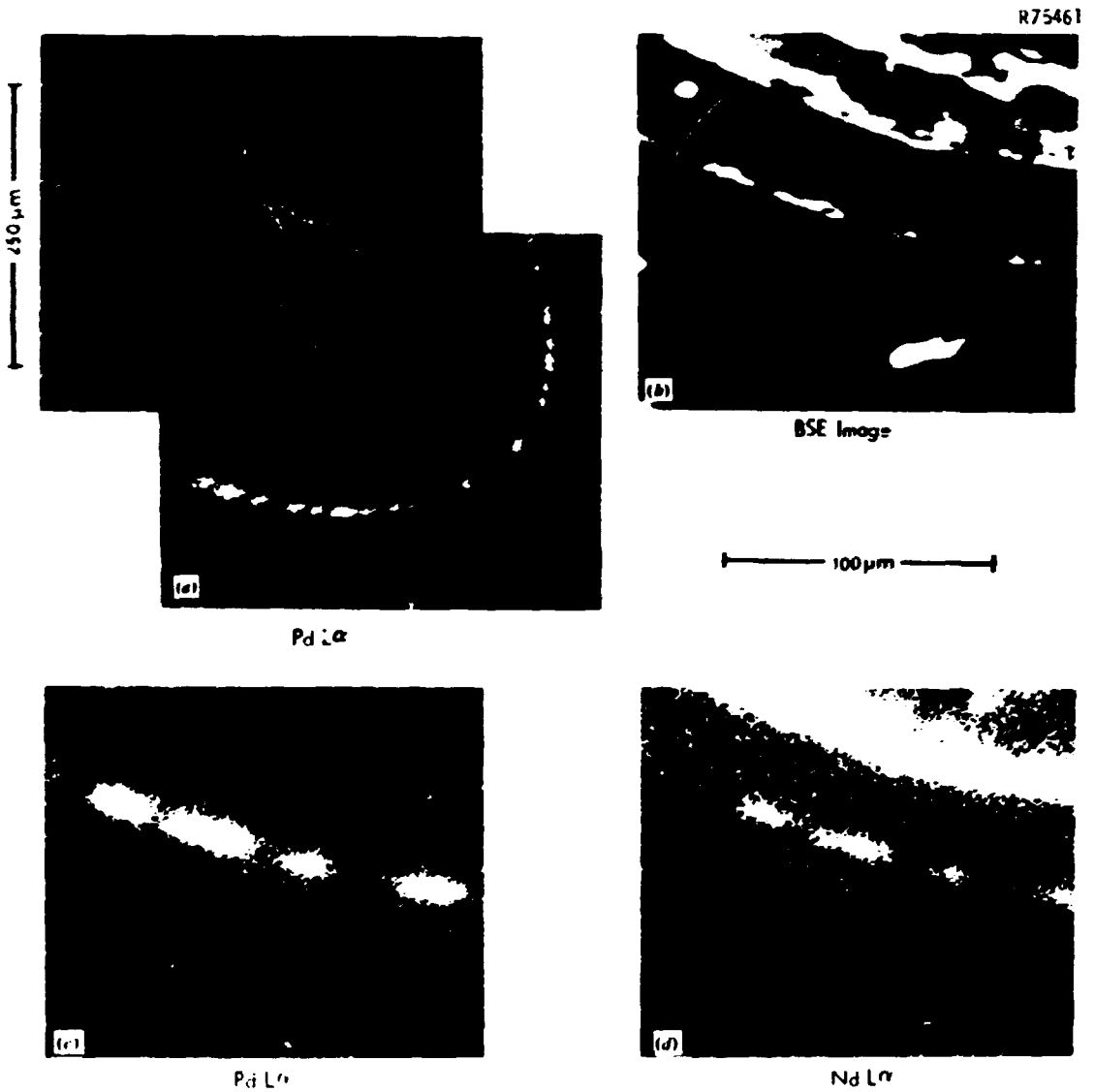

Fig. 3.60. Particle from Batch A-601. (a) Pd x-ray display is in same orientation as in Fig. 3.56. (b) Backscattered electron image of cold side of particle. (c) Pd x-ray display of cold side of particle. (d) Nd Lα x-ray display – representative of other rare earths – of cold side of particle.

Fig. 3.6i. Batch A-6J1 Fissile Particle Examined with Electron Microprobe. The particle was irradiated in fuel rod C-2-1 and was 3000 μm from the outer surface of the rod. Rod's surface is to the right of the micrographs. 150×. (a) Bright field. (b) Polarized light.

The backscattered electron image as well as the distributions of uranium and chlorine are presented in Fig. 3.62. The uranium was heavily concentrated in the kernel phases dispersed throughout the densified buffer. Small concentrations were observed in the densified buffer itself. Although chlorine was also associated with the kernel phases, none was observed outside the densified kernel and buffer. The observations agree with previous results.[11]

The rare earth fission product distributions — Nd, Ce, La, Pr — are presented in Fig. 3.63. They were preferentially located in the kernel phase, but relatively high concentrations were observed in the densified buffer and along the inner surface of the iLTI coating. These results resemble previous studies[11] of partially converted WAR particles. We observed no migration of the rare earth fission products to the SiC coating. In particles with such a high initial oxygen content — the ratio of oxygen to uranium being 1.75 — most of the rare earths were expected to remain in the kernel.

The fission product distributions for zirconium, strontium, and barium are shown in Fig. 3.64. Like the particle from batch A-601 just discussed, the zirconium also was observed in the kernel phase, in the densified buffer, along the entire inner surface of the iLTI coating, and in the iLTI coating in low concentrations. The strontium was also in the kernel phase and densified buffer, but it appeared preferentially deposited along the inner surface of the iLTI coating on the cold side of the particle. Again strontium was evident in the SiC coating. Barium was present in the kernel phase, densified buffer, and in the iLTI coating in low concentrations.

The volatile fission product, cesium, had migrated from the kernel into the surrounding densified buffer and iLTI coating (Fig. 3.65). No xenon x-ray display could be made because the xenon count rate was too low to make a discernible image. Thus, we assume that much of the xenon was originally present in the void volume.

The fission products molybdenum and ruthenium were preferentially located in the densified buffer (Fig. 3.65). . the surfaces of the kernel phase, noble metal inclusions were identified. Evidently the molybdenum and ruthenium precipitate out of solution in the kernel

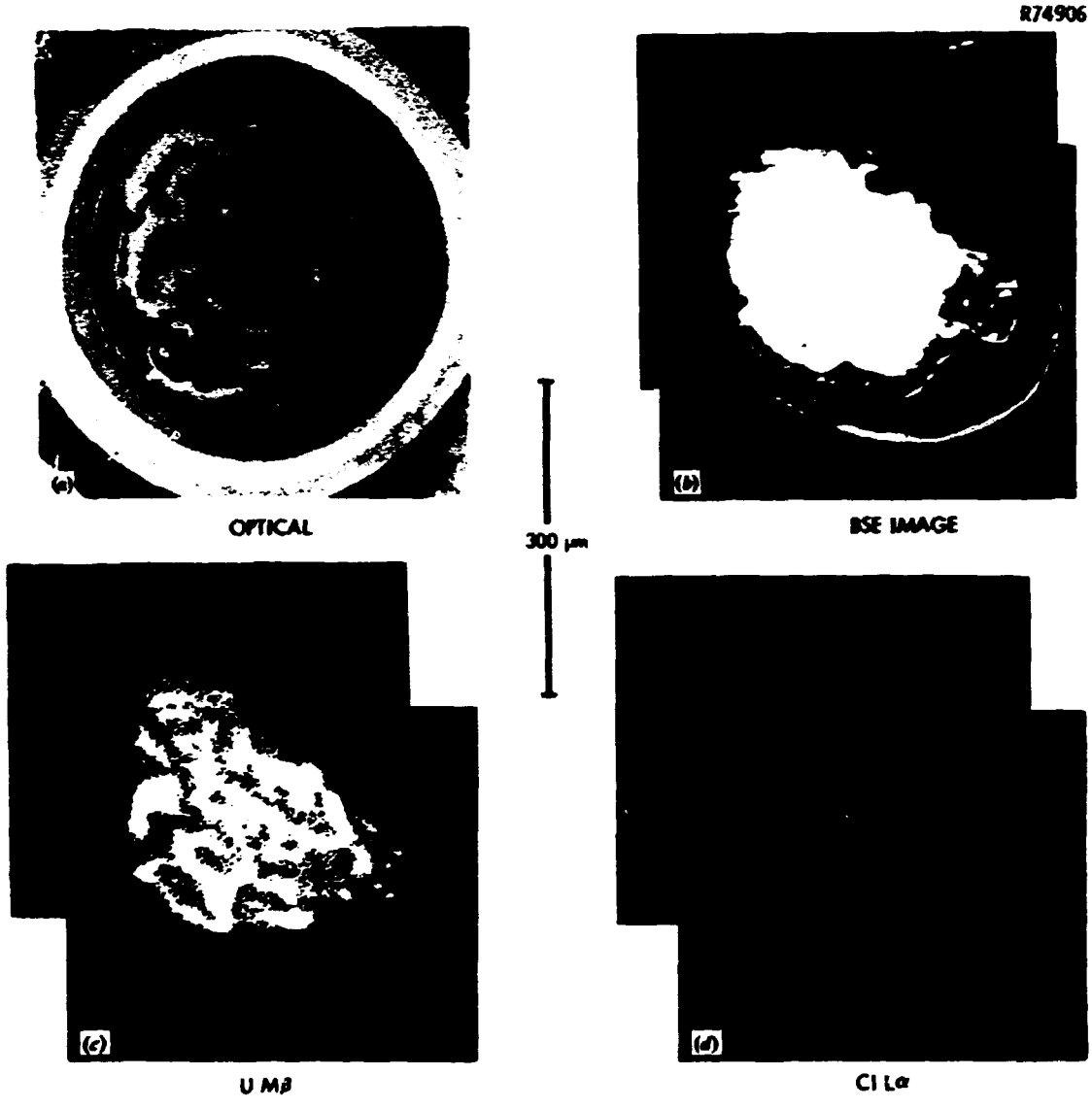

Fig. 3.62. Particle from Batch A-611. Cold side of particle is at lower right corner of figures. (a) Optical. Bright field. (b) Back-scattered electron image. (c) U Mβ x-ray display. (d) Cl Lα x-ray display.

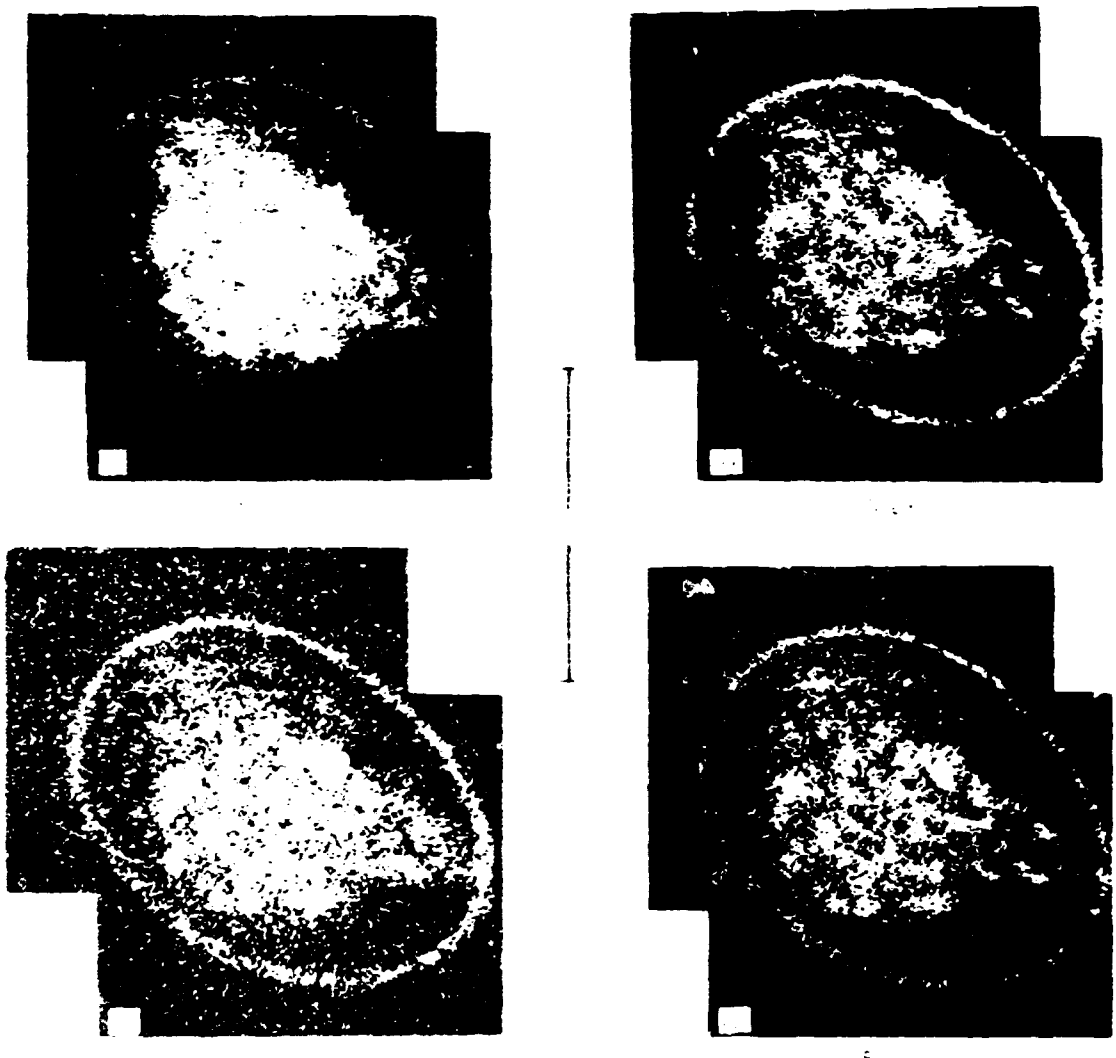

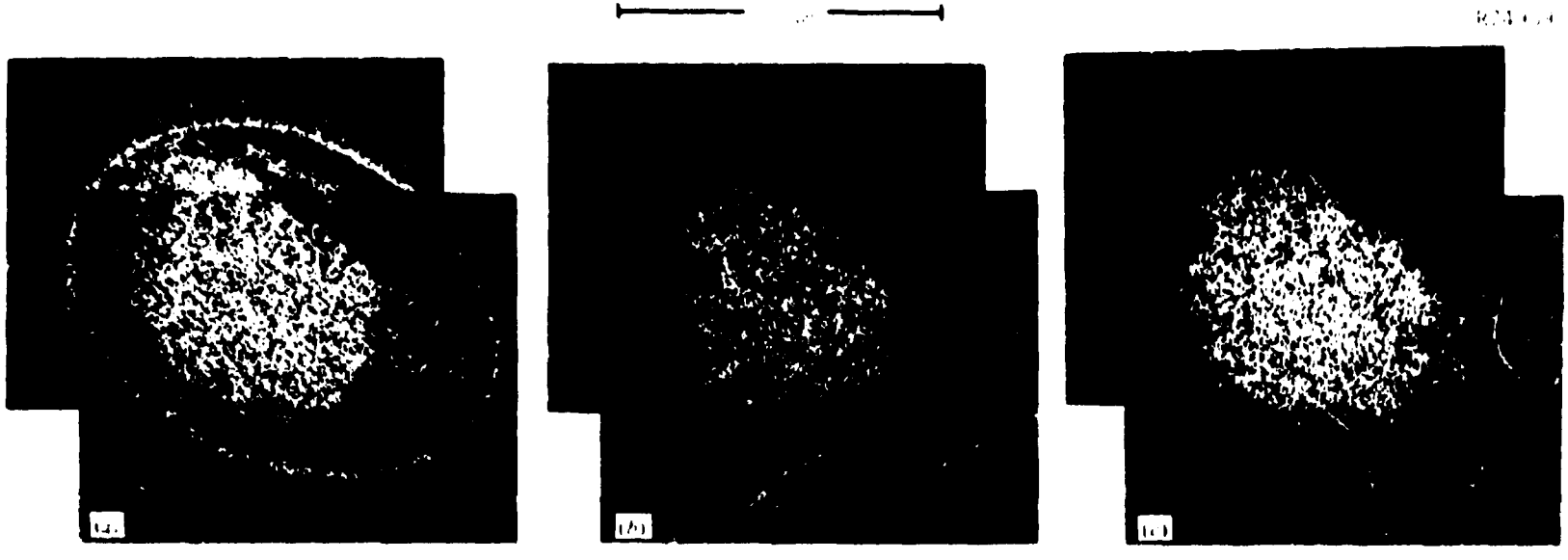

[illegible]

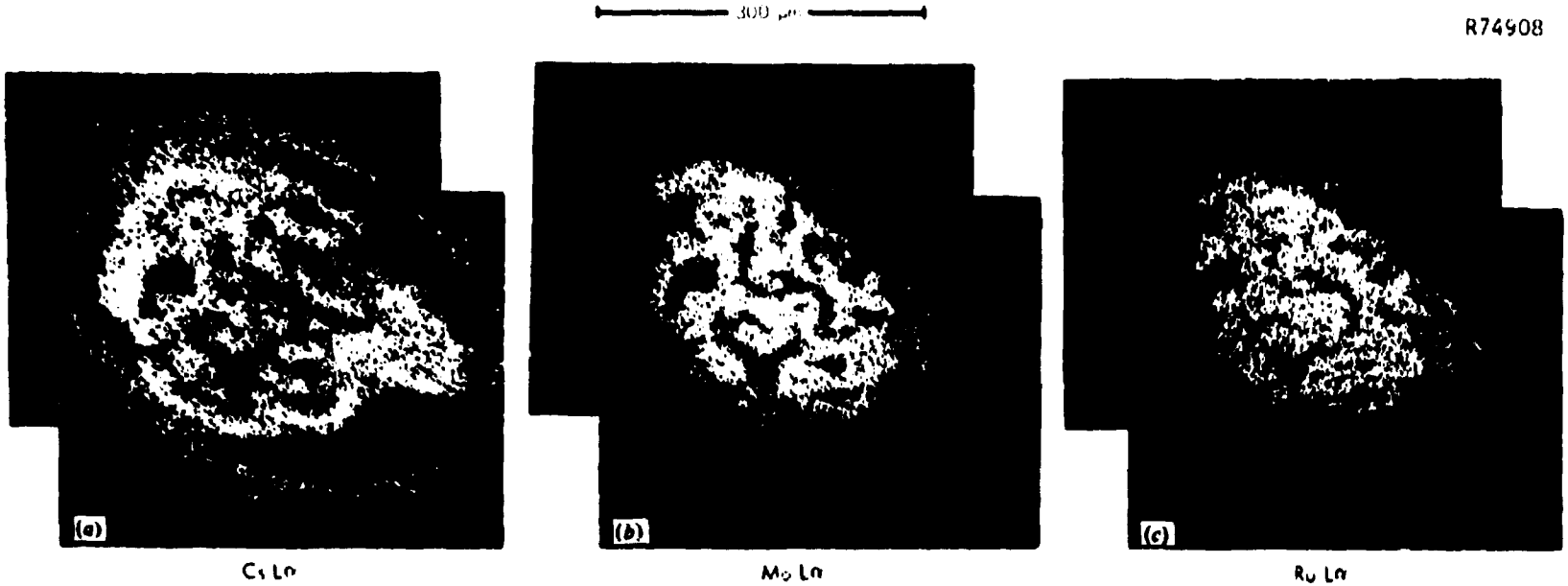

Fig. 3.65. Particle from Batch A-611. Orientation identical to that of Fig. 3.62. X-ray — Lα line — displays of (a) cesium, (b) molybdenum, and (c) ruthenium.

(presumably an oxide) and migrate out. These results resemble those of previous studies.

Palladium again had migrated out of the kernel and accumulated at the SiC coating on the cold side of the particle near the kernel's point of attachment to the iLTI coating (Fig. 3.66). However, unlike particle batch A-601, in this case the rare earth fission products were not associated with the palladium accumulations.

Electron microprobe analysis showed that the behavior of fission products from partially converted WAR particles depends on the initial oxygen content of the kernel. The results on the fissile WAR particles coated in the 0.13-m-diam coater resemble those on partially converted WAR particles coated in 0.025-m-diam and 0.063-m-diam coaters.[11] Therefore, many previous results on fission product behavior in WAR particles apply to particles coated in the 0.13-m-diam coater.

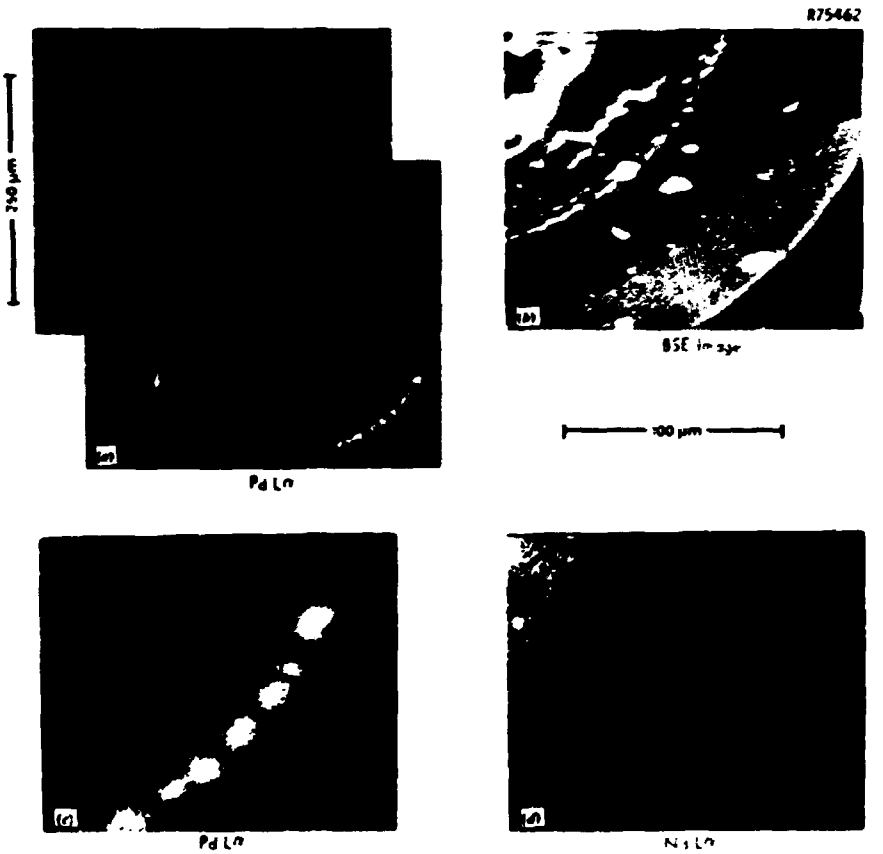

Fig. 3.66. Particle from Batch A-611. (a) Pd Lα x-ray display in same orientation as in Fig. 3.63. (b) Backscattered electron image of cold side of particle. (c) Pd Lα x-ray display of cold side of particle. (d) Nd Lα x-ray display – representative of those of other rare earths – on cold side of particle.

4. CONCLUSIONS

The OF-2 capsule tested various HTGR fuel types under a wide range of irradiation conditions. These included Triso-coated fissile particles and Biso-coated fertile particles.

Triso-coated WAR particles coated in the 0.13-m-diam coater with a fritted gas distributor showed good irradiation performance. However, in similar particles coated by a cone gas distributor, the oLTI coatings had high failure fractions. The failures were attributed to the anisotropy of the pyrocarbon layer, a characteristic of the coatings made by the cone gas distributor. The fissile particles chosen for the Fort St. Vrain Early Validation Tests[23] were coated by the fritted gas distributor in the 0.13-m-diam coater. We believe they will perform well under actual HTGR irradiation conditions.

During the metallographic examination, we could not confidently distinguish between coating failures caused by matrix-particle interaction and those by fast-neutron damage. Most coating failures occurred in the oLTI coating on the Triso-coated particles. (Only one coating failure was observed among the Biso-coated particles.) The most important property of the oLTI coating was its anisotropy. Those fuel particles with an oLTI Bacon Anisotropy Factor of less than 1.069 appear to have performed best. Also important were the pitch-coke yields of the matrices and the amount of open porosity of the pyrocarbon. Matrices with pitch-coke yields above 30% had significantly more oLTI-coating failures than did matrices with yields below 30%.

The Biso-coated ThO_2 particles were coated under various conditions of gas concentration, deposition rate, deposition temperature, and batch size (see Table 1.2). From the limited results obtained during metallography, the irradiation behavior of all the particles except one appeared excellent. That exception had the lowest rupture load (22.42 N, 5.40 lb), but none of the coating conditions distinguish it from particles from the other batches. Because the particle coatings may have been permeable during irradiation, further tests of the irradiation performance are being pursued.[13]

The Triso-coated WAR particles with stoichiometries ranging from 0 to 100% converted performed as expected. The high-oxygen-content particles (0% converted) showed amoeba of the kernel up the temperature gradient. In the low-oxygen-content particles (100% converted) tested previously,[18] high-yield rare earth fission products accumulated at the SiC coating on the cold side of the particle. However, this accumulation was not observed in the particles in OF-2. This difference resulted from irradiation temperatures lower than 1150°C (1423 K) facing these particles. We expect that 100%-converted particles from Magazine B will show rare earth migration down the temperature gradient. Magazine B had a higher average temperature [1350°C (1623 K)] than did Magazine A.

The partially (15%-75%) converted WAR particles showed good irradiation performance. No amoeba migration was observed. However, some rare earth fission product migration to the SiC coating was observed in particles from Magazine C, which had relatively high temperatures (a maximum of 1350°C, 1623 K). The partially converted WAR particles from Magazine A showed no evidence of rare earth migration (maximum temperature of 1150°C, 1423 K).

The fuel rods were easily removed from their respective magazines. This included fuel rods carbonized in-block and out-of-block. In previous tests the fuel rods had been difficult to remove after in-block carbonization. However, the pitch-coke yields of the rods carbonized in-block in OF-2 were very much lower (~25 versus ~40%), so very little bonding between the rods and the graphite occurred.

The findings from the postirradiation examination we described in this report are typical of the previous capsule tests. Most of the objectives of the OF-2 capsule test were achieved. However, this capsule test indicates that more analyses are needed to determine particle performance so as to qualify a fuel for licensing. Conventional methods do not provide sufficient information. For example, virtually all the Biso-coated ThO_2 particles appeared to be in good condition after irradiation. These particles were used to demonstrate the irradiation behavior of various coating microstructures arising from a variation of the coating process conditions. However, other tests[19,23] have shown that

intact Biso-coated ThO_2 particles may have permeable pyrocarbon coatings, which can leak fission gases. Such particles, therefore, are actually failed. Additional PIE, in the form of IMGA analysis and internal gas pressure measurements, will be performed on these Biso-coated ThO_2 particles and reported later.[13] In addition, many observations are required to ascertain whether the performance of fuel particles is adequate. Metallographic examinations do not provide a statistically definitive number of observations to do this. Therefore, additional use of the IMGA system to statistically determine fuel particle performance at high confidence levels will be done.[13] When the IMGA analysis is completed, all the objectives of the OF-2 capsule irradiation test will have been met.

ACKNOWLEDGMENTS

The authors wish to acknowledge the efforts of many people who made significant contributions to the planning and implementation of this experiment. W. P. Eatherly, F. J. Homan, R. L. Beatty, R. A. Bradley, W. J. Lackey, Jr., and E. L. Long, Jr., of the Metals and Ceramics Division; T. B. Lindemer of the Chemical Technology Division; and J. A. Conlin of the Reactor Division participated in the planning and design of the experiment. A. J. Caputo, J M Robbins, J. C. McLaughlin, and D. E. Rossin of the Metals and Ceramics Division fabricated and characterized the slug-injected fuel rods. The fissile and fertile particles were coated and characterized by R. L. Beatty, W. J. Lackey, Jr., C. E. Devore, and C. Hamby, Jr., of the Metals and Ceramics Division. D. R. Johnson and R. L. Beatty were responsible for carbonization and conversion of the fissile particles. Dosimetry for the capsule was provided by E. J. Allen, H. T. Kerr, and D. L. Reed of the Reactor Division. Thermometry for the capsule was provided by R. L. Shepard of the Instrumentation and Controls Division. Fuel specimens from Los Alamos Scientific Laboratory were provided by P. Wagner. The postirradiation examination was done by the staff of the High Radiation Level Examination Laboratory and E. L. Ryan; metallography was carried out by L. G. Shrader and E. R. Boyd; and electron microprobe examination by T. J. Henson. The authors

also acknowledge the editorial work by N. Richards and the help of the Technical Publications Department, Information Division, in the preparation of this report.

REFERENCES

1. T. N. Tiegs, "Irradiation Tests in the ORR," *Thorium Utilization Programs Prog. Rep., July 1, 1975–Dec. 31, 1976,* ORNL-5274, pp. 299–308.

2. T. N. Tiegs, E. L. Long, Jr., E. J. Allen, M. J. Kania, and K. R. Thoms, *Irradiation Experiment OF-1: Accelerated Testing of HTGR Fuel,* ORNL-5234 (August 1977).

3. K. R. Thoms and M. J. Kania, *Design, Fabrication, and Initial Operation of HTGR-ORR Capsule OF-2,* ORNL/TM-5459 (March 1977).

4. M. J. Kania, K. R. Thoms, and T. N. Tiegs, "Irradiation Tests in the ORR," *HTGR Base-Technology Program Prog. Rep. Jan. 1, 1974–June 30, 1975,* ORNL-5108, pp. 360–95.

5. P. Wagner et al., *Irradiation Test OF-2: High-Temperature Irradiation Behavior of LASL-Made Fuel Rods and LASL-Made Coated Particles,* LA-6988-MS (October 1977).

6. M. J. Kania and A. M. Howard, *Thermal Analysis of ORR Capsule OF-2,* (report in preparation).

7. P. Angelini, J. L. Long, and D. E. Starnes, "Effect of Blending on Fuel Rod Temperature Distributions," *Thorium Utilization Programs Prog. Rep. July 1, 1975–Sept. 30, 1976,* ORNL-5266, pp. 197–201.

8. *Public Service Company of Colorado 330-MW(e) High-Temperature Gas-Cooled Reactor Research and Development Program Quart. Prog. Rep. Sept. 30, 1970,* GA-10313.

9. C. B. Scott and D. P. Harmon, *Postirradiation Examination of Capsule F-30,* GA-A13208, April 1, 1975.

10. F. J. Homan, E. L. Long, Jr., T. B. Lindemer, R. L. Beatty, and T. N. Tiegs, *Development of a Fissile Particle for HTGR Fuel Recycle*, ORNL/TM-5602 (December 1976).

11. T. N. Tiegs and T. J. Henson, *Fission Product Behavior in HTGR Fuel Particles Made from Weak-Acid-Resins* (report in preparation).

12. K. H. Valentine and E. L. Long, Jr., "Fuel Particle Inspection with Irradiated Microsphere Gamma Analyzer," *Trans. Am. Nucl. Soc.* 22 (TANSAO 22): 213–14 (November 1975).

13. M. J. Kania, *Gamma Analysis of Irradiated Fuel Particles from ORR Capsule OF-2* (in preparation).

14. F. J. Homan, T. B. Lindemer, E. L. Long, Jr., T. N. Tiegs, and R. L. Beatty, "Stoichiometric Effects on Performance of High-Temperature Gas-Cooled Reactor Fuels from the U-C-O System," *Nucl. Technol.* 35(2): 428–41 (September 1977).

15. T. N. Tiegs, T. J. Henson, and L. G. Shrader, Unpublished results on Irradiation Test HRB-12.

16. T. N. Tiegs, T. J. Henson, and L. G. Shrader, *Electron Microprobe Study of Low-Enriched HTGR Fuel Particles* (in preparation).

17. K. H. Valentine, F. J. Homan, E. L. Long, Jr., T. N. Tiegs, B. H. Montgomery, R. L. Hamner, and R. L. Beatty, *Irradiation Performance of HTGR Fuel Rods in HFIR Experiments HRB-7 and -8*, ORNL-5778 (May 1977).

18. F. J. Homan, E. L. Long, Jr., B. H. Montgomery, T. N. Tiegs, M. J. Kania, R. L. Hamner, R. L. Beatty, and B. A. Thiele, *Irradiation Performance of HTGR Fuel Rods in HFIR Experiments HRB-9 and -10*, ORNL-5254 (February 1978).

19. H. Grübmeier, A. Naoumidis, and B. A. Thiele, *Silicon Carbide Corrosion in HTGR Fuel Particles*, Kernforschungsanlage Jülich Gmbtt, Jül 1382 (January 1977).

20. R. A. Bradley and B. A. Thiele, "Neutron Induced Permeability of Pyrocarbon-Coated High Temperature Gas-Cooled Reactor Fuel Particles," *Nucl. Technol.* 35(2): 353–358 (September 1977).

21. M. J. Kania, T. B. Lindemer, M. T. Morgan, and J M Robbins, *Irradiation Performance of HTGR Fertile Fuel in HFIR Target Capsules HT-12 through HT-15: Part 1 — Experiment Description and Fission Product Behavior*, ORNL/TM-5305 (February 1977).

22. P. E. Brown and R. L. Faircloth, "Metal Fission Product Behavior in High Temperature Reactors — UO_2 Coated Particle Fuel," *J. Nucl. Mater.* 59: 29–41 (1976).

23. T. N. Tiegs, "FSVR Early Validation Tests," *Thorium Utilization Program Prog. Rep. July 1, 1975–Sept. 30, 1976*, ORNL-5266, pp. 265–67.

APPENDIX

GAMMA SPECTRA OF INDIVIDUAL FUEL RODS FROM OF-2

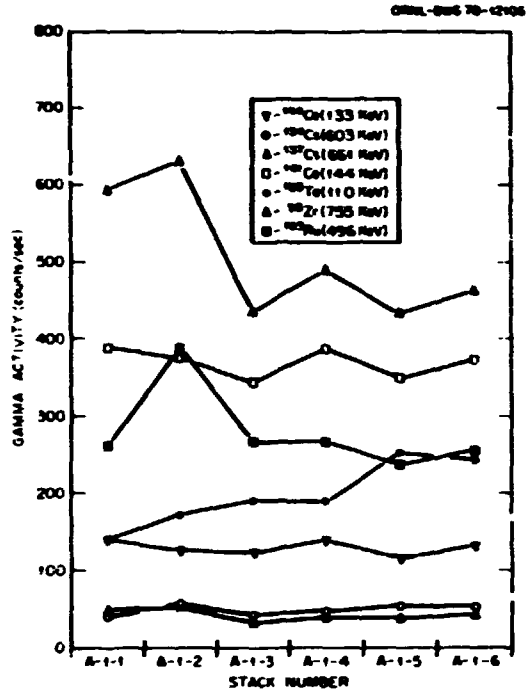

Fig. A.1. Gamma Activity of Fuel Rods from Stack A-1.

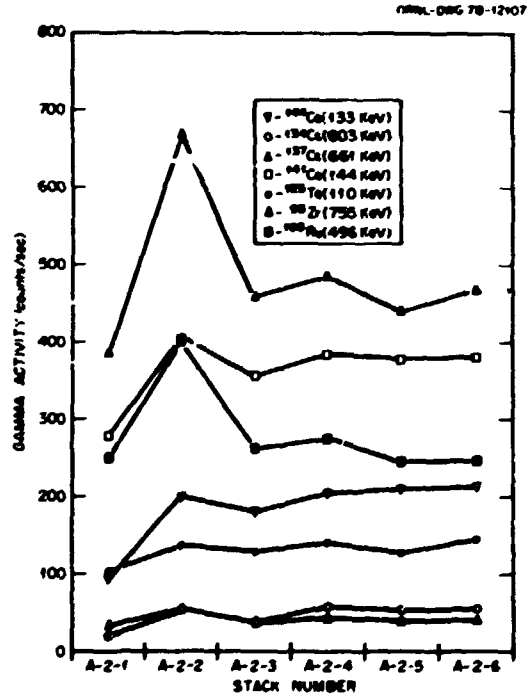

Fig. A.2. Gamma Activity of Fuel Rods from Stack A-2.

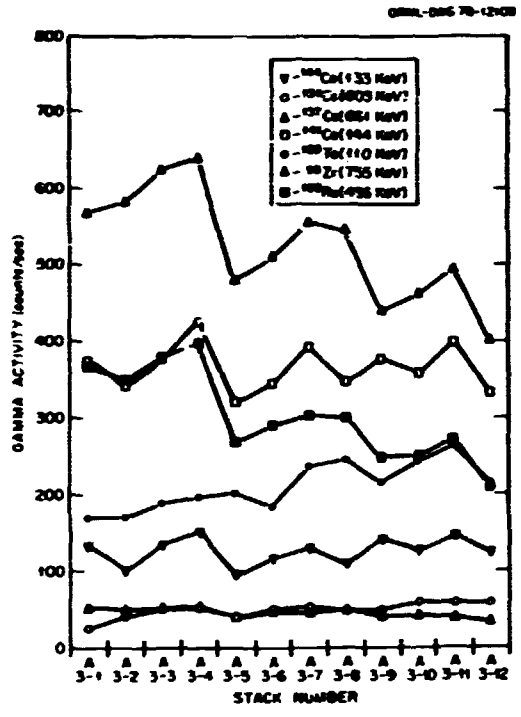

Fig. A.3. Gamma Activity of Fuel Rods from Stack A-3.

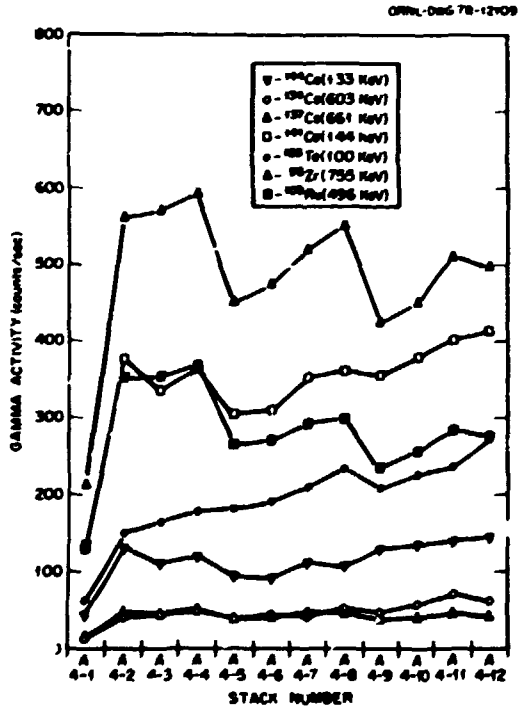

Fig. A.4. Gamma Activity of Fuel Rods from Stack A-4.

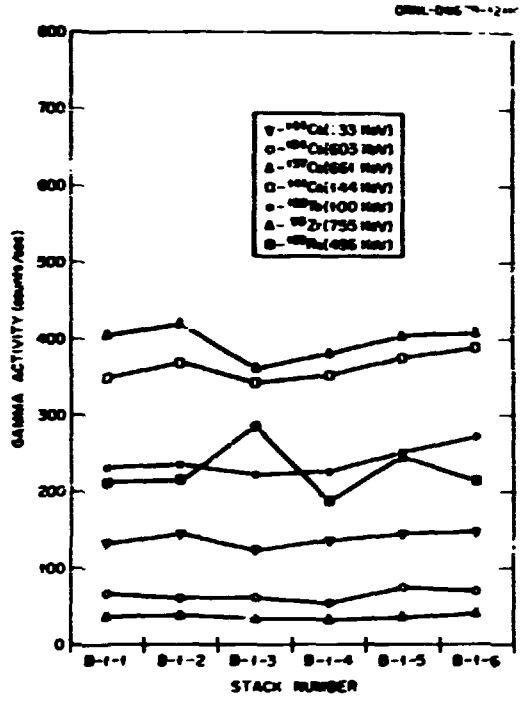

Fig. A.5. Gamma Activity of Fuel Rods from Stack B-1.

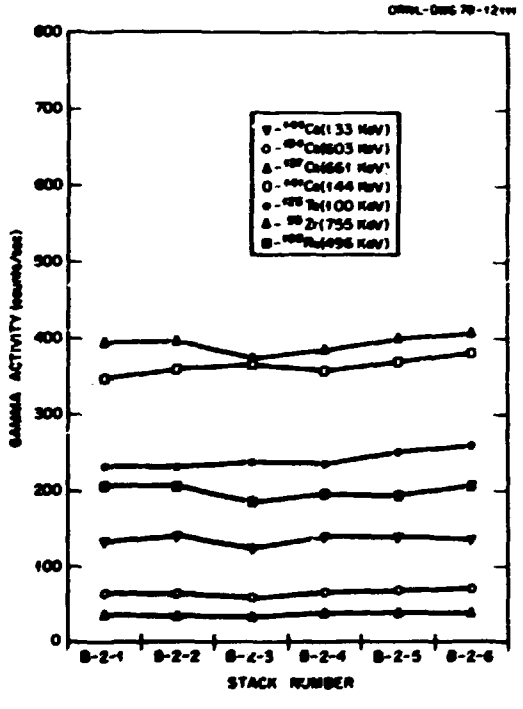

Fig. A.6. Gamma Activity of Fuel Rods from Stack B-2.

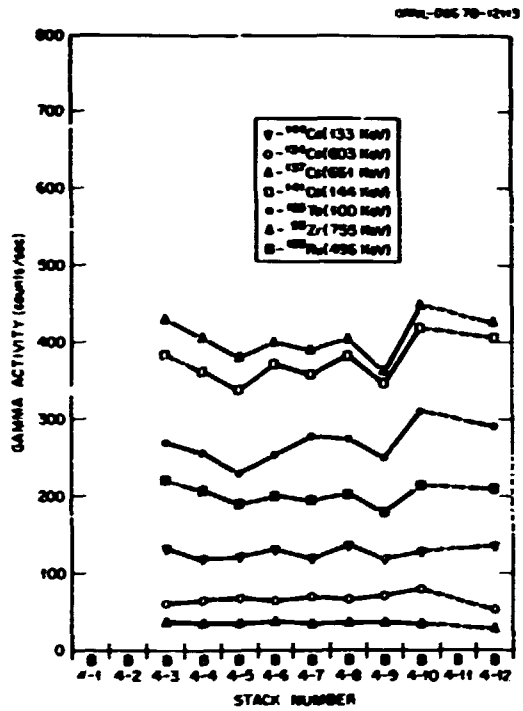

Fig. A.7. Gamma Activity of Fuel Rods from Stack B-3.

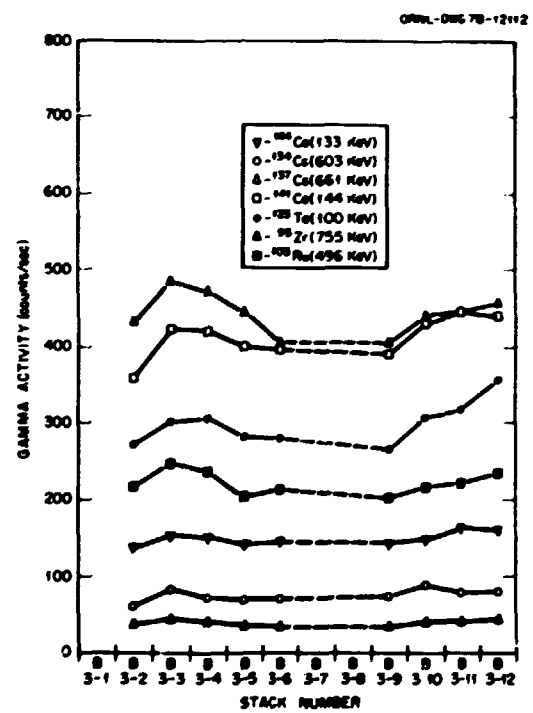

Fig. A.8. Gamma Activity of Fuel Rods from Stack B-4.

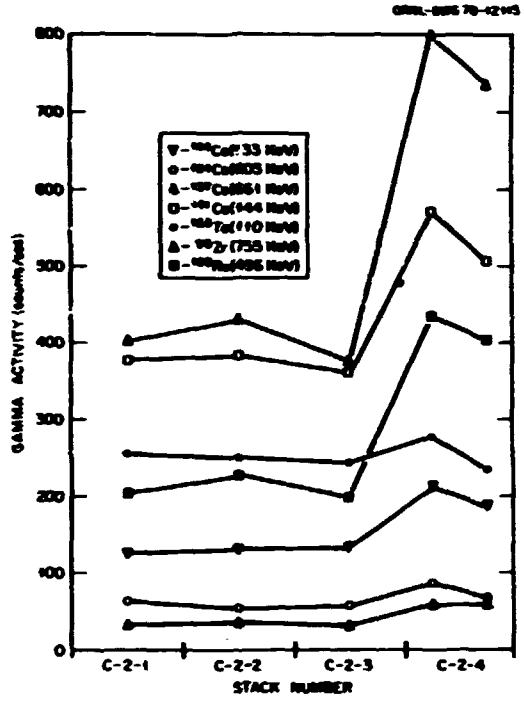

Fig. A.9. Gamma Activity of Fuel Rods from Stack C-1.

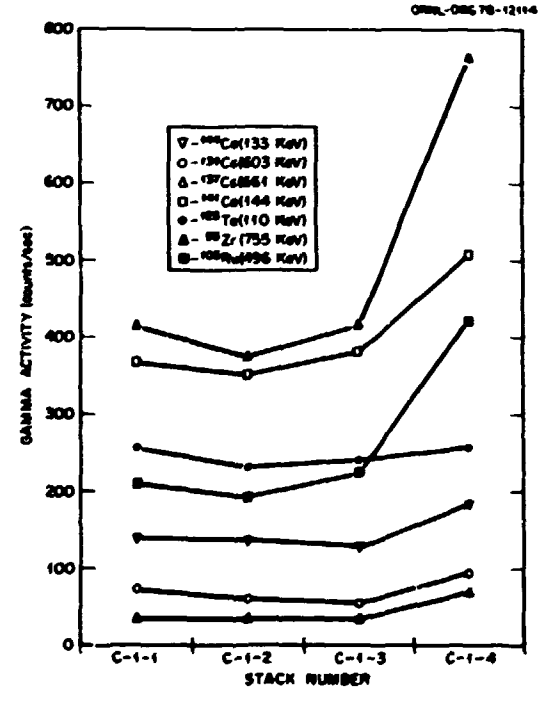

Fig. A.10. Gamma Activity of Fuel Rods from Stack C-2.

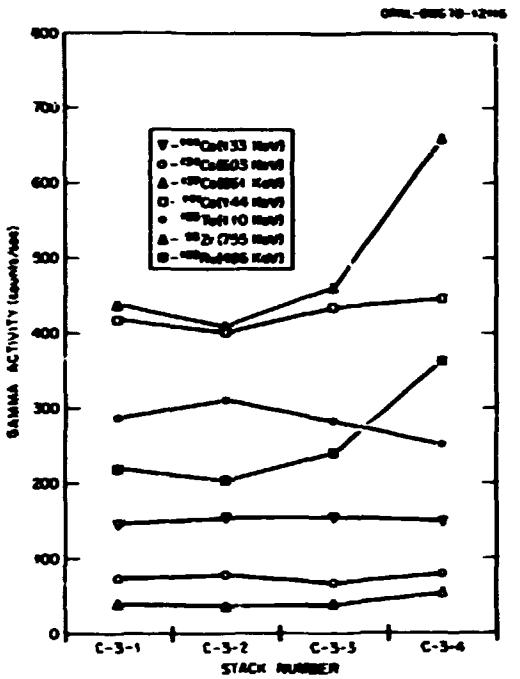

Fig. A.11. Gamma Activity of Fuel Rods from Stack C-3.

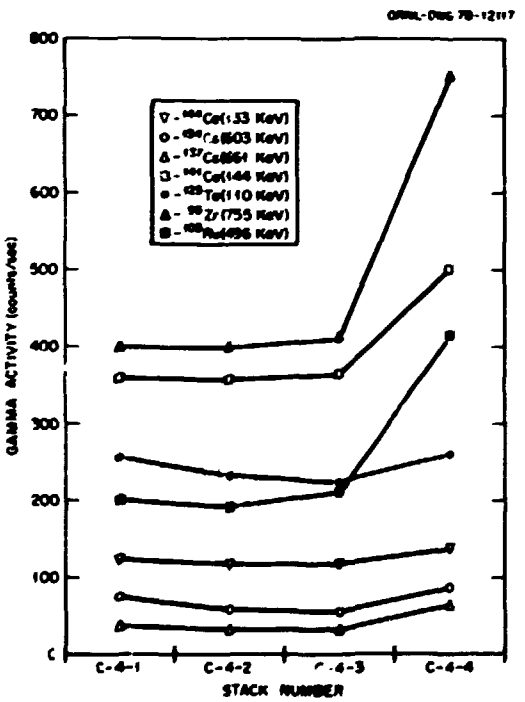

Fig. A.12. Gamma Activity of Fuel Rods from Stack C-4.